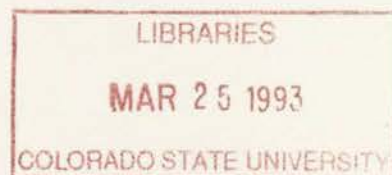


QC852
.C6
no.521
ATSL

Colorado Agricultural Experiment Station #COL00692
Air Force Office of Scientific Research #AFOSR-91-0269

PROTOTYPE REAL-TIME MESOSCALE PREDICTION
DURING 1991-92 WINTER SEASON AND
STATISTICAL VERIFICATION OF MODEL DATA

by Gregory Thompson



William R. Cotton, P.I.

**Colorado
State
University**

**DEPARTMENT OF
ATMOSPHERIC SCIENCE**

PAPER NO. 521

PROTOTYPE REAL-TIME MESOSCALE PREDICTION
DURING THE 1991-92 WINTER SEASON AND
STATISTICAL VERIFICATION OF MODEL DATA

by

Gregory Thompson

Department of Atmospheric Science

Colorado State University

Fort Collins, CO 80523

Research Supported by

Colorado Agricultural Experiment Station

under Grant #COL00692

Air Force Office of Scientific Research

under Grant #AFOSR-91-0269

March 9, 1993

Atmospheric Science Paper No. 521



U18400 7249980

CR

40002
. C6
no. 521
ATSL

ABSTRACT

PROTOTYPE REAL-TIME MESOSCALE PREDICTION DURING THE 1991-92 WINTER SEASON AND STATISTICAL VERIFICATION OF MODEL DATA

With the advent of faster, more powerful computers has come an opportunity to perform real-time mesoscale numerical weather prediction. The Regional Atmospheric Modeling System (RAMS) developed at CSU has been modified to become a prototype real-time forecast model. Surprisingly, a substantially complex model configuration can attain real-time forecasts on CSU workstations, as well as a CRAY supercomputer, although more sacrifices must be made on local machines in order to maintain the real-time restrictions.

Real-time forecasting began in November 1991 with two main objectives at the time. The first was to predict orographically-forced precipitation in the Colorado region. In this effort the RAMS model was run throughout the winter season of 1991-92 and continues again for the winter season of 1992-93. Through investigation of a case study day (9 March 1992) in which a major winter storm produced blizzard conditions along the Colorado Front Range, the true potential of RAMS real-time forecasting is demonstrated. The second goal was to provide real-time forecasts of cirrus-level clouds to investigators involved in the FIRE II field program in Kansas from 13 Nov. to 6 Dec. 1991. Again a case study day is analyzed in order to assess the possibility that RAMS could improve local mesoscale forecast capabilities.

COLORADO STATE UNIVERSITY LIBRARIES

Lastly, a comprehensive statistical analysis of all model data is discussed. The analysis uses multivariate randomized block permutation methods (MRBP) to illustrate model forecast skill for a variety of categories. These categories are comprised of case study model verification and entire season verification for forecasts of lengths 12, 24, 36, 48 hours as well as a brief comparison with established numerical models.

Gregory Thompson
Department of Atmospheric Science
Colorado State University
Fort Collins, Colorado 80523
Spring 1993

ACKNOWLEDGEMENTS

I'd like to thank my advisor, Dr. William Cotton for his guidance and support throughout the past few years. Spear-heading the real-time RAMS forecasting effort with him will no doubt pay dividends beyond graduate school. Committee members Dr. Roger Pielke and statistics professor Paul Mielke Jr. are also thanked for their contributions to this thesis.

I am likewise indebted to Dr. Craig Tremback whom I pestered so often with questions concerning RAMS code. His help in modifying the RAMS code to enable the ingest of the MAPS and NGM datasets was greatly appreciated as well as his help in learning much of the RAMS code. Paul Schultz of Forecast Systems Laboratory in Boulder was instrumental in providing the MAPS datasets and NGM model output for the duration of the study. Tom Parker provided help in setting up the real-time priority queue for running on the CRAY Y-MP at NCAR.

All of Dr. Cotton's group is thanked for valuable discussions concerning RAMS modeling as well as putting up with my disgust of machine problems throughout the real-time forecasting periods, particularly Jason Nachamkin. Brenda Thompson (no relation) is thanked for her help in preparing this manuscript and providing moral support while taking classes and simultaneously running the model.

Finally, I'd like to thank my wife, Dee, for her support throughout this research, even while 1500 miles across the country. The miles that separated us during the first year and a half only contributed to high phone bills; her support was unwavering during this time as well as the past year of marriage.

Cray Research provided the grant (#35081185) to use the NCAR CRAY-YMP for the FIRE experiment computations. NCAR is partially supported by the National Science Foundation. The CSU Student RISC workstation was purchased under support of the Dept. of Energy, DOE contract #DE-FG02-90ER61066. RAMS was developed under

support of NSF and ARO. This research was made possible by the Colorado Agricultural Experiment Station's grant #COL00692 and by the Air Force Office of Scientific Research's grant #AFOSR-91-0269.

TABLE OF CONTENTS

1	INTRODUCTION	1
2	BACKGROUND	3
3	REAL-TIME FORECAST SYSTEM	7
3.1	General Model Description	7
3.2	Initialization - MAPS	9
3.3	Time-dependent Lateral Boundary Conditions - NGM	13
4	PROTOTYPE REAL-TIME FORECASTING INVESTIGATIONS	17
4.1	Colorado Investigation	17
4.1.1	Description and model configuration	17
4.1.2	Discussion of forecasts for the entire season	18
4.1.3	Case study: 8-9 March 1992	20
4.1.4	Problems/discrepancies	38
4.1.5	Rhea-CSU model interface	42
4.1.6	Future: winter season 1992-93	45
4.2	FIRE II Investigation	45
4.2.1	Description and model configuration	46
4.2.2	Discussion of overall forecasts	47
4.2.3	Case study: 26 November 1991	50
4.2.4	Future & preliminary sensitivity studies	54
4.3	Computer Resources	57
5	STATISTICAL VERIFICATION	59
5.1	Introduction	59
5.2	Description of MRBP	61
5.3	Procedure of Analysis	63
5.4	Results	66
5.4.1	Whole season	68
5.4.2	8-9 March case study	73
5.4.3	MRBP analysis of a 23 November 1992 forecast	86
5.4.4	26 November FIRE II case study	91
6	SUMMARY AND CONCLUSIONS	94
6.1	Summary	94
6.2	Conclusions	96
6.3	Suggestions for Further Research	98

LIST OF FIGURES

3.1	Grid points and domain of 60 km MAPS data.	11
3.2	East-west cross-section of the MAPS domain illustrating the hybrid sigma-isentropic vertical coordinate system. (From Benjamin et al., 1991)	12
3.3	Grid points and domain of the NGM datasets. Note that these grid points are not the actual resolution of the NGM model.	15
4.1	Grid points and domain of Colorado investigation real-time forecast system. The course grid has a 100 km grid increment and the fine grid has 25 km spacing.	19
4.2	RAMS 24-hr forecast valid 0000 UTC 9 March, 1992 showing a) mean sea-level pressure (mb) with wind vectors and b) 500 mb heights/vorticity.	22
4.3	a) NMC surface and b) NGM 0-hour 500 mb heights/vorticity analyses valid 0000 UTC 9 March, 1992.	23
4.3	continued.	24
4.4	RAMS 36-hr forecast valid 1200 UTC 9 March, 1992 showing a) mean sea-level pressure (mb) with wind vectors and b) 500 mb heights/vorticity.	25
4.5	a) NMC surface and b) LFM 0-hr 500 mb heights/vorticity analyses valid 1200 UTC 9 March, 1992.	26
4.5	continued.	27
4.6	RAMS 24-hour grid 2 surface temperature (F) forecast valid 0000 UTC 9 March.	28
4.7	RAMS 36-hour accumulated precipitation (mm) valid 1200 UTC 9 March. . . .	29
4.8	FAA surface airway observations indicating three-letter station identifiers, 24-hour accum. liquid precipitation (<i>cm</i>) (upper-right), 24-hour snowfall (<i>cm</i>) (lower-right), and 12-hour liquid precipitation (<i>cm</i>) (lower-left) valid 1200 UTC 9 March, 1992.	30
4.9	RAMS 24-hr forecast mean sea-level pressure (mb) and surface wind vectors valid 0000 UTC 9 March, 1992.	31
4.10	SKEW-T/LOG-P diagrams for a RAMS gridpoint near Denver, Colorado at 0000 UTC 9 March, 1992. a) RAMS 24-hr forecast, b) RAMS with MICRO 24-hr forecast, and c) RAMS 0-hr forecast.	32
4.11	SKEW-T/LOG-P diagrams for a RAMS gridpoint near Denver, Colorado at 1200 UTC 9 March, 1992. a) RAMS 36-hr forecast, b) RAMS with MICRO 36-hr forecast, and c) RAMS 0-hr forecast.	33
4.12	RAMS (with MICRO) 36-hr accum. precipitation ending 1200 UTC 9 March, 1992.	34
4.13	RAMS 36-hr time-series of precipitation for a model grid point near Denver, Colorado depicting rain (solid) and snow (dashed) valid 0000 UTC 8 March through 1200 UTC 9 March, 1992.	36

4.14	Time-series of surface observations at Denver, Colorado and corresponding RAMS forecast surface information from 1200 UTC 8 March to 1200 UTC 9 March, 1992. Standard plotting with: temperature (upper-left), dewpoint temperature (lower-left), sea-level pressure (upper-right) and wind barb (each full barb representing 10 knots while half barbs represent 5 knots).	37
4.15	NGM 24-hr forecast valid 0000 UTC 9 March, 1992 showing a) mean sea-level pressure (mb) and b) 500 mb heights/vorticity.	39
4.16	RAMS relative humidity E-W cross-sections near Denver, Colorado valid 1200 UTC 9 March, 1992. a) RAMS 36-hr forecast, b) RAMS 0-hr forecast, and c) RAMS with MICRO 36-hr forecast.	41
4.17	CSU-Rhea model domain, border interpolation points and upper-air stations (from Rhea, 1978).	43
4.18	CSU-Rhea 36-hr predicted precipitation through 1200 UTC 9 March, 1992. . .	44
4.19	Grid points and domain of FIRE II investigation real-time forecast system. The course grid has a 80 km grid increment and the fine grid has 20 km spacing.	48
4.20	Infra-red satellite picture taken by NOAA-12 at 1443 UTC 26 November, 1991. Notice the high level clouds oriented north-south through the center of Kansas.	52
4.21	RAMS 16-hr forecast ice concentration (/L) valid 1600 UTC 26 November, 1991. Notice the similarities between this plot and the clouds shown in Figure 4.20.	53
4.22	RAMS 24-hr time-height ice concentration (/L) plot valid at a model grid point near Coffeyville, Kansas from 0000 UTC 26 November to 0000 UTC 27 November, 1991.	54
4.23	Lidar instrument time-height observations taken at Coffeyville, Kansas from 1652 UTC to 2214 UTC 26 November, 1991 indicating the locations of clouds.	55
4.24	RAMS 40-hr forecast ice concentration (/L) valid 1600 UTC 26 November, 1991.	56
5.1	MRBP results for whole season of RAMS 12 hour forecasts. Statistical agreement measure is plotted versus model sigma level (see text for details). Panel a shows wind-related variables for grid 1, while thermodynamic variables for grid 1 are shown in panel b. Panels c and d have same information but for grid 2.	69
5.2	MRBP results for whole season of RAMS 24 hour forecasts, otherwise same as Figure 5.1.	70
5.3	MRBP results for whole season of RAMS 36 hour forecasts, otherwise same as Figure 5.1.	71
5.4	MRBP results for whole season of RAMS 48 hour forecasts, otherwise same as Figure 5.1.	72
5.5	MRBP results for a single RAMS 24-hour forecast from sensitivity run V2c beginning 0000 UTC 8 March, 1992, otherwise same as Figure 5.1	74
5.6	MRBP results for a single RAMS 24-hour forecast from sensitivity run NEW2c, otherwise same as Figure 5.5.	76
5.7	MRBP results for a single RAMS 36-hour forecast from sensitivity run NEW2c, otherwise same as Figure 5.6.	77
5.8	RAMS grid 2 mean sea-level pressure (mb) with wind vectors valid 0000 UTC 9 March, 1992 a) 24-hour forecast and b) 0-hour forecast.	78
5.9	MRBP results for a single RAMS 24-hour forecast from sensitivity run MICRO, otherwise same as Figure 5.7.	79

5.10 MRBP results for a single RAMS 24-hour forecast from sensitivity run LBC-ETA, otherwise same as Figure 5.9.	81
5.11 MRBP results for a single RAMS 36-hour forecast from sensitivity run LBC-ETA, otherwise same as Figure 5.7.	82
5.12 MRBP results for a single NGM 24-hour forecast beginning 0000 UTC 8 March, 1992, otherwise same as Figure 5.6.	84
5.13 MRBP results for a single NGM 36-hour forecast beginning 0000 UTC 8 March, 1992, otherwise same as Figure 5.7.	85
5.14 MRBP results for a single ETA 24-hour forecast beginning 0000 UTC 8 March, 1992, otherwise same as Figure 5.12.	87
5.15 MRBP results for a single ETA 36-hour forecast beginning 0000 UTC 8 March, 1992, otherwise same as Figure 5.13.	88
5.16 MRBP results for a single RAMS 36-hour forecast beginning 0000 UTC 23 November 1992, otherwise same as Figure 5.7.	89
5.17 MRBP results for a single NGM 36-hour forecast beginning 0000 UTC 23 November 1992, otherwise same as Figure 5.16.	90
5.18 MRBP results for a single RAMS 18-hour forecast beginning 0000 UTC 26 November 1991, otherwise same as Figure 5.16.	92
5.19 MRBP results for a single NGM 18-hour forecast beginning 0000 UTC 26 November 1991, otherwise same as Figure 5.17.	93

Chapter 1

INTRODUCTION

Operational numerical models have become established in real-time weather prediction over the past few decades. For the most part, numerical models are executed on large supercomputers by major government agencies like the National Meteorological Center (NMC) in Washington, D.C. , the British Meteorology Office in London, the European Center for Medium Range Forecasting in Reading, England, and Japan's Meteorological Agency in Tokyo. The model-generated forecasts are disseminated all across the globe to local forecast offices which use them for guidance in local weather prediction. Some would argue that today's forecasters rely too heavily on model output when making forecasting decisions. Unfortunately, forecasters all across the U.S. are given the same model output encompassing the Northern Hemisphere, but not products which are specific to their locality. The problem is two-fold. First, current numerical models are designed to forecast synoptic-scale weather situations and, as a result, cannot accurately predict mesoscale features which the local forecaster needs to aid in local weather prediction. Second, local forecasters are not provided with model output products which are specific to their location.

Recently, research mesoscale numerical models have begun addressing this problem while successfully simulating a variety of mesoscale weather phenomena, including: thunderstorm morphology, sea-breeze circulations, and flow over complex terrain. Although these mesoscale models are based on the same primitive equations of momentum and thermodynamics as their operational counterparts, their complexity has previously restricted their potential for operational forecasting. This complexity is a result of the incorporation of more complete physical parameterizations and finer vertical and horizontal resolution. Only the significant advances in computer technology of the past few years have made real-time forecasting by mesoscale numerical models feasible.

One such example is the Regional Atmospheric Modeling System (RAMS) developed at Colorado State University (CSU). RAMS has been modified to become a prototype real-time forecast model (Chapter 3). To address the problem that current operational models cannot accurately predict mesoscale weather phenomena nor provide region-specific forecast products, RAMS was configured for two forecast applications. The objective of the first forecast application was to predict orographically-forced precipitation for much of Colorado. The objective of the second was to provide real-time forecasts of cirrus-level clouds to investigators involved in the FIRE Phase II field program. It is the goal of this study to show RAMS' ability to forecast accurately mesoscale phenomena important to the two forecast applications within the time restrictions of operating in real-time. This will be accomplished through the discussion of two case studies (one for each application - Chapter 4), whereby real-time model output from each application is compared with corresponding observations. Finally, a comprehensive statistical analysis of all model data is discussed (Chapter 5) in an effort to quantify what is meant by the accuracy of RAMS forecasts.

Chapter 2

BACKGROUND

In the last century or so, technological advances have provided meteorologists with the information necessary to predict reliably, and for the most part, accurately the daily weather. Today, not a single hurricane goes unnoticed, most tornadic thunderstorms receive warnings, and many a blinding snowstorm is seen well ahead of its arrival. The end result of most meteorological research is to improve weather forecasting. Improving weather forecasting benefits everyone because of the many impacts weather has on our daily lives. The most obvious impacts relate to severe weather where lives may be at stake. Each year tornadoes, hurricanes, lightning and hail take hundreds of lives and destroy countless dollars of personal property. More docile weather phenomena have more subtle implications. Fog may close an airport, delaying thousands of travelers; strong winds spread wildfires, destroying thousands of acres of forest; frost destroys crops, raising prices at the grocery store; air stagnation hinders pollution dispersion, creating health problems in densely populated areas, to name a few.

Recurring themes eluded to above focus on weather impacts to agriculture, recreation and transportation/shipping (land, sea or air). Common sense dictates that forecasting be directed appropriately into these categories. This is often the case, especially in the media. Across the country, countless television forecasters advise viewers not to travel the following day because of an incoming snowstorm or will suggest an outdoor picnic based on a "warm and sunny" forecast. Agriculture is the category for which weather forecasts are least often tailored.

Mesoscale numerical models are well suited for forecasting applications to agriculture. Most of the applications involve the optimal utilization of water resources. Rainfall, dew/frost and evaporation/transpiration all contribute to the water budget which are so

critical to agriculture. These agricultural concerns relate as much to mesoscale weather features as to synoptic scale weather. For instance, summer rains in the western high plains are primarily provided by thunderstorms which exist on the mesoscale. Likewise, frost may occur over an area of 30 square kilometers due to drainage flow into a local valley. Mesoscale models are beginning to incorporate the characteristics necessary to predict these events. Highly detailed topography, prognostic soil and vegetation models and meso α - scale (250 - 2500 *km*) convective parameterizations are now included into many atmospheric mesoscale models. Furthermore, ever increasing computer power is allowing complex numerical models to predict in real-time. With the nearly limitless increase in future computer power comes a multitude of forecast applications.

Weather prediction by numerical models consists of three basic ingredients: data collection/model initialization, model time integration, and a post-processing step to display/disseminate model output. Model initialization requires numerical quantification of the state of atmospheric variables such as winds, temperature and moisture. Initialization has been accomplished traditionally by one of two methods. The first method is to assume a horizontally homogeneous atmospheric state. This is where the model's wind, temperature and moisture variables are obtained by an atmospheric sounding and held constant in the horizontal throughout the model domain. Examples of which can be found in Grasso (1992), Meyers (1990) and Bossert (1990) among others. The other method of model initialization is to describe the atmosphere via horizontally inhomogeneous conditions, a more realistic atmospheric description. This is often referred to as variable initialization, examples of which are found in Tremback (1990), Heckman (1991) and Henry (1991) to name a few. The variable initialization in these studies used archived data from NCAR as described by Cram (1990), however, a new data source has been used for this study, details of which are provided in the next Chapter.

The second ingredient, model time integration, conserves mass, momentum, and water substance while accounting for all important sources and sinks. More complete details of the numerical model are given in Chapter 3, however one of the distinguishing features of this study needs to be mentioned here. Assuming the atmosphere does not remain steady-state for long periods, the expected atmospheric state at later times must be communicated to

the model's lateral boundaries. This is necessary because meteorological conditions outside the model domain (of which the model has no information) often influence the meteorology occurring on the model boundaries. Hence, the model must be told what the boundary tendencies are with time. This is referred to as time-dependent lateral boundary conditions and is discussed more thoroughly in the next Chapter. In the studies using variable initialization mentioned above, this was accomplished by supplying the model with observed conditions via the same type of data sets which were used for the initialization. Throughout this study, though, forecast atmospheric conditions were used to update the lateral boundary tendencies, not observations. A true forecast numerical model has been achieved since daily observations are used for initialization while model forecasts are used to update the boundary conditions. Earlier work with mesoscale models have produced retroactive simulations and used observations in order to specify lateral boundary regions, however, this work is only the second of its type in a university environment. The Pennsylvania State University (PSU) has recently adapted their mesoscale model, PSU/NCAR MM4, to operate in real-time (Warner and Seaman, 1990). The MM4 mesoscale model has also been used occasionally by the NMC as additional model guidance.

The MM4 mesoscale model has been quasi-operational since April 1989. Warner and Seaman (1990) discuss the real-time forecast system and illustrate it using two real-time forecasts produced by MM4. The first involved a frontal passage through Pennsylvania with relatively light precipitation. The forecast position of the front, the wind shift and the forecast precipitation all agreed well with observations. The second involved a heavy rainfall case in which a series of fronts and troughs moved through the northeastern United States in association with the eastern portion of an omega blocking pattern. Again, the MM4 produced respectable forecasts with the only problems isolated to precipitation forecasts. Warner and Seaman (1990) also discuss the research, teaching and public service applications of the real-time mesoscale model prediction tool. Specifically, they point out three situations that make this real-time forecasting system so valuable: "1) when an objective of the research is the development of techniques for real-time interpretation and utilization of mesoscale forecasts; 2) when it is used in conjunction with measurement programs that

require short-range mesoscale forecasts; and 3) when a setting is desired in which modelers, operational forecasters (faculty, staff, and students) and diagnosticians can interact to better understand mesoscale processes and how to predict them, through real-time daily interpretation of mesoscale model output and the assessment of model performance." The value of the first two situations has been proven throughout the past two years at Colorado State University (CSU). An entire section of Chapter 4 is devoted to the discussion of real-time forecasting applications to measurement programs and utilization of mesoscale forecasts. In particular, real-time forecasting was performed daily in support of the FIRE II field program from 13 November to 6 December 1991. The results of this investigation will show potential for repeated real-time forecasting in future field programs. The third point by Warner and Seaman has only recently come to fruition as faculty, staff and students are just beginning to inquire, interpret and discuss the real-time mesoscale forecasting underway at CSU. Furthermore, the assessment of model performance has really emerged via this study as a comprehensive statistical analysis has been performed for nearly all of the real-time forecasting results presented here.

Chapter 3

REAL-TIME FORECAST SYSTEM

3.1 General Model Description

The numerical model employed throughout this research is the Regional Atmospheric Modeling System (RAMS) developed at CSU. It is a completely new code that is a merger of a non-hydrostatic cloud model (Tripoli and Cotton, 1982) and a hydrostatic mesoscale model (Mahrer and Pielke, 1977). A general description of the model can be found in Tripoli and Cotton (1982), Cotton et al. (1982), Tremback et al. (1985), Tripoli (1986), Tremback (1990), and Pielke et al. (1992). The non-hydrostatic version of RAMS was used and the numerical procedures are described in Tripoli and Cotton (1982) and Tripoli (1986). This version uses the leapfrog time differencing with an Asselin filter and a time-split scheme (Klemp and Wilhelmson, 1978) to integrate acoustic terms on a short time step and all other terms on a long time step. The advection scheme used was of second order. RAMS predicts u , v , and w wind components, ice/liquid water equivalent potential temperature, θ_{ii} , dry air density, total water mixing ratio, and the mixing ratios of the various water variables (rain, snow, pristine ice, aggregates and graupel). From these, pressure, potential temperature, vapor mixing ratio and cloud mixing ratio are diagnosed.

RAMS uses a standard Arakawa-C grid (Arakawa and Lamb, 1981) which is staggered in both the vertical and horizontal directions. Scalar variables such as pressure, temperature and mixing ratio are defined at the center of each grid volume; whereas velocity components are defined on the faces of grid volumes. Horizontally, RAMS utilizes a polar stereographic grid (Version 2c) and vertically, a sigma-z terrain-following system (Gal-Chen and Somerville, 1975) with user-specified spacing. Specific features to particular investigations are mentioned in subsequent subsections, however, additional common features between investigations are listed below. The turbulence scheme used was the deformation

eddy viscosity described by Tripoli and Cotton (1982) where adjustments to the vertical exchange coefficients were made using a Richardson number/moist Brunt-Väisälä frequency enhancement factor. This study used a 5-level prognostic soil model described by Tremback and Kessler (1985). The radiation scheme employed here is described in Mahrer and Pielke (1977). This scheme considers the influence of water vapor, ozone, and carbon dioxide on shortwave and longwave radiative transfer. It does not consider radiative influences due to condensate or microphysical species. For this reason, the model does not account for reflected/absorbed shortwave radiation due to clouds nor does it include additional downward longwave radiation. RAMS does have a radiation option to consider these effects, however, its implementation causes the model to run much slower, hence, one cannot forecast in real-time.

The "wall on top" condition where w is set to zero at the model top is used as a top boundary condition. The modified Rayleigh friction scheme described by Heckman (1991) and Cram (1990) was not utilized for this study because of the additional time involved, however, future real-time RAMS forecasts will include a damping mechanism at the top since the wall proves to be reflective (Heckman, 1991).

There are four levels of moisture complexity in RAMS. The first level is completely dry; the second causes moisture to be a passive tracer; the third dictates that all supersaturation is condensed into liquid water; and the final option has the highest complexity - microphysics. A complete description of the Cloud Microphysical Module (CMM) is found in Flatau et al. (1989). The CMM simulates nucleation, growth, collection, and precipitation processes for pristine ice crystals, snow, aggregates, graupel and rain. Pristine crystals are considered to be a mono-dispersed size distribution with the characteristic diameter diagnosed from the predicted concentration and mixing ratios. Simulated crystal nucleation was achieved using a modified Fletcher scheme (Cotton et al., 1986). This scheme allowed larger numbers of crystals at colder temperatures with an adjustment for ice supersaturation. Hexagonal plates is assumed for vapor depositional growth and terminal velocity is computed based on characteristic diameters. Crystals can then aggregate, melt into rain drops and evaporate. Features lacking in this treatment include: explicit representations of

particle size distributions; a homogeneous freezing mechanism for crystal nucleation; and additional crystal geometries for depositional growth.

3.2 Initialization - MAPS

The first step of numerical weather prediction is model initialization. This is accomplished through quantification of atmospheric variables such as horizontal winds, temperature and moisture (e.g. relative humidity). These quantities must be known for all of the model's grid volumes at the initial time of the simulation. Unfortunately, routinely available observational data does not come already gridded at the exact resolution of numerical models. As a result, irregularly spaced data such as surface airway observations (SAO) and rawinsondes must be objectively analyzed and processed into data in a gridded format. Ideally, all models would include a data ingest procedure which would take the observations and create a gridded data set which exactly matches the model's grid spacing. Instead, as is the case with this study, models often rely on gridded data provided by an outside source which have to be interpolated to the model's grid spacing. This can not only create uncertainty concerning the interpolation procedure, but also adds significantly to the time involved in initializing the model. The latter being of extreme importance when forecasting operationally. Receiving already gridded data does, however, have an advantage: less time and energy needs to be spent on writing the code for the objective analysis scheme used and more time can be shifted toward improving the model. We feel we have gained just that through the use of NOAA's Forecast System Laboratory's (FSL) Mesoscale Analysis and Prediction System (MAPS).

MAPS is both a data assimilation system and a primitive equation model. A full description of MAPS' formulation can be found in Benjamin (1989) and Benjamin et al. (1991). Although MAPS is also a primitive equation forecast model, only MAPS analyses were used for this study not forecasts. The biggest advantage of the MAPS data sets over the NMC's products is the resolution. MAPS is a hybrid sigma-isentropic (constant theta) dataset with 60 *km* horizontal grid spacing. NMC's datasets available at the time had much coarser resolution which is of great importance when initializing a mesoscale model. Many important mesoscale features are lost on grids with spacing greater than 60 *km*.

Another advantageous aspect of the MAPS dataset is the isentropic coordinate system. Tremback (1990) points out that, "isentropic coordinate data analysis has inherent advantages over other coordinate systems. First, since synoptic scale flow tends to be adiabatic, objective analyses performed on isentropic surfaces better approximate interstation variability of atmospheric fields. Second, isentropes provide enhanced resolution along discontinuities especially baroclinic zones since isentropes tend to be packed more closely. Finally, because isentropes are sloped in the vicinity of fronts, short wavelength features are transformed into longer wavelengths that can be more accurately analyzed objectively with much less smoothing than with other coordinate systems." Relating to the first point mentioned above, Black (1987) notes that "isentropic surfaces describe the locus of trajectories of all parcels which initially possess a given potential temperature and which move under adiabatic, frictionless conditions". Black claims that isentropic coordinates render motion essentially two-dimensional on the synoptic scale. He continues by mathematically showing how errors associated with finite-difference approximations in the third dimension are decreased or eliminated.

The main disadvantage of an isentropic coordinate system is that details within an adiabatic boundary layer are impossible to analyze. FSL, however, included a hybrid-sigma coordinate system as well. This sigma vertical coordinate exists as six levels in the lowest 150 *mb* thus retaining highly detailed planetary boundary layer information. The preset isentropic levels exist below ground during the warmest weather, within the sigma levels, and, most of all, above the sigma levels.

Another advantage MAPS has over NMC products is the incorporation of aircraft reports (ACARS), wind profiler data and surface mesonetwork data along with the standard surface airway observations (SAO) and rawinsondes into the analysis. It is currently not known whether the additional high resolution data or the analysis technique (an optimal interpolation scheme) has a larger impact on the quality of the MAPS analysis products.

FSL generously transferred the 0000 and 1200 UTC MAPS analysis each day roughly 3 hours after data time. RAMS was initialized with the 0000 UTC dataset for two reasons. First, simulations were performed on a multi-user computer so running from 0000 UTC data caused most of the computations to be performed during off-peak nighttime hours. Second,

nightly runs produced forecasts (albeit 12 hours older than NMC's products) which were available first thing in the morning.

The MAPS datasets contained the following variables: grid relative east wind component, grid relative north wind component, pressure, theta, condensation pressure (lifting condensation level, LCL) and Montgomery streamfunction ($\psi = gz + C_p T_v$). Code was painstakingly pieced together to convert from these to more easily ingested ones such as: true north and east wind components, heights, relative humidity, pressure and theta. MAPS variables are provided at the horizontal grid points shown in Figure 3.1 and vertically on the six sigma levels and 19 isentropic levels listed in Table 3.1 and shown in Figure 3.2.

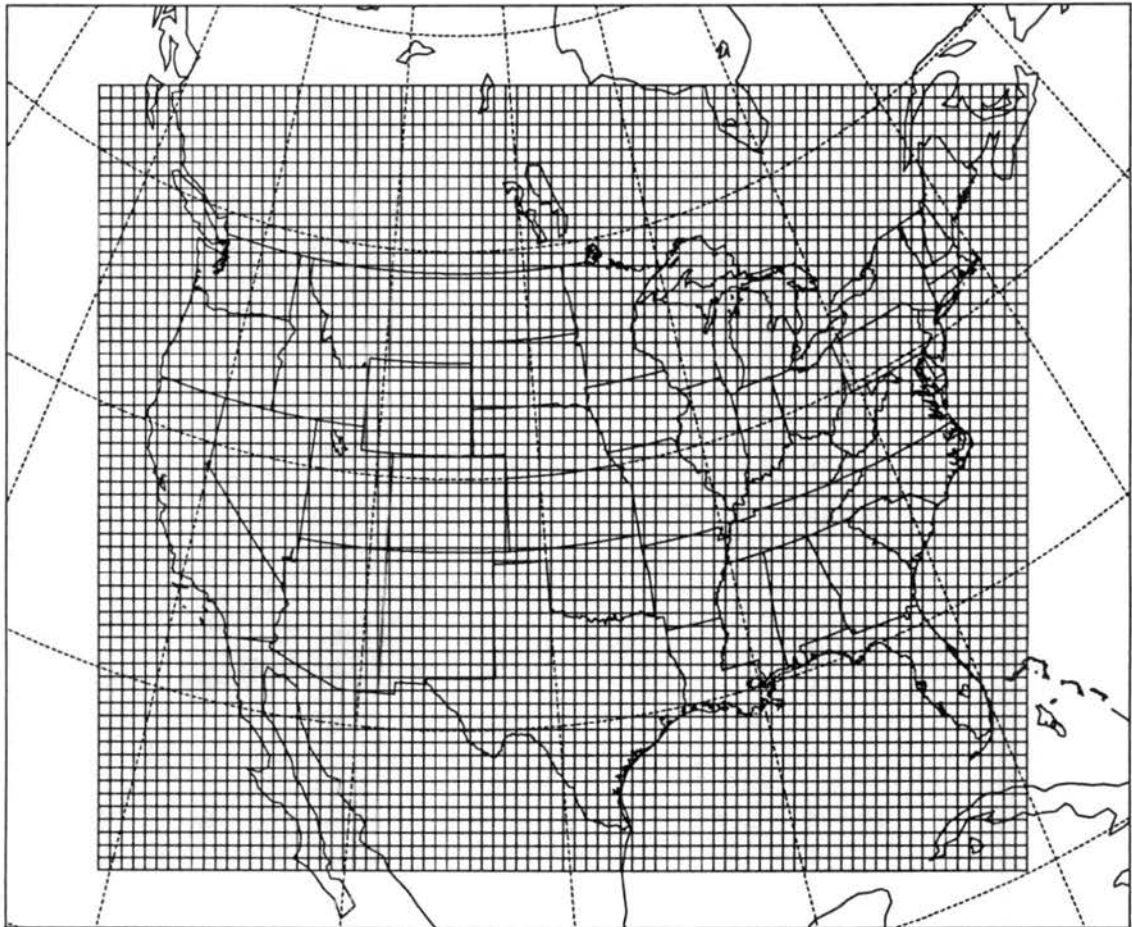


Figure 3.1: Grid points and domain of 60 km MAPS data.

Obviously theta values on isentropic surfaces are a bit redundant, however, theta values within the sigma levels are absolutely necessary.

Ingesting the MAPS data into RAMS was accomplished in the following manner. First, MAPS variables were converted to true east and north wind components, theta, relative humidity and Montgomery streamfunction. Then a horizontal interpolation was performed transforming variables from MAPS' horizontal grid to RAMS' horizontal grid. Variables were then vertically interpolated (linearly in z) to our sigma vertical coordinate system. This was first performed for the first 6 sigma levels of MAPS, then for the isentropic surfaces, beginning with the first isentrope above the top sigma level. This meant that, in a given column, any isentropic level information would be ignored if the isentrope crossed into the sigma levels. A schematic of this is shown in Figure 3.2 where the isentrope is not drawn

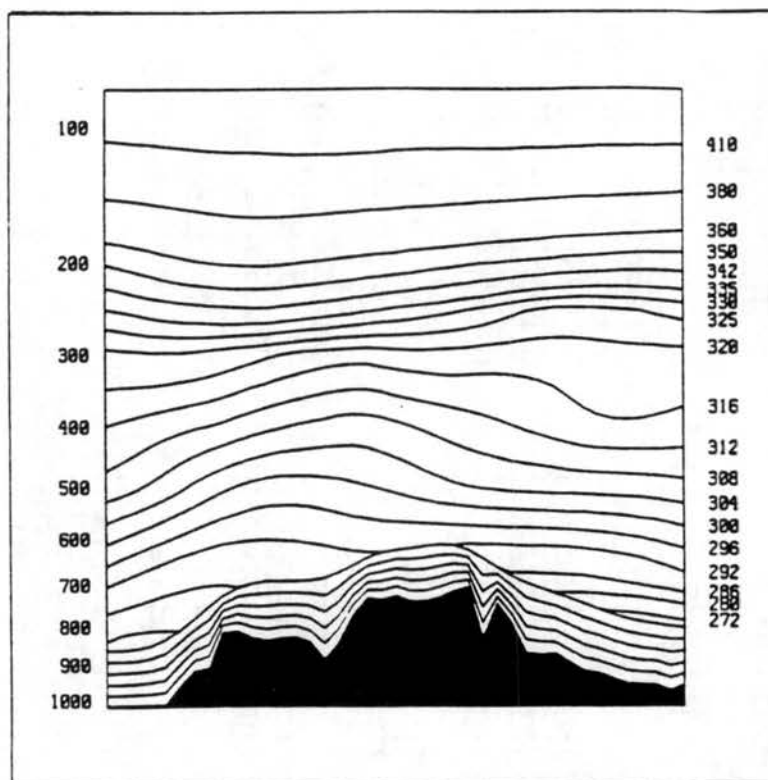


Figure 3.2: East-west cross-section of the MAPS domain illustrating the hybrid sigma-isentropic vertical coordinate system. (From Benjamin et al., 1991)

if it intersects the sigma level information. Finally, Exner function ($\pi = (p/p_0)^{R/C_p}$) values were obtained by a hydrostatic integration from the MAPS 360 K objectively analyzed streamfunction "boundary condition".

3.3 Time-dependent Lateral Boundary Conditions - NGM

As mentioned in Chapter 2, time-dependent lateral boundary conditions are necessary for variably initialized simulations. The two choices in RAMS are a Perkey and Kreitzberg (1976) sponge and a Davies (1983) relaxation. In either case, data at two times (initial and 12 hours later, for example) are used to force the boundary values of the variable tendencies. In the Davies scheme, which was utilized for this research, boundary values of u , v , θ , r and π are forced to externally-specified values although the model's internally defined tendencies are used in the model integration (Cram, 1990). More specifically, an extra tendency term is added to each prognostic equation which forces the predicted variable towards the available observations or forecasts. Again, as mentioned in Chapter 2, when nudging toward observations a type of retroactive simulation is achieved, while using forecasts of boundary conditions, a true forecast modeling system is achieved.

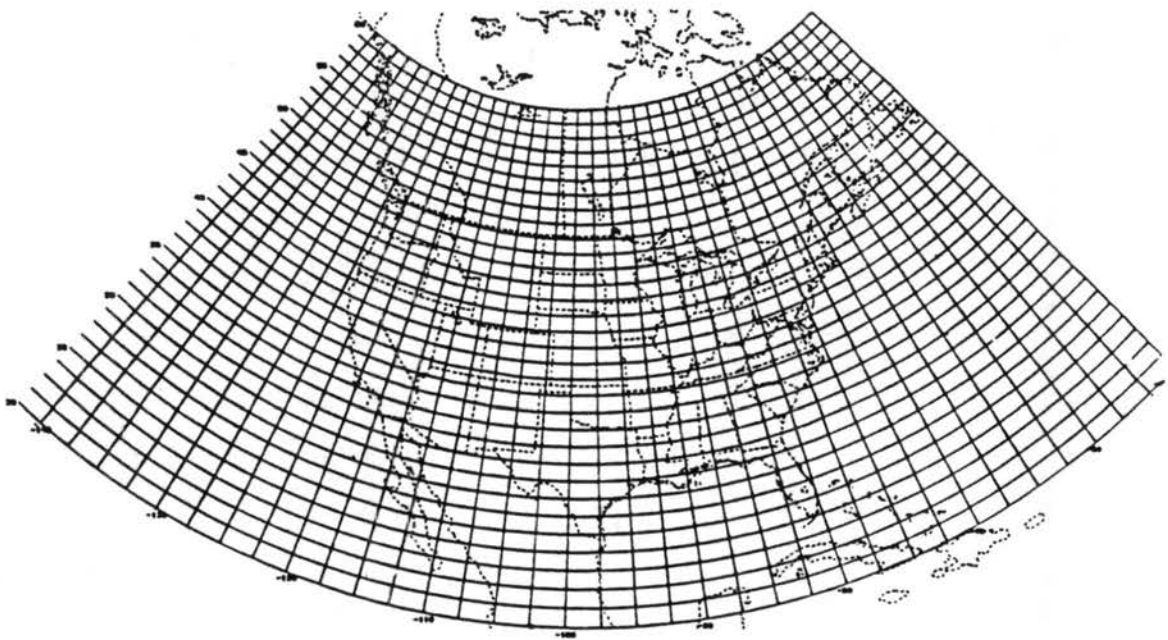
The time-dependent lateral boundary conditions were provided by the NGM forecasts disseminated by NMC. A thorough description of the NGM model can be found in Hoke et al. (1989). This was the most restrictive part of the real-time forecasting at CSU. Whenever NMC had computer problems, an unfortunate chain of events resulted. FSL would receive the NGM forecasts later. Then, upon transmitting at the same time each day, only portions of the NGM forecasts received by CSU were complete. This resulted in forecasts of lengths 24, 30 or 36 hours instead of 48. RAMS, then, would only have forecast boundary conditions out to this time and thus could not run beyond 24, 30 or 36 hours. To further illustrate this point, over one-hundred 12-hour forecasts were made between mid-November and early April, while eighty 24-hour forecasts, fifty 36-hour and only forty 48-hour forecasts were made for this period. Fortunately this problem has been averted for the 1992-93 winter season as a new NGM data link has been created. In an attempt to remedy the incomplete NGM datasets, FSL would transmit at later times, sometimes as much as 5 1/2 hours after data time. This becomes a major problem when forecasting in real-time because the longer one waits for data, the longer one has to wait for the simulation to begin. The conclusion reached was to wait a specified period of time in which most, but not all, data would be received.

The NGM datasets used throughout this study are summarized below and in Table 3.1. The NGM model has three nested grids with polar stereographic projections. The smallest nested grid has a horizontal grid-spacing of approximately 84 km at 45° north latitude. Unfortunately, the NGM datasets received were not this spacing but instead had spacing of 1.25° latitude by 2.5° longitude. This spacing translates to nearly 150 km at 45°. A plot of this grid can be found in Figure 3.3. Vertically, the NGM model has 16 sigma levels however, CSU received the degraded version in which 10 pressure levels were provided. The NGM datasets provided horizontal wind components, heights, temperatures and relative humidity at 1000, 850, 700, 500, 400, 300, 250, 200, 150, 100 mb. Unfortunately, relative humidity was not provided at 1000 mb but at 900 mb instead. This was the only variable provided at 900 mb so it was extrapolated to the 1000 mb level. Relative humidity above 300 mb was also missing. Unfortunately, NMC does not distribute freely the original NGM grid point datasets not even within their own organization.

Table 3.1: Description of resolution and variables provided in MAPS and NGM datasets.

DATASET	RESOLUTION	VARIABLES
MAPS	Horizontal: 81 x 62 points 60 x 60 km Vertical: 6 σ_z in lowest 150 mb 19 preset θ levels $\theta = 272, 280, 286, 292,$ 300, 304, 308, 312, 316, 320, 325, 330, 335, 342, 350, 360, 380, 410	u - grid rel. i wind component v - grid rel. j wind component p - pressure ψ - Montgomery streamfunction θ - theta cp - condensation pressure
NGM	Horizontal: 36 x 33 points 1.25° Lat x 2.5° Lon Vertical: 10 pressure levels p = 1000, 850, 700, 500, 400, 300, 250, 200, 150, 100 mb	u - east wind component v - north wind component z - geopotential heights T - temperature RH - relative humidity except RH at 900 mb and not above 300 mb

NGM datasets provided forecasts at the following times: 0, 6, 12, 18, 24, 30, 36, and 48 hours. The lateral boundary conditions were first updated at 12 hours and then at all



GRID SPACING: 2.5 LON X 1.25 LAT

Figure 3.3: Grid points and domain of the NGM datasets. Note that these grid points are not the actual resolution of the NGM model.

subsequent NGM forecast times listed. The boundary conditions were linearly interpolated between the time intervals mentioned. This implies the variables on a zone of points (5 in this study) along the domain's lateral boundaries were assumed to undergo a linear transition from initialization to 12 hours, 12 to 18 hours and so on.

A much more complete dataset used experimentally for the task of updating boundary conditions was provided by the ETA model which is NMC's experimental numerical model (Mesinger et al., 1988, 1990). This was a far superior dataset because of its resolution. ETA datasets contained heights, wind components, temperatures and relative humidity at 50 *mb* vertical increments and 80 *km* horizontal grid spacing. This dataset, however, was available for a limited time and only used experimentally up to this point.

Ingesting the NGM datasets into our model was accomplished by using the data assimilation package described by Tremback (1990) and Cram (1990). This package was used because it is designed for data which are gridded horizontally on a lat/lon grid and vertically on pressure levels. The ISentropic ANalysis package, or ISAN as it is called, outputs a dataset which is gridded horizontally on a user-specified spaced lat/lon grid and vertically on isentropic levels. This makes the output datasets very similar to the MAPS format except that MAPS is on a polar stereographic grid. Once NGM datasets are passed through the isentropic package, they are horizontally and vertically interpolated following the methods mentioned in the above section in order to transform all variables to the RAMS horizontal and vertical structure.

Chapter 4

PROTOTYPE REAL-TIME FORECASTING INVESTIGATIONS

There were two real-time forecasting investigations performed during the winter of 1991-92. The goal of the first was to forecast orographic snowfall throughout the state of Colorado. The goal of the second was to provide real-time forecasts of cirrus level clouds to scientists involved in the FIRE II experiment centered in Coffeyville, Kansas. Each will be discussed separately in this chapter. Through discussion of a case study from each investigation, it will be demonstrated that improvement of real-time local weather prediction can be achieved using the RAMS model.

4.1 Colorado Investigation

4.1.1 Description and model configuration

During the winter months in Colorado, most precipitation falls as snow. Branson (1991) and Rhea (1978) among others speculate that the majority of precipitation for mountainous regions is produced by three components: 1) synoptic vertical forcing, 2) convective precipitation, and 3) orographic (forced lifting) precipitation. Through review of orographic studies, they have determined that the dominant control factor in mountain precipitation is topography. In particular, Rhea and Grant (1974) demonstrated that a high correlation exists between certain western Colorado snowcourse water equivalent measurements and the influencing factors of upstream topographic slope, 700 *mb* wind direction, and the number of upstream "shadowing" barriers. The highest correlations were found for water-year and monthly averages but significant correlations also existed for particular events. For this reason, one might expect that given a reasonable representation of the topography and a correct prediction of the mesoscale winds, one could predict the amount and placement of snowfall. With this in mind RAMS was configured in such a way as to predict

orographically-forced precipitation over the Colorado region. While this has been done in past studies (e.g. Meyers (1991), Wesley (1991)), the true test here was to attempt numerical prediction in real-time. Simulations were performed daily from mid-November 1991 through the first week of April 1992 on a workstation at CSU. RAMS was initialized daily with 0000 UTC data and, as often as data allowed, would forecast out to 48 hours. A 48-hr simulation on the CSU Stardent workstation took from 10 to 12 hours of wall-clock time depending on machine load. The model configuration used had to be compromised in order to simulate in real-time. One of the best features of the RAMS model is the modularity/flexibility as the user can specify many options which allow the model to run faster. Although these options often cause the model to run quicker, they often consist of compromises in the physical parameterizations. This is the compromise that one must make in order to run in real-time. Perhaps a larger compromise, though, comes with grid spacing. The Colorado experiment had two interactive nested grids. The course grid covered the western three-fourths of the U.S. with 100 *km* grid increment and the fine grid covered Colorado with 25 *km* spacing. A plot of these grids is shown in Figure 4.1. There were 24 vertical levels with spacing of 300 *m* near the surface stretching to a constant 1000 *m* near model top of 17.5 *km*. Because of time considerations, we could not implement the bulk microphysics option of RAMS, however, a crude scheme which allowed precipitation was coded. This scheme assumed that any supersaturation was immediately translated to the ground with a precipitation efficiency based on cloud-top temperature. The scheme did not include ice phase nucleation, precipitation processes, latent heat release or evaporation. It only translated the equivalent amount of water in excess of 100% relative humidity to the surface, reduced by a coefficient resembling precipitation efficiency. This provided a crude "dump bucket" method of liquid precipitation. All other model options used for this investigation are described at the start of this chapter.

4.1.2 Discussion of forecasts for the entire season

Operating a mesoscale model as complex as RAMS daily for more than four months was no trivial task, especially while taking classes. To simplify the problem of running overnight, code was written which would automate the 3-step process of data ingest/model

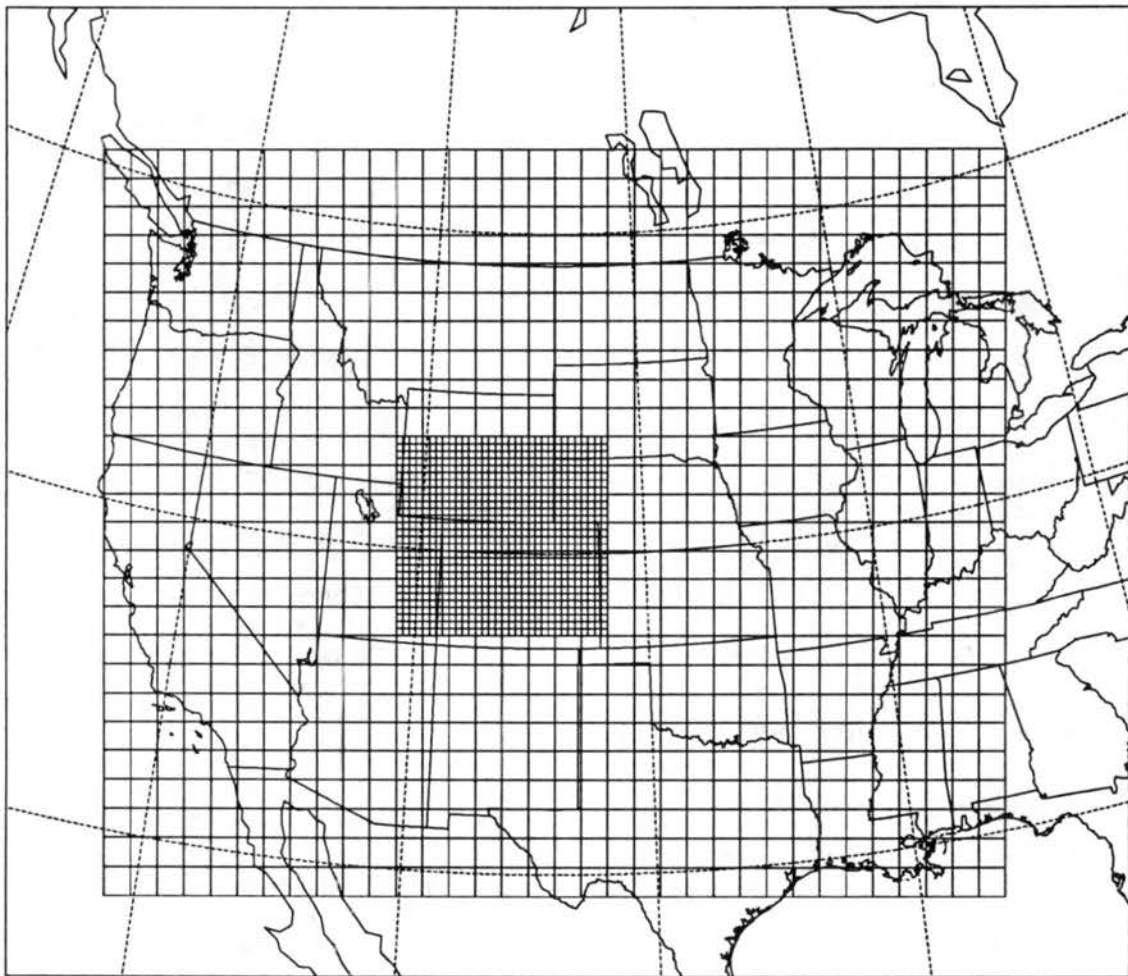


Figure 4.1: Grid points and domain of Colorado investigation real-time forecast system. The course grid has a 100 km grid increment and the fine grid has 25 km spacing.

initialization, model integration and post-processing. Once automation was accomplished and RAMS needed no outside intervention to run daily, emphasis was placed on improving forecasts.

Attempting to improve the daily forecasts was a seemingly endless and humbling experience. Modifying user-input parameters often had varying effects in which for certain days improvement was achieved and other days the opposite occurred. Often, modeling efforts involve months of "tuning" the model to obtain the desired effect for a single case study. That luxury could not be afforded in this research since a new simulation began each day. Besides, these desired effects may not have the same desired effects for other days. Only the most serious problems were truly resolved. For instance, it became obvious that surface-based sensible/latent heat fluxes were incorrect. By modifying the way in which the soil moisture was initialized, this problem was mitigated. Also, grid scale convection occasionally caused the model to "blow up" thus the tunable, user-input diffusion parameters were adjusted. Overall, the entire season of modeling in real-time was exhausting, exhilarating and enraging all rolled into one. Perhaps the most exhilarating portion of the entire season was the Colorado Front Range blizzard that occurred on 8-9 March 1992.

4.1.3 Case study: 8-9 March 1992

Synoptic overview

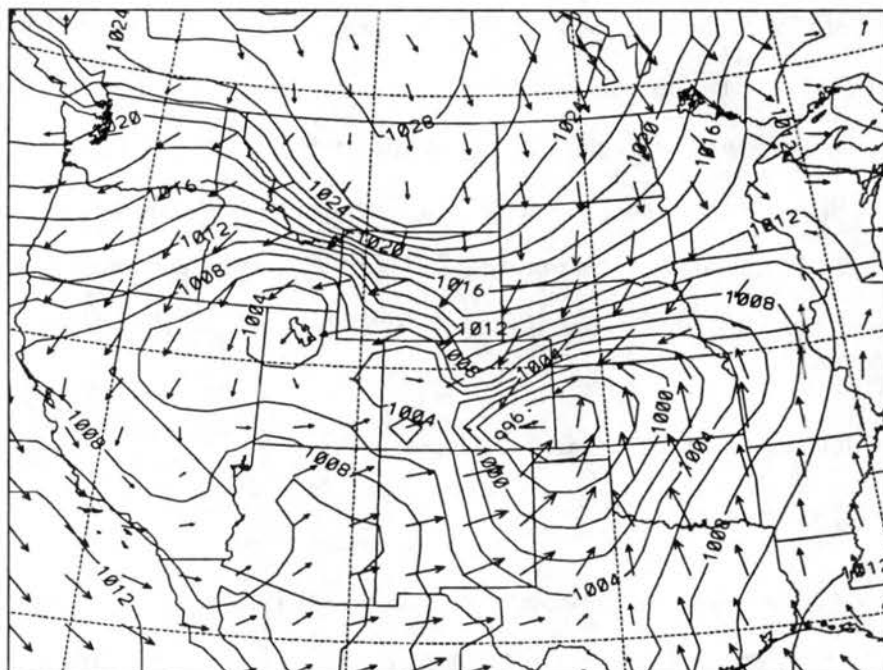
On 8 March 1992 a synoptic situation favorable for heavy snow along the Colorado Front Range was developing. At the surface, an arctic front was approaching from the north while lee cyclogenesis was occurring in the southeastern portion of Colorado. Moisture was being fed into the storm as a strong fetch of air from the Gulf of Mexico protruded northward and westward through Kansas and into Colorado. Aloft, a split flow regime allowed a cut-off low to move from Southern California toward the Four Corners region. By 0000 UTC 9 March the arctic front was pushing through Colorado causing an upslope flow regime to develop along the Front Range and snow followed soon after. The snow began in the northern portions of the state first and intensified throughout the nighttime hours. Embedded convection aided in localized heavy snowfall and many communities reported blizzard conditions and occasional lightning. In fact, pre-frontal convection was

also present as evidenced by the report of a tornado just to the south of Limon, Colorado the afternoon of 8 March. By 1200 UTC 9 March, Fort Collins reported 33 *cm* of snow while residents in the foothills just west of town reported snowfall amounts as large as 71 *cm*. The surface low at this time had moved into central Kansas and incorporated the arctic front into the system creating a trailing cold front and more classical extra-tropical cyclone. The 500 *mb* cut-off was centered on the Colorado-Kansas border and was beginning to be absorbed in the northern branch of the jet. By 0000 UTC 10 March the whole system had moved into the Great Lakes region leaving Colorado and the Central Plains in a cold arctic air mass dominated by large-scale subsidence.

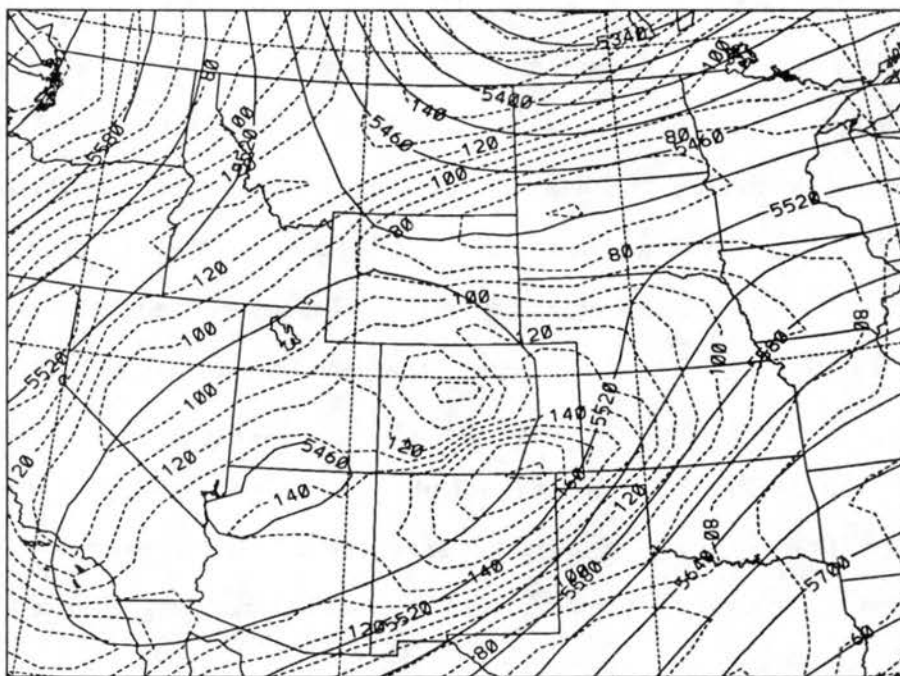
Real-time RAMS forecast

RAMS simulated this developing storm system very well during this 48 hour time period. The cyclogenesis in southeast Colorado was modeled particularly well. As shown in Figure 4.2a the 24-hr predicted mean sea level reduced pressure valid at 0000 UTC 9 March exhibited a 994 *mb* low in southeast Colorado and associated cyclonic winds. Elsewhere in the figure, we see a tight pressure gradient between this low and the approaching arctic anticyclone as the arctic front noses down the Front Range in the center of the figure. This is where we see the largest discrepancy between the model and observations. Shown in Figure 4.3a is the analyzed surface chart valid at the same time. Notice that the modeled position and central pressure of the low correspond extremely well with observations. The observed arctic cold front, however, moved along the 105 meridian to just north of Denver whereas, the model advanced the cold front to just south of Colorado Springs. A closer inspection of the RAMS forecast revealed frontal passage approximately two hours earlier in Denver. Based on a 24 hour forecast, the prediction of frontal passage within two hours is still considered good. The model's faster propagation might be attributed to the stronger low-level wind speeds and smoothed terrain.

The associated 500 *mb* characteristics were also predicted quite well at this time. Shown in Figure 4.2b is the 24-hr predicted 500 *mb* height and vorticity pattern. Here we see the cut-off low centered over the Four Corners region with the main vorticity maximum on the Colorado-New Mexico border. Again, comparing with the analysis of the 500 *mb*



REDUCED MSLP (mb)
24HR FCST VALID 0000 UTC 03/09/92



GEOPOTENTIAL HEIGHTS (m)
24HR FCST VALID 0000 UTC 03/09/92

TOTAL VORTICITY (1/s)

Figure 4.2: RAMS 24-hr forecast valid 0000 UTC 9 March, 1992 showing a) mean sea-level pressure (mb) with wind vectors and b) 500 mb heights/vorticity.

b)

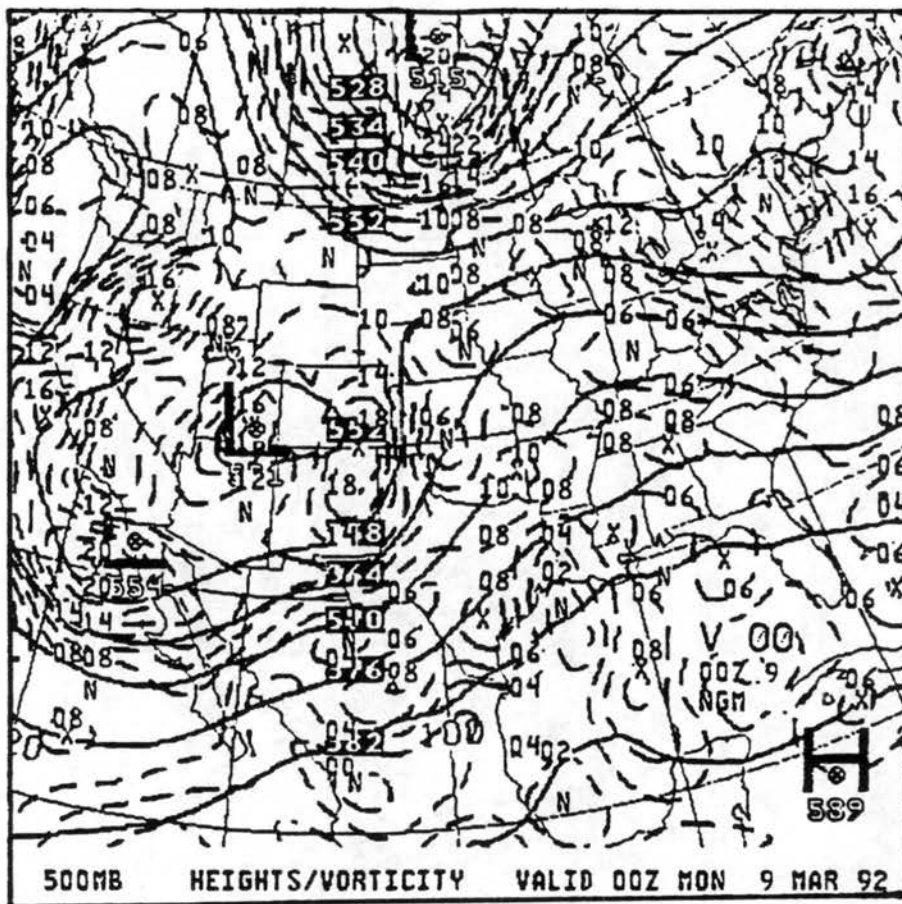
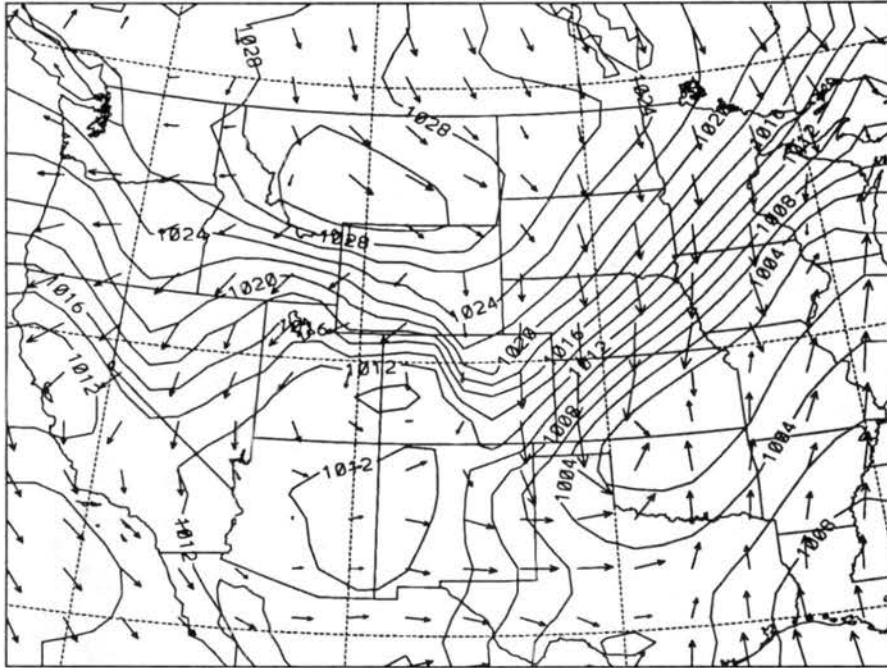


Figure 4.3: continued.

heights/vorticity shown in Figure 4.3b, we see the analyzed cut-off low over the Four Corners region and associated vorticity maximum on the Colorado-New Mexico border.

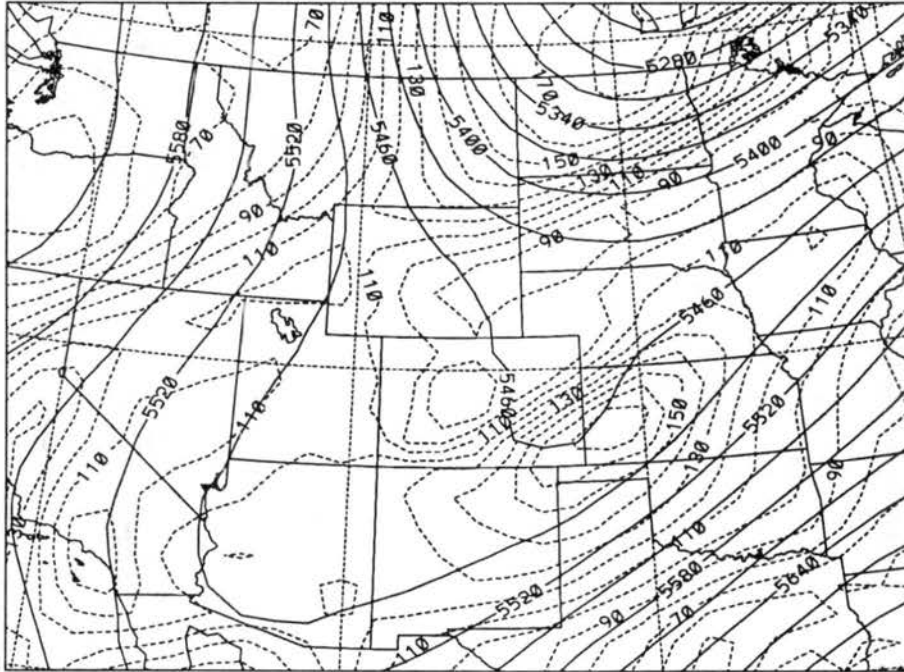
Continuing on in time to 1200 UTC 9 March, we see that at 36 hours RAMS predicted the surface low to move into east-central Kansas and elongate toward the Great Lakes region (Figure 4.4a) while the surface analysis (Figure 4.5a) has the surface low analyzed over the center of the state of Kansas. Again, looking at the features aloft, RAMS predicted that much of the energy would be lifting northeastward and weakening as the cut-off became absorbed into the more energetic system to the north. The heights predicted by RAMS shown in Figure 4.4b again agree well with the analysis shown in Figure 4.5b with the vorticity maximum predicted also over west-central Kansas.

a)



REDUCED MSLP (mb)
36HR FCST VALID 1200 UTC 03/09/92

b)



GEOPOTENTIAL HEIGHTS (m)
36HR FCST VALID 1200 UTC 03/09/92

TOTAL VORTICITY (1/s)

Figure 4.4: RAMS 36-hr forecast valid 1200 UTC 9 March, 1992 showing a) mean sea-level pressure (mb) with wind vectors and b) 500 mb heights/vorticity.

a)

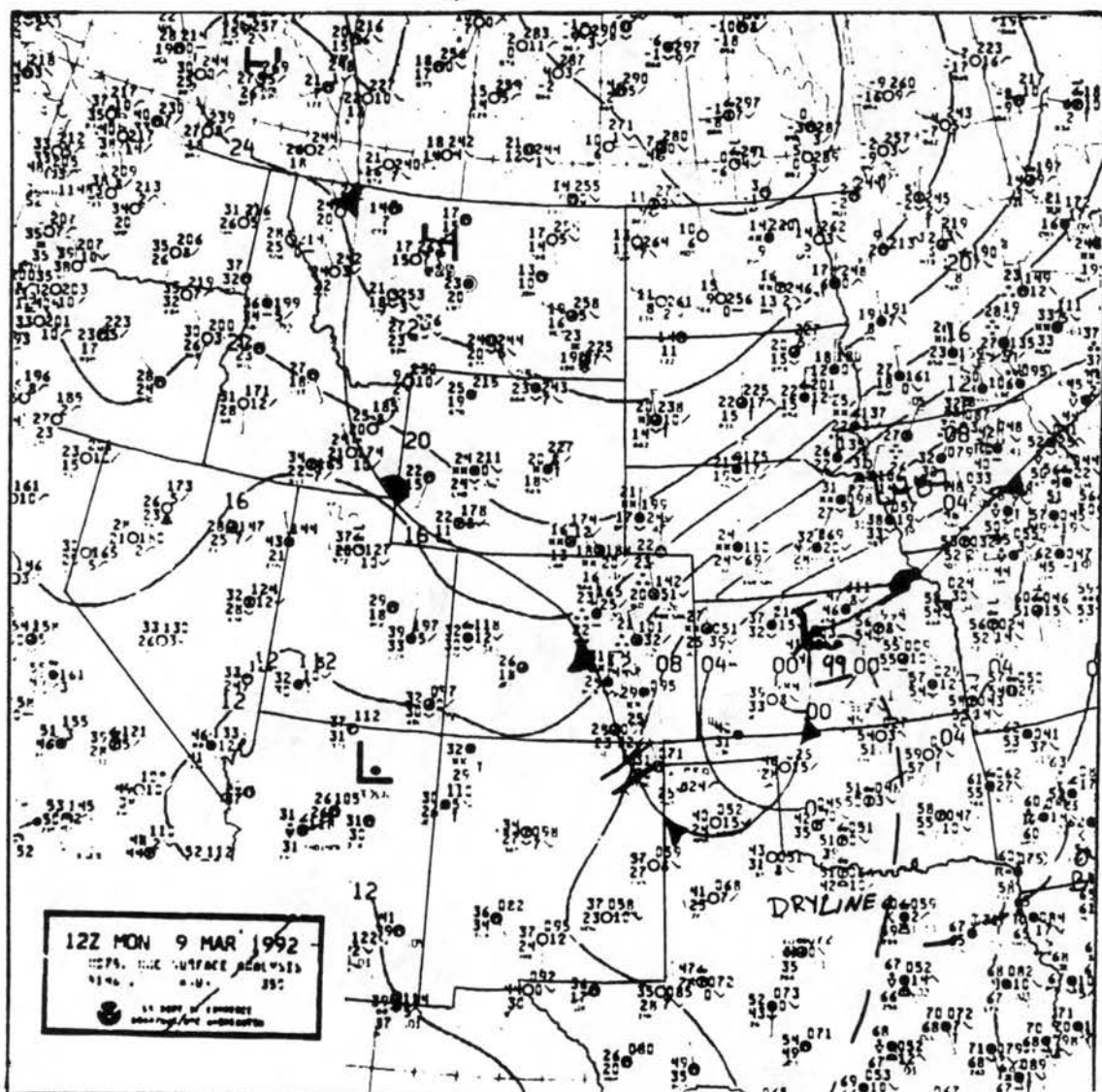


Figure 4.5: a) NMC surface and b) LFM 0-hr 500 mb heights/vorticity analyses valid 1200 UTC 9 March, 1992.

b)

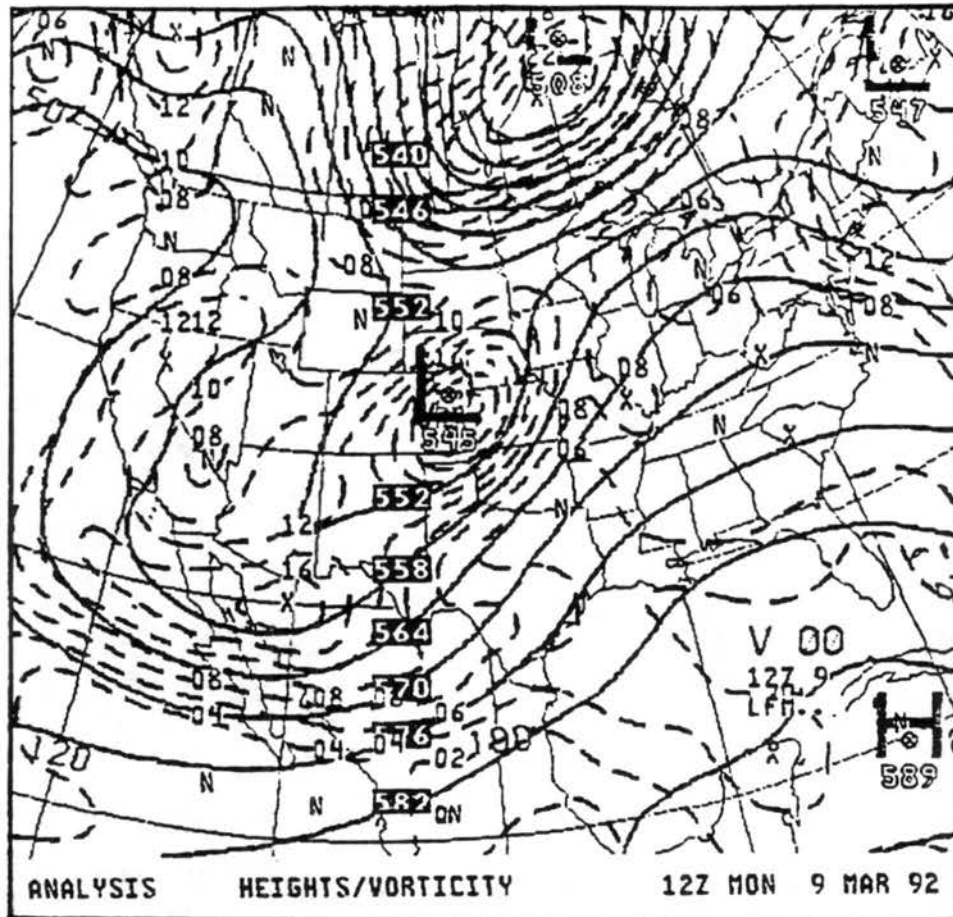
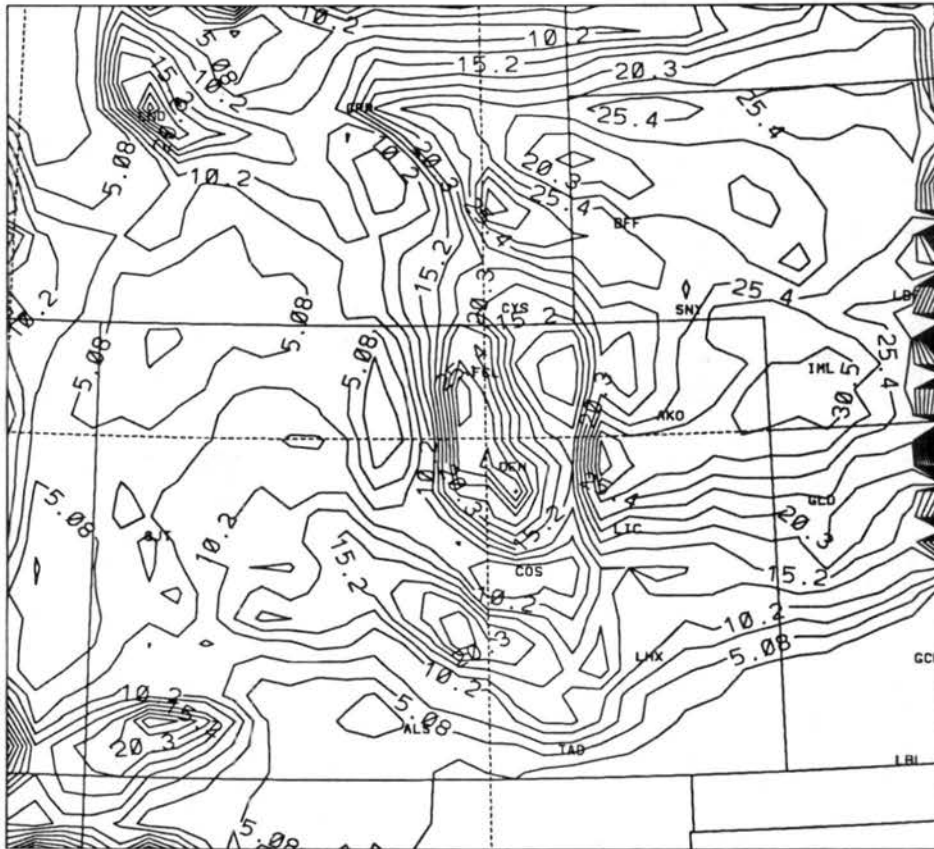


Figure 4.5: continued.

Finally, at 48 hours, or 0000 UTC 10 March, the whole system has moved into the Great Lakes region and just beyond the RAMS course grid. RAMS continued the northeast track of the storm and propagated the energy out of the model domain in a timely fashion.

Summarizing briefly, RAMS predicted the strength and movement of the storm system with a fair degree of accuracy throughout the 48 hour time frame. Quantification of the degree of accuracy is the subject of Chapter 5, however presented here is a more in-depth look at specific features of the storm, particularly temperatures and precipitation.

A discrepancy noted earlier was that RAMS predicted the cold front south of Colorado Springs at 0000 UTC 8 March when, in fact, the cold front was analyzed over Denver. The associated predicted surface temperature pattern is shown in Figure 4.6. As expected, there are discrepancies between modeled and observed surface temperatures in the region between the modeled and observed cold front; however, comparing Figure 4.6 with Figure



ACCUMULATED PRECIP RAIN (mm)
36HR FCST VALID 1200 UTC 03/09/92

Figure 4.7: RAMS 36-hour accumulated precipitation (mm) valid 1200 UTC 9 March.

[0.30 cm] and, likewise, from Imperial (IML) [2.54 cm] to Goodland (GLD) [0.05 cm]. RAMS predicted a sharp gradient in precipitation as well, but was shifted further south on a line from Trinidad (TAD) to Garden City (GCK). The errors in the precipitation forecast can be explained, at least in part, through the use of the crude precipitation scheme and also the embedded convection which this RAMS configuration could not model. In fact, most of Colorado Springs' precipitation was convective in nature as they reported 2.24 cm of precipitation during the three hours of thundershowers and snow pellets prior to 0000 UTC 9 March. Improving the predicted precipitation by using a convective parameterization was not attempted, however, inclusion of a more complete precipitation scheme was.

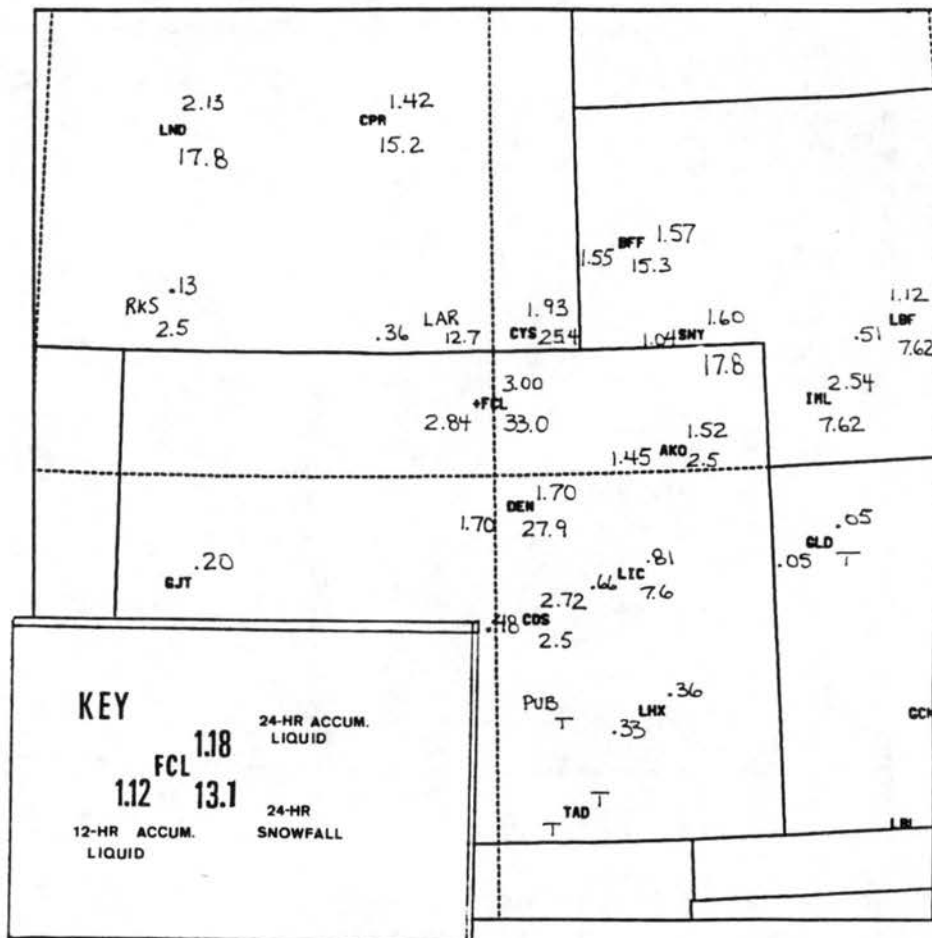


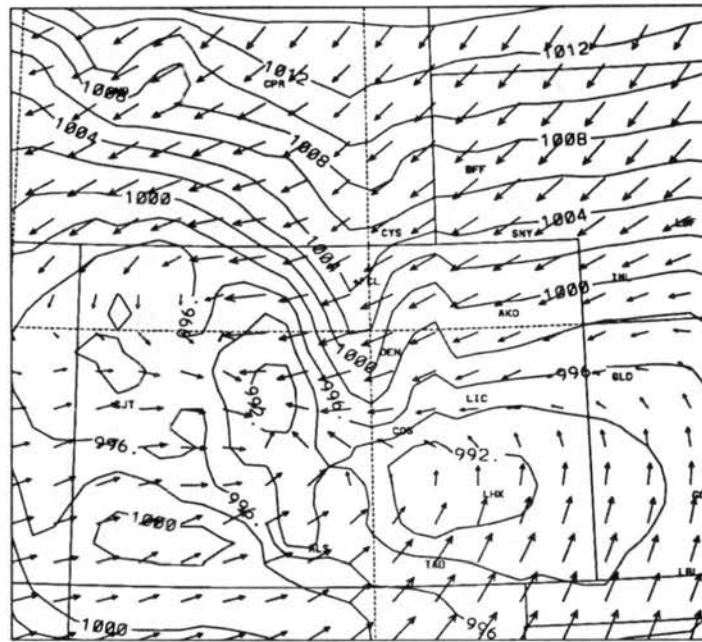
Figure 4.8: FAA surface airway observations indicating three-letter station identifiers, 24-hour accum. liquid precipitation (*cm*) (upper-right), 24-hour snowfall (*cm*) (lower-right), and 12-hour liquid precipitation (*cm*) (lower-left) valid 1200 UTC 9 March, 1992.

Addition of microphysics

The microphysics option of RAMS accounts for all the atmospheric processes deleted by the crude “dump bucket” precipitation scheme mentioned earlier. For instance, latent heat release, nucleation processes, ice phase precipitation physics and evaporation are all handled by the inclusion of RAMS’ microphysics option. This option could not be afforded when running on CSU workstations available to this project, however, if run on a CRAY, then real-time forecasting can be attained as shown in Section 4.2. There are five different species which may be individually activated for any given simulation: rain, snow, pristine ice crystals, aggregates and graupel. Of these, all except graupel were activated for the simulation discussed. Pristine ice crystal mixing ratio and concentration were predicted but

all other species' mixing ratios and concentrations were diagnosed from their characteristic diameters.

Addition of the RAMS microphysics option produced some surprising improvements. First, the cold front, which originally was forecast south of Colorado Springs, was predicted to be just south of Denver at 0000 UTC 9 March. The mean sea level pressure and surface wind vectors depicting this are shown in Figure 4.9. The center of the low pressure lowered



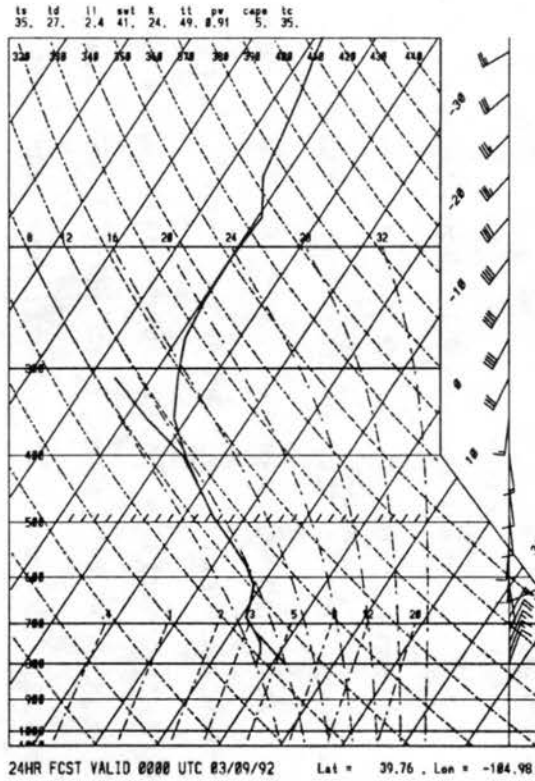
REDUCED MSLP (mb)
24HR FCST VALID 0000 UTC 03/09/92

Figure 4.9: RAMS 24-hr forecast mean sea-level pressure (mb) and surface wind vectors valid 0000 UTC 9 March, 1992.

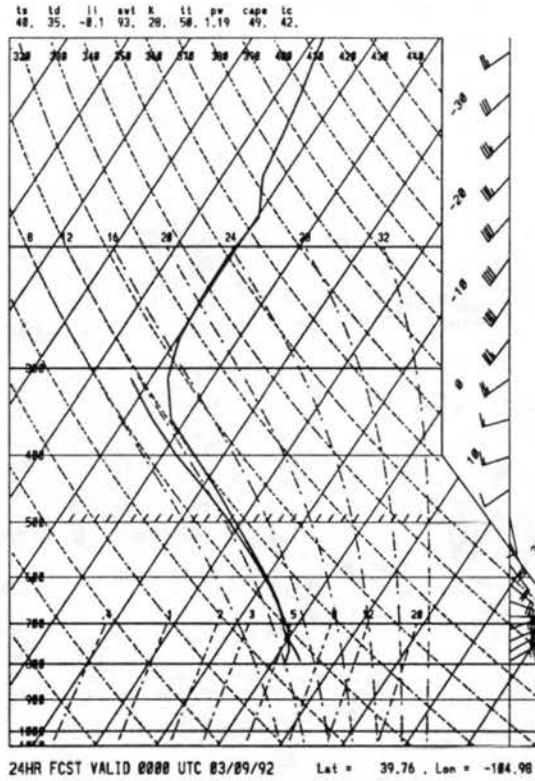
by 2 mb and shifted slightly west, however, the cold front propagated more slowly agreeing more with observations. Perhaps the latent heat released triggered additional upward motion and slowed the progress of the surface convergence and associated cold front.

Second, improvements were noted in the low-level winds as shown in a series of skew-T/log-p diagrams valid for a grid point near Denver shown in Figures 4.10 and 4.11. Figure 4.10a shows a 24-hr forecast skew-T diagram from the original real-time simulation without microphysics valid 0000 UTC 9 March; part b shows the same diagram except from the simulation that included microphysics; and part c shows an interpolated analysis for ease of comparison. Upon inspection of all three diagrams, one can readily see that the simulation

a)



b)



c)

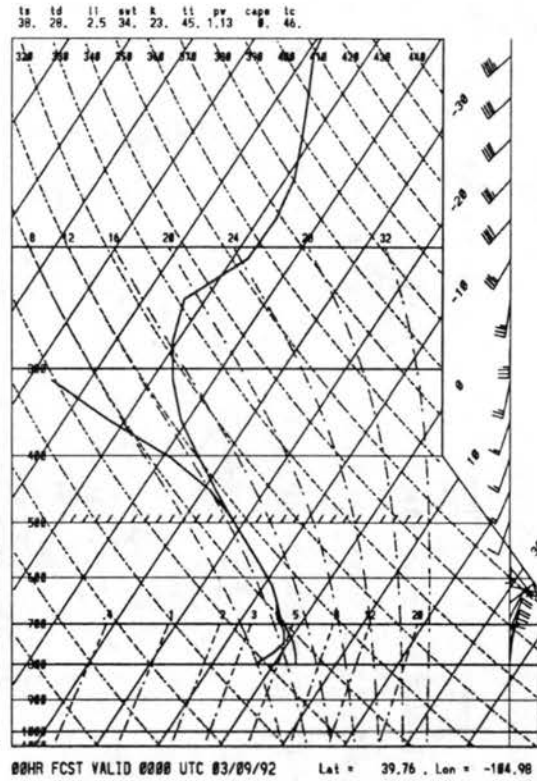
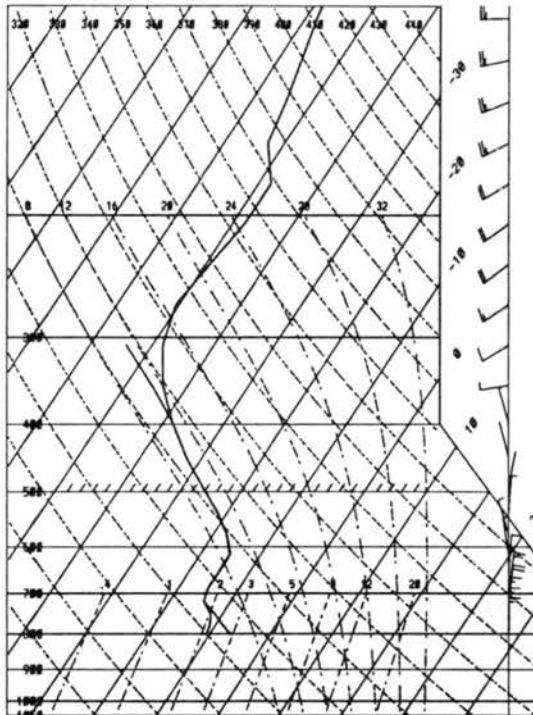


Figure 4.10: SKEW-T/LOG-P diagrams for a RAMS gridpoint near Denver, Colorado at 0000 UTC 9 March, 1992. a) RAMS 24-hr forecast, b) RAMS with MICRO 24-hr forecast, and c) RAMS 0-hr forecast.

a)

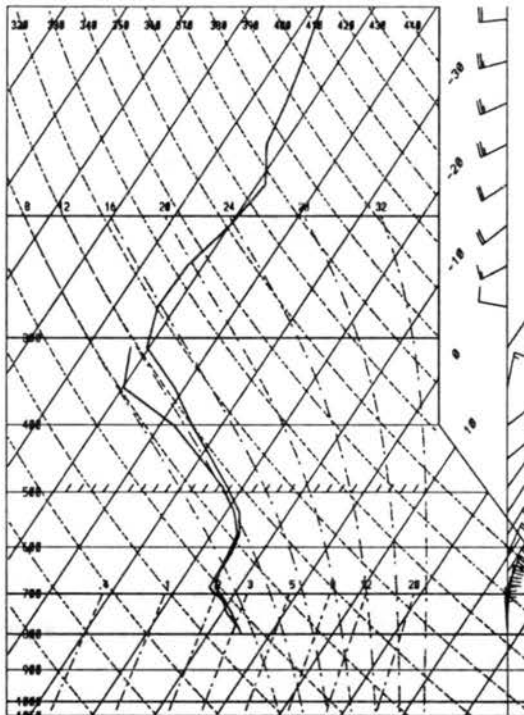
ts td ll wet k tt pw cape tc
28. 13. 11.2 29. 18. 37. 8.62 8. 21.



36HR FCST VALID 1200 UTC 03/09/92 Lat = 39.76 , Lon = -104.98

b)

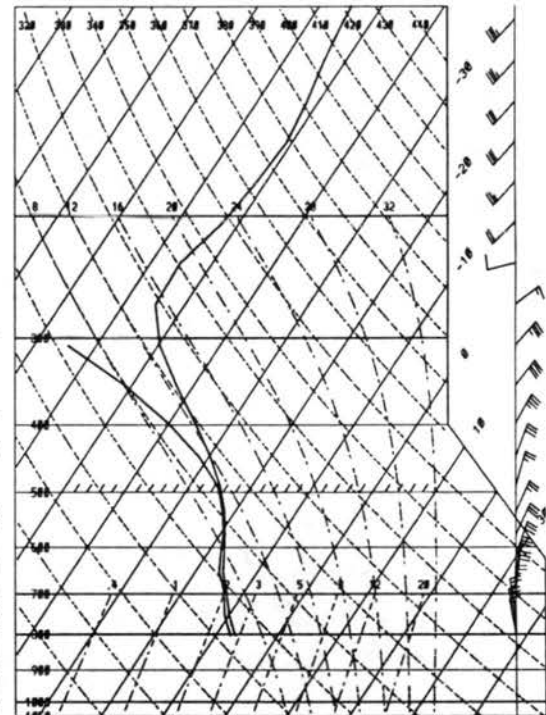
ts td ll wet k tt pw cape tc
24. 21. 11.9 49. 12. 34. 8.73 8. 26.



36HR FCST VALID 1200 UTC 03/09/92 Lat = 39.76 , Lon = -104.98

c)

ts td ll wet k tt pw cape tc
28. 17. 12.3 53. 11. 36. 8.63 8. 23.

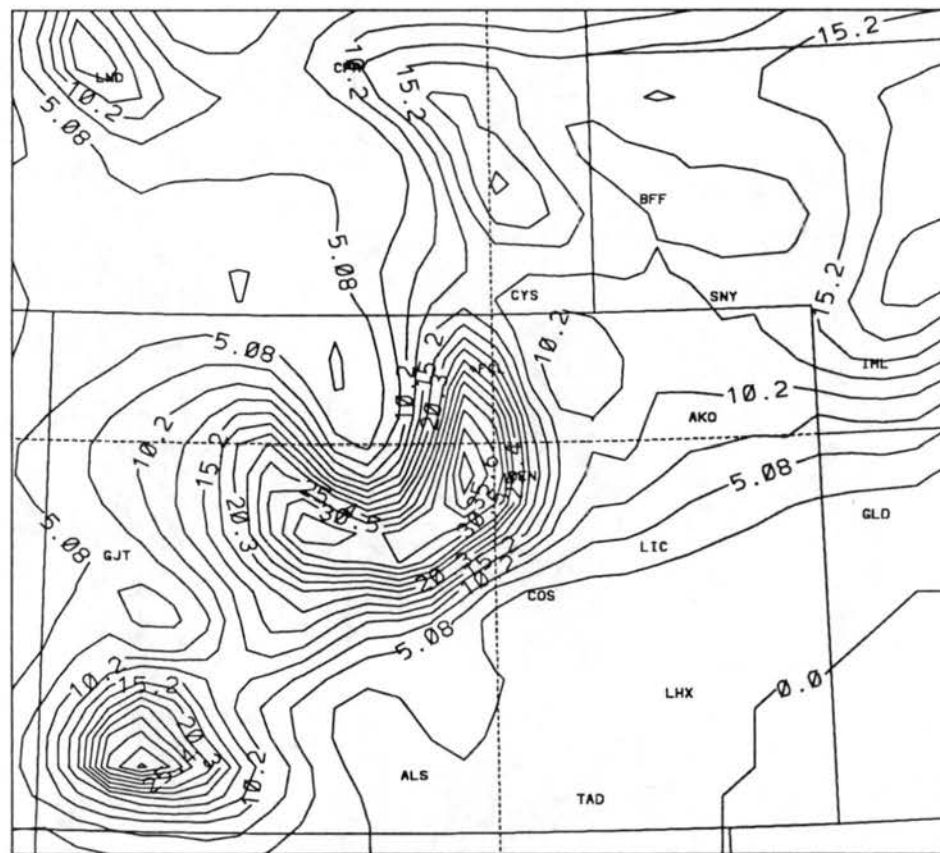


00HR FCST VALID 1200 UTC 03/09/92 Lat = 39.76 , Lon = -104.98

Figure 4.11: SKEW-T/LOG-P diagrams for a RAMS gridpoint near Denver, Colorado at 1200 UTC 9 March, 1992. a) RAMS 36-hr forecast, b) RAMS with MICRO 36-hr forecast, and c) RAMS 0-hr forecast.

with microphysics more closely resembles the analysis. In particular, the thermodynamic and wind information below 500 *mb* is predicted much better by the run which included microphysics. Likewise, this pattern is repeated in the 36-hour forecast shown in Figure 4.11b as the microphysics run more closely resembles the analysis.

Lastly, as anticipated, improvement in forecast precipitation was achieved through the addition of microphysics. The RAMS-predicted total precipitation including snow, rain, aggregates and pristine ice crystals through 36 hours is shown in Figure 4.12. Notice the southern extent of precipitation now agrees more closely with observations (Figure



TOTAL PRECIP (mm)
36HR FCST VALID 1200 UTC 03/09/92

Figure 4.12: RAMS (with MICRO) 36-hr accum. precipitation ending 1200 UTC 9 March, 1992.

4.8), particularly from COS to GLD. The forecast accumulation at COS was the worst single station forecast precipitation amount as RAMS predicted only 0.25 *cm* and they received 2.72 *cm*. As mentioned earlier, however, 2.24 *cm* of that amount was mainly

due to convection and COS reported only 0.48 *cm* of precipitation after the convective component had ceased, or at least subsided.

Note the differences between the predicted precipitation in this simulation and the precipitation from the "dump bucket" scheme shown earlier in Figure 4.7. The maxima in southwest Colorado (San Juan mountains) and the central mountains east of Grand Junction (denoted by GJT) were the result of snow during the first 24 hours of the simulation and were also reflected in the original real-time forecast. These maxima were supported by "snotel" measurements of 1.78 *cm* liquid water equivalent at Wolf Creek Pass in SW Colorado, 1.78 *cm* in the exact center of the state, and 2.03 *cm* 100 or so *km* due west of DEN. The minimum due west of FCL was also supported by a snotel site at Columbine which reported only 0.25 *cm* of liquid equivalent precipitation. Snotel observations are not as reliable as SAOs since they are taken at varying times and also not taken immediately when precipitation ceases. Nonetheless, measurements are taken daily roughly at 1400 UTC and are included here for comparison purposes since a lack of observational data exists in the Colorado mountains. Further information on snotel measurements can be found in Doesken (1987). The precipitation along and east of the 105 meridian was the result of precipitation during the 12 hour period from 0000 UTC to 1200 UTC 9 March. This is also evidenced by a time-series plot of precipitation for a grid point close to Denver shown in Figure 4.13. Shown here is that onset of precipitation occurred with frontal passage between 22 and 24 hours. RAMS predicted the precipitation to begin as rain in Denver and continue to 28 hours or 0400 UTC 9 March totaling 1.4 *cm* before changing to snow. The forecast snow continued through 36 hours or 1200 UTC 9 March with liquid water equivalents equalling the rain accumulation of 1.4 *cm*. Denver's FAA surface airway observations (SAO) reflected rainshowers from 2200 UTC 8 March to 0050 UTC 9 March with an abrupt change-over to snow at 0056 UTC. The SAOs are plotted for the 24-hour period beginning 1200 UTC 8 March and ending 1200 UTC 9 March in Figure 4.14 along with the companion RAMS forecast plotted in a similar manner. Here we see the reason why RAMS miss-timed the change-over to snow by 2 hours. RAMS-predicted surface temperatures were 34°F and 32°F at 0200 UTC and 0400 UTC respectively while observed temperatures were 32°F and

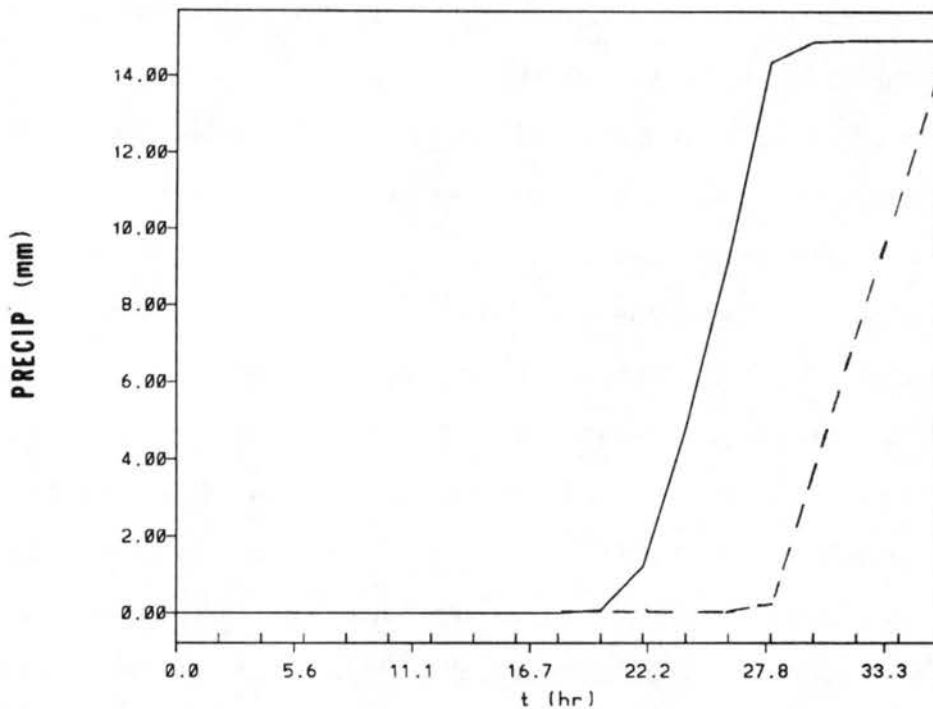


Figure 4.13: RAMS 36-hr time-series of precipitation for a model grid point near Denver, Colorado depicting rain (solid) and snow (dashed) valid 0000 UTC 8 March through 1200 UTC 9 March, 1992.

30°F. This 2 degree discrepancy was obviously enough to incorrectly predict the change from rain to snow.

A larger discrepancy noted in this Figure involves the wind field. RAMS predicted northeast flow throughout most of the first 16 hours. Observations showed variable wind direction for the first 6 hours with speeds around 5 *kts*. Then, at 2000 UTC 8 March, the wind increased to 10 *kts* from the northeast and continued until frontal passage when the wind increased dramatically to 30 *kts* (with higher gusts) from the north-northwest for the next 5 hours. Finally, during the last 7 hours, the winds slowly decreased and maintained a northerly component. Perhaps this is evidence of the blocking mechanisms discussed by Wesley and Pielke (1990) since Akron, Colorado reported mostly northeast flow during the same period while Denver reported the northwest flow. If this is the case, then perhaps a finer resolution simulation would be needed to simulate a blocking-induced convergence zone.

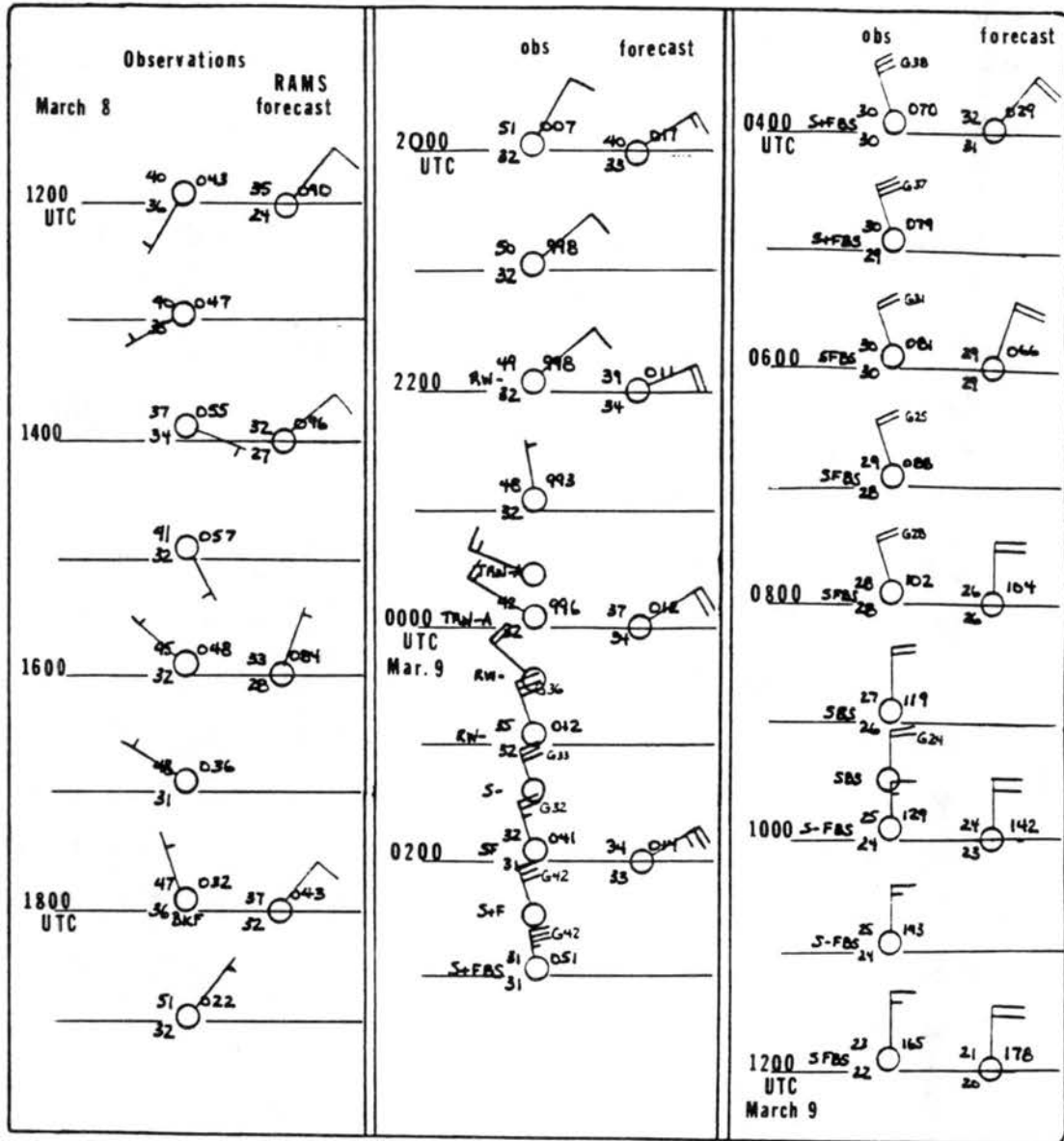


Figure 4.14: Time-series of surface observations at Denver, Colorado and corresponding RAMS forecast surface information from 1200 UTC 8 March to 1200 UTC 9 March, 1992. Standard plotting with: temperature (upper-left), dewpoint temperature (lower-left), sea-level pressure (upper-right) and wind barb (each full barb representing 10 knots while half barbs represent 5 knots).

Summarizing briefly, it was shown that the overall forecast was improved through the addition of the RAMS microphysics option. In particular, features like timing of the arctic cold front, forecast precipitation and low-level wind prediction reflected dramatic improvements from the simulation using the crude precipitation scheme. The trade-off with the model configuration using the microphysics option is that a faster machine must be utilized in order to attain real-time forecasts. This may not be the case for long, however, since a new microphysics code is being implemented in RAMS which is a factor of ten faster than the current module. It is emphasized here that this forecasting system can achieve real-time output when run on a CRAY-YMP and the previously discussed configuration (which did a respectable job as well) will operate in real-time on workstations. A further discussion of computer throughput is found in Section 4.3 at the end of this chapter.

Remarks concerning the NGM simulation

The NGM model has a rather well-known bias for these type storms along the Front Range in which the surface low is moved too fast and too far north, in conjunction with an arctic front being too far north. For the 8-9 March simulation initialized at 0000 UTC 8 March, the north bias is evident, not just at the surface, but aloft too. The 24-hr NGM forecast valid 0000 UTC 9 March is presented in Figure 4.15. The NGM model predicted the surface (part a) low at the Colorado-Kansas-Nebraska border and the 500 *mb* (part b) cut-off low directly over Denver, Colorado. Recall the analysis shown earlier which showed the 500 *mb* cut-off over the Four Corners and the surface low to the south and east of Colorado Springs. This trend continued into the 36-hr NGM forecast as these same features were predicted too far north and east.

4.1.4 Problems/discrepancies

A few major problems/discrepancies were discovered throughout the season of real-time forecasting. It was eluded to in the previous section that the RAMS 24-hr forecast advanced the cold front a bit too far south because of stronger than observed surface winds. It seemed as though the model had a tendency to attain stronger than observed surface winds on many occasions. This could be due to the turbulence parameterization used.

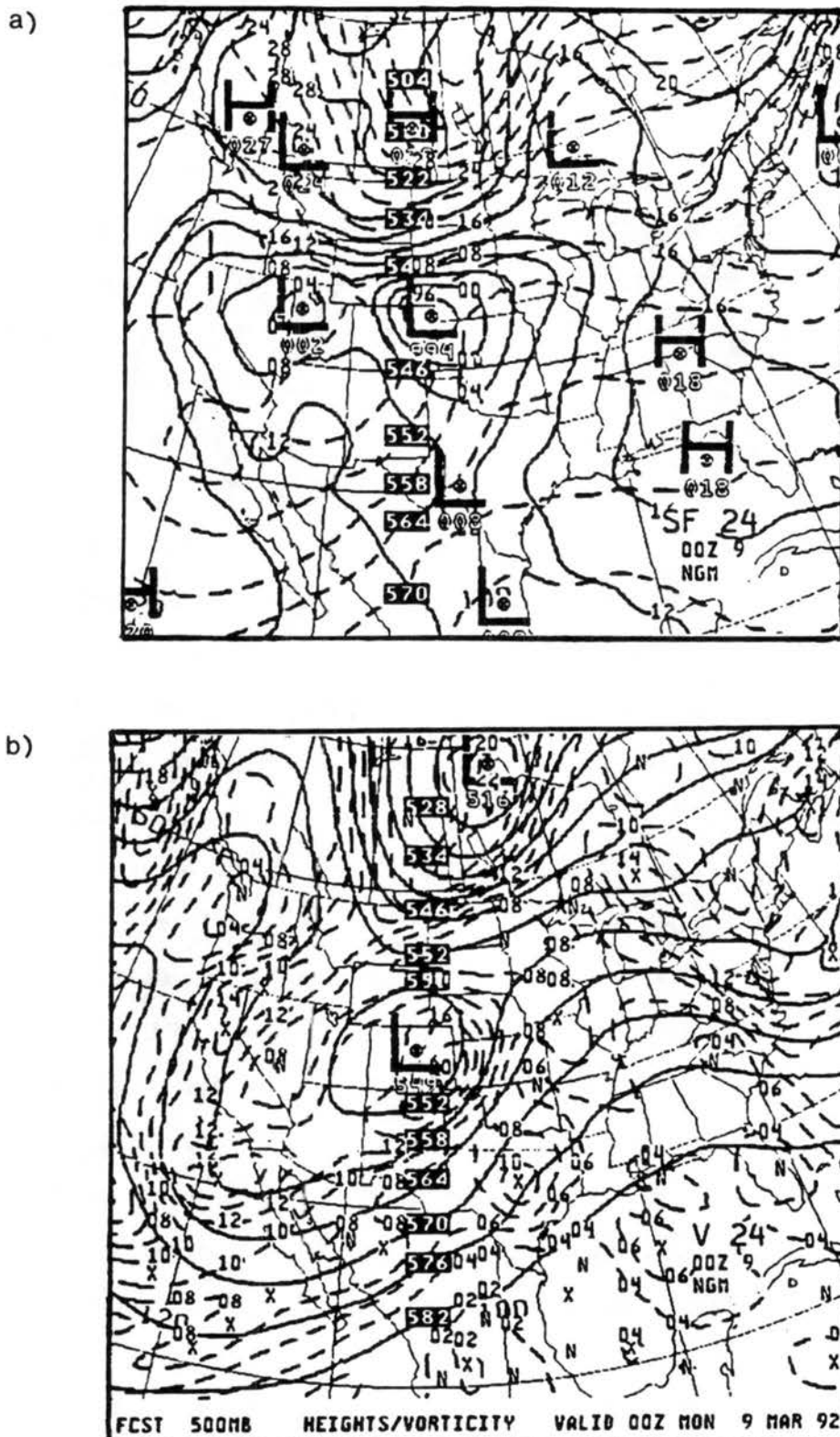


Figure 4.15: NGM 24-hr forecast valid 0000 UTC 9 March, 1992 showing a) mean sea-level pressure (mb) and b) 500 mb heights/vorticity.

Higher-order schemes do exist in RAMS, however, no sensitivity studies were performed. Another attributing factor could be that the model had a constant surface roughness length of 0.2 *m* across the domain. Perhaps the inclusion of variable roughness and other surface characteristics would impact the translation of the surface cold front.

Another problem area for RAMS was the moisture field. There appeared to be a major discrepancy between modeled and observed moisture fields after storm systems departed. The model tended to have too deep a moist layer which remained in place for too long. Looking at Figure 4.16a, one can see a region of 90% relative humidity from 3 to 8 *km* in the RAMS 36 h forecast whereas observed relative humidity values at this time, shown in Figure 4.16b, were much lower at altitudes from 6 to 8 *km*. The simulation including the microphysics option, however, improved the predicted moisture field dramatically. This is expected since the crude “dump bucket” precipitation scheme does not effectively remove large enough quantities of moisture from the atmosphere. An identical cross-section from the simulation including microphysics is shown in Figure 4.16c. Here we see that forecast relative humidity (RH) values agree much more with the observations as the 80% RH contour now lowers in altitude to near 6 *km* when previously it could be found near 8 *km*.

Another possibility arises from the time-dependent lateral boundary conditions. As stated earlier, the moisture field from the NGM forecasts is one of the variable fields towards which RAMS' lateral boundaries are nudged. Also stated earlier was the extremely poor resolution of these data sets and, in particular, the relative humidity. Therefore, if the NGM model forecasts erroneous high values of RH, then RAMS exaggerates these when interpolating to its grid points. Although the nudging only affects the zone of points along lateral boundaries, a quick look at advective processes shows how rapidly these poorly specified values propagate into the interior of the model. To investigate this further, RAMS was run on the case study discussed above with the ETA model forecasts used as input to the time-dependent lateral boundary condition information (as opposed to NGM forecasts used earlier). As stated in Chapter 3, the ETA model data sets provided much better vertical and horizontal resolution. The results of this simulation were discouraging. A plot of the 24-hr predicted sea level pressure pattern exhibited the surface low further south and east of its observed position at 0000 UTC 9 March. This trend continued through 36 hours

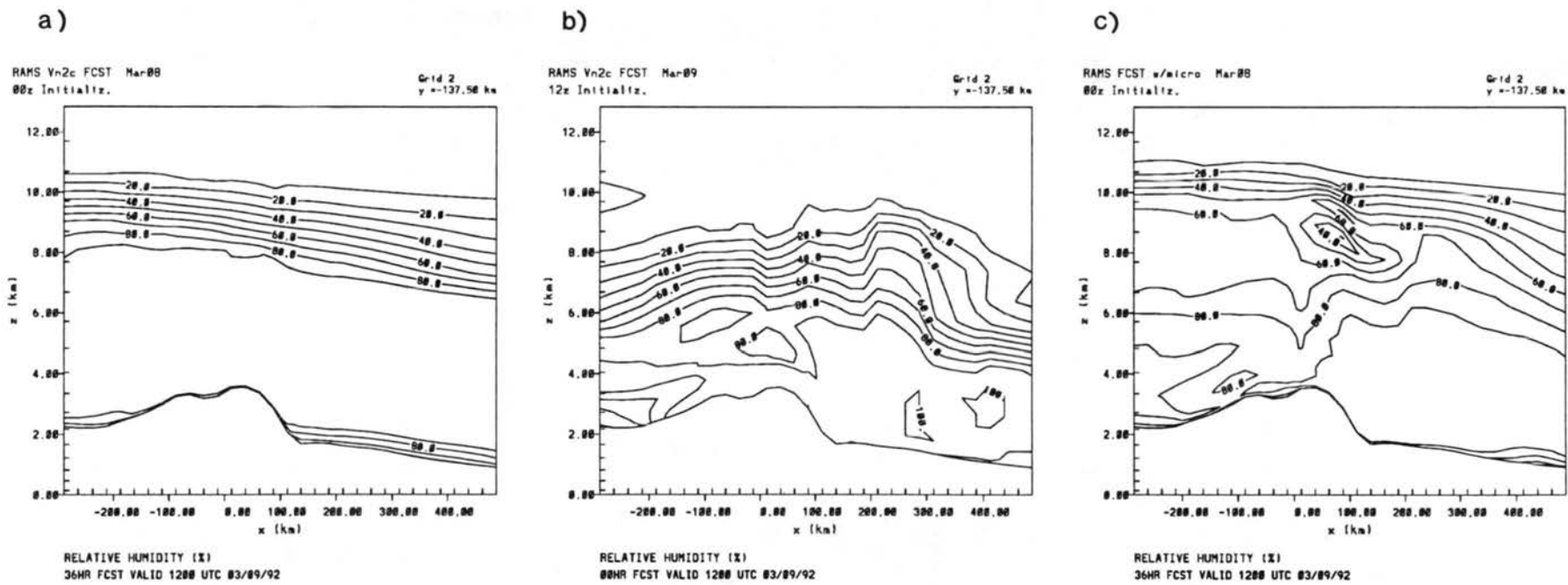


Figure 4.16: RAMS relative humidity E-W cross-sections near Denver, Colorado valid 1200 UTC 9 March, 1992. a) RAMS 36-hr forecast, b) RAMS 0-hr forecast, and c) RAMS with MICRO 36-hr forecast.

which showed many storm features south and east of their observed position. The cross-section depicting the forecast relative humidity field showed little change from the original RAMS forecast although other regions of the domain were not compared. Nonetheless, the need for a higher resolution (especially in the vertical) data set to provide time-dependent lateral boundary conditions is justified.

4.1.5 Rhea-CSU model interface

The Rhea-CSU model is a fast-running model that was initially developed by J. Owen Rhea in the late 1970s to determine if winter precipitation distribution in the Colorado Rockies could be diagnosed using only routine upper air atmospheric soundings along with topographic grid data (Rhea, 1978). Historical comparisons of model precipitation amounts to observed snowcourse water equivalent, precipitation gauge readings and streamflow runoff showed favorable correlations (Rhea, 1978; Branson, 1991). These calculations were originally made for 13 winter seasons by Rhea and were more recently extended to 26 seasons by Branson. Basically, the Rhea-CSU model took 6 routine upper air soundings from Colorado and surrounding states and interpolated a mean 700 *mb* level wind to advect parcels over terrain of 10km grid spacing. The grid used for this encompassed the Colorado Rockies with its north and south boundaries on the northern and southern borders of Colorado. The west boundary of the grid was the western border of Colorado while the east boundary was the 105th meridian. A plot of this domain is shown in Figure 4.17. Through empirical experiments, Rhea determined that a parcel need not be advected (ie. the model is not run at all) over the terrain if the 750, 700, 650 *mb* relative humidity was less than 50%. Furthermore, he determined a precipitation efficiency proportional to cloud-top temperature which worked well for the Colorado Rockies. The formula for this is the following:

$$E = -0.01T_{ct}$$

where T_{ct} is the temperature ($^{\circ}C$) of the unlifted cloud top. As an example, assume a Denver cloud top at 500 *mb* ($-20^{\circ}C$) at 1200 UTC 8 March, then the precipitation efficiency is approximately $(-0.01) \times (-20) = 20\%$. Other research indicates that this efficiency is rather low. For example, Chappell (1970) inferred precipitation efficiencies for Wolf Creek Pass,

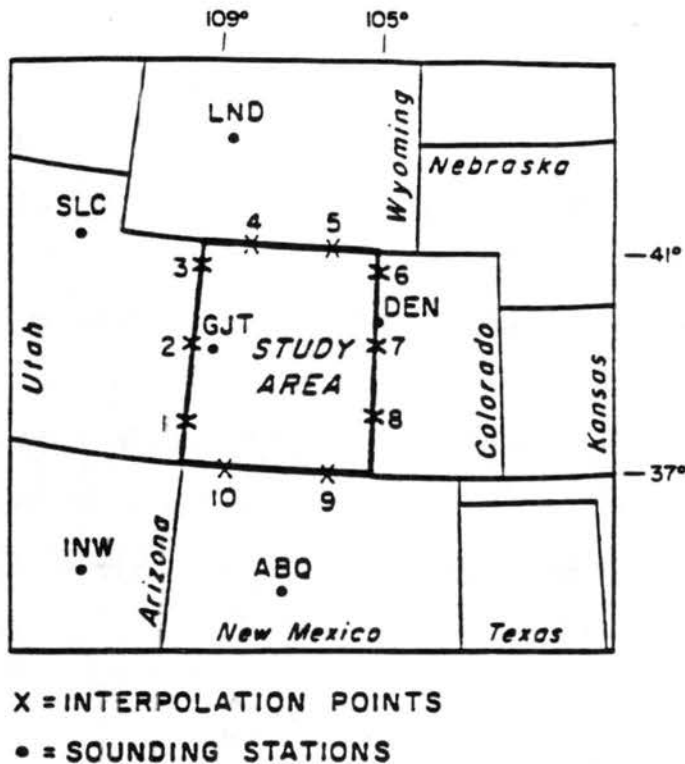


Figure 4.17: CSU-Rhea model domain, border interpolation points and upper-air stations (from Rhea, 1978).

CO of near 100% at temperatures colder than -20°C and between 25 and 35% at warmer temperatures. Dirks (1973) found efficiencies ranging between 25 and 80% for a Wyoming mountain. He claimed the lowest efficiencies were at very cold temperatures and strong winds, and the highest efficiencies were under moderately cold cloud tops and moderate wind speeds. This contradicts the Rhea type efficiency whereby the colder the cloud top the larger the efficiency. Rhea's model also takes into account the large-scale vertical motions derived from the divergence of the horizontal wind in the soundings. Unfortunately, Branson (personal communication) has determined that precipitation output by this model can vary greatly due to small changes in these vertical motions.

During the winter of 1991-92 the Rhea-CSU model was interfaced with the RAMS model. Here, RAMS provided the thermodynamic variables and wind information from the RAMS forecast in order for the Rhea-CSU model to forecast precipitation. In effect, RAMS provided the Rhea-CSU model with the sounding information at given locations on the boundaries at shorter time intervals (2 hrs); thus improving forecasts via more frequent

time updates of the mean 700 *mb* wind and interpolation of this wind because actual border point soundings could be supplied instead of rawinsonde station soundings as much as 300 *km* away from the grid borders. One of the biggest advantages of using the Rhea model is its high speed. It takes only a matter of minutes to integrate through 48 hours as described here.

Only a few times during this winter was the Rhea model run in this configuration. One particular case was the 8-9 March storm discussed earlier. A plot of the 36-hr predicted precipitation by the Rhea model is shown in Figure 4.18. Comparisons with observations is difficult since the few observations recorded were spread far apart in the mountains. The

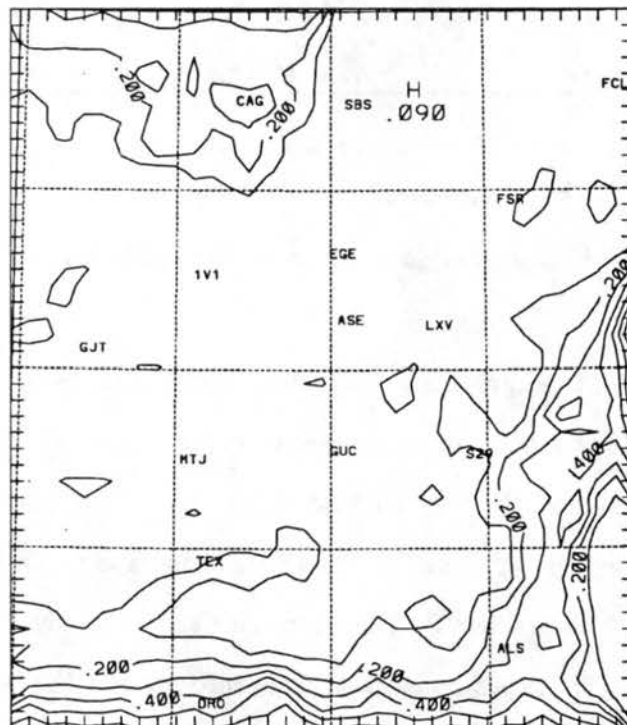


Figure 4.18: CSU-Rhea 36-hr predicted precipitation through 1200 UTC 9 March, 1992.

Rhea model predicted under 0.25 *cm* liquid precipitation over most of the central mountains and northeast foothills and larger amounts along the southern border, northwest plateau and along the 105th meridian (eastern edge of domain). Overall the model predictions were poor with the worst correspondence over the central mountains and northeast foothills near FCL which received 3.00 *cm* liquid precipitation. Only the northwest plateau was predicted

well with low precipitation amounts from GJT to CAG. These precipitation amounts contrast greatly with the RAMS forecast which included microphysics shown in Figure 4.12. A possible reason for the discrepancy is the lack of dynamical and convective forcing in the Rhea model. Most of the precipitation during the 8-9 March storm was produced by dynamical forcing and convection, not upslope forcing. Perhaps further investigation of the interpolated large-scale vertical motion is necessary to produce better predictions for this case.

4.1.6 Future: winter season 1992-93

Real-time RAMS forecasting is currently underway for the winter season of 1992-93. Improvements for this season include a vegetation module as described by Lee (1992). To complement this, a variably initialized vegetated surface is also used. The classes of vegetation are described in Lee (1992) and are allowed to vary across the domain. Another major improvement is radiative interactions with "pseudo" clouds. The term pseudo is used because the model has no knowledge of cloud mixing ratio. (This is an option in RAMS, however, its use causes large amounts of computational time which slow the model to where real-time forecasts can no longer be achieved on the available workstations.) Instead, a cloud is defined simply by a threshold relative humidity. As for shortwave radiation, a curve by Neiburger (1949) which relates cloud depth to cloud albedo is used. This certainly isn't the best scheme possible, but provides a crude mechanism whereby shortwave radiation is reflected due to "clouds"; whereas in the 1991-92 season "clouds" were transparent to incoming shortwave radiation. As for longwave radiation, the presence of pseudo clouds causes the addition of downward radiative flux equal to that of a blackbody, σT^4 where T is the temperature at the bottom of the assumed cloud base. Through the addition of this simple scheme, forecast surface temperatures have improved dramatically. Before, predicted daytime surface temperatures were far too high under cloudy skies and nighttime temperatures far too low as one would expect. Lastly an absorbing layer at the top of the model is included since numerical reflection problems exist when using the "wall on top" top boundary condition.

4.2 FIRE II Investigation

4.2.1 Description and model configuration

The importance of real-time forecasting as it applies to measurement programs was mentioned in Chapter 2. A mesoscale numerical model such as RAMS run operationally can address some program-specific concerns. One such program, the First ISSCP (International Satellite Cloud Climatology Program) Regional Experiment Phase II (FIRE II), provided the opportunity to supplement real-time forecast products by established operational centers like NMC and FSL with real-time RAMS forecasts. The major difference between our forecasts and that of NMC's was that we could provide specific forecasts relating to high-level clouds which were of much interest to field scientists. The original FIRE sponsored an intensive field observation (IFO) for cirrus in Wisconsin during October, 1986. Then, FIRE II sponsored another IFO in Kansas from 13 November to 6 December, 1991. During this experiment, RAMS was run daily in an effort to provide real-time mesoscale forecasts of cirrus-level clouds to scientists in the field in Coffeyville, Kansas.

The idea behind this evolved from previous RAMS modeling by Heckman (1991), and Heckman and Cotton (1993) where a successful modeling study of cirrus clouds during the first FIRE experiment is discussed. Heckman produced very respectable cirrus-level cloud simulations for 28 October 1986 reproducing layering, cloud top generation and fallstreaks. Unfortunately his model configuration could not be run for the real-time simulations because of its computational expense. The first model parameterization that had to be eliminated was the radiation scheme. Heckman used the Chen and Cotton (1983) radiation parameterization which included the effects of condensate on radiative transfer. Owing to the large number of vertical levels, this scheme was thought to account for nearly 70% of the computational cost of his simulations although only activated at 15 minute intervals! The other RAMS radiation option as described earlier and in Mahrer and Pielke (1977) was utilized instead.

Another major time-consumer in Heckman's simulations was vertical grid-spacing and number of levels. Heckman had 69 points from the surface to 19.2 *km* with 200 *m* spacing between 5 and 11 *km*. The real-time RAMS configuration had 42 vertical levels with a constant 300 *m* spacing up to 9 *km* then slowly increasing gaps to 1000 *m* spacing near

16 km. Again, the non-hydrostatic mode and two interactive nested grids were used. The course grid had 45 points in the x-direction and 35 in the y-direction with spacing of 80 km. The nested grid was 50 by 34 points with 20 km spacing. A plot of these grid points is shown in Figure 4.19.

The biggest difference between this investigation and the Colorado snow investigation discussed previously is the use of the bulk microphysics option of RAMS. Because simulations were performed on the NCAR CRAY Y-MP, real-time forecasting could be accomplished with the microphysics activated. In this study, timely forecasts were essential so only pristine ice, snow and rain were activated. Both the concentration and mixing ratio of pristine crystals were predicted while the concentrations of rain, snow and cloud water were diagnosed assuming a characteristic diameter of each species.

4.2.2 Discussion of overall forecasts

If the 8-9 March Front Range blizzard was the most exhilarating portion of the entire season, then this portion was the most exhausting. The FIRE II experiment began 13 November 1991. Barely a single real-time forecast in the history of RAMS had been produced up to this time however. To use the word prototype was a huge understatement. NCAR did everything possible to allow a smooth start-up/break-in period of the model including supplying us with a test account to make a few sample runs; but we were unable to utilize their generosity as we hadn't yet made final preparations. Miraculously, the first night's forecast ran out through 24 hours although manual intervention was required for data ingest and model initialization as automation code was still in the making. Unfortunately, this luck did not continue as is evidenced by the nightly log detailing the problems encountered.

A calendar format of this log is shown in Table 4.1. Many problems were data related as discussed for the Colorado investigation (lack of NGM or MAPS data sets). Others such as grid-scale convection were not anticipated because of the time of year. In November, 1991 the southern U.S. was frequented with an unusually warm pattern and some regions experienced early September convective patterns. This was mitigated by extending the

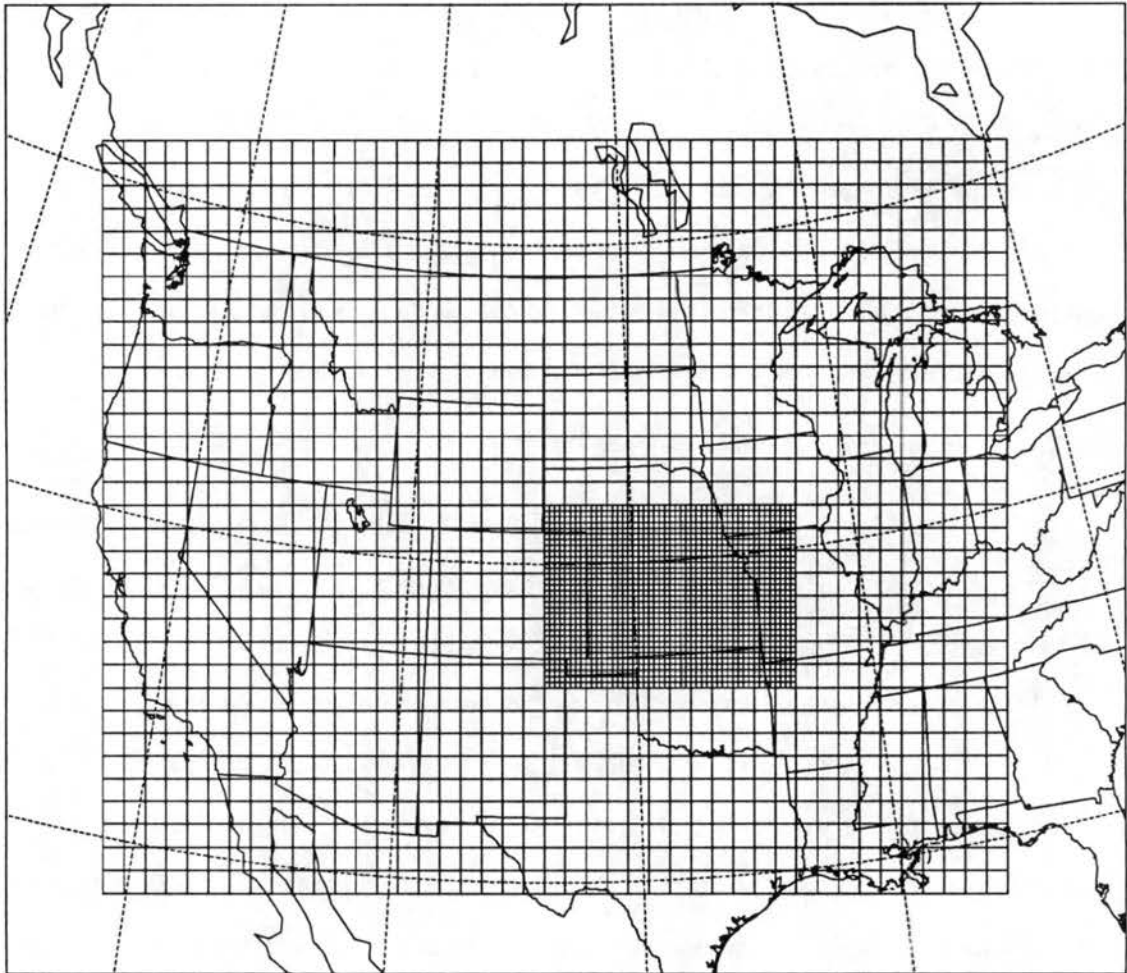


Figure 4.19: Grid points and domain of FIRE II investigation real-time forecast system. The course grid has a 80 km grid increment and the fine grid has 20 km spacing.

Table 4.1: Calendar format nightly log of activity for RAMS FIRE II real-time forecast experiment detailing problems encountered.

November 1991

Sun	Mon	Tue	Wed	Thu	Fri	Sat
10	11	12	13 local disc filled; managed 24 hr run	14 no MAPS data; ran entirely from NGM data; full 24 hr run	15 no NGM data at all; NMC 6+ hrs. late; no RAMS run	16 only 12 hrs of NGM convec. blew up at 9hrs. ran 9 hrs.
17 convec. blew at 13 hrs; solution: extend model top 2 km higher ran 13 hrs.	18 incorrectly handles multiple b.c. files; ran 12 hrs.	19 same as yesterday; ran 12 hrs.	20 same as past 2 days; fixed bug; ran 12 hrs.	21 GOOD RUN; full 24 hrs.	22 convec. blew at 1 hr; ran only 1 hr.	23 only 12 hrs. of NGM; ran 12 hrs.
24 only 12 hrs NGM convection blew at 11 hrs; solution: changed timestep and diffusion parameter	25 CRAY preventative maintenance at 7 AM otherwise OK; ran 15+ hrs.	26 local machine crash; manually submit jobs; OK ran 24 hrs.	27 MAPS data full of zeroes; no run.	28 THANKSGIVING GOOD RUN ran 24 hrs.	29 no MAPS or NGM; holiday? no run.	30 simply forgot; my holiday; no run.

December 1991

1 automation screwed up because of forgetfulness no run.	2 memory overwrite near 8 hours; ran 8 hrs.	3 same as yesterday; no run.	4 memory overwrite near 17 hours; ran 16+ hrs.	5 memory overwrite near 11 hours; ran 11+ hrs.	6 GOOD RUN full 24 hrs.	7
---	---	---	--	--	--------------------------------------	----------

model two kilometers higher, reducing the timesteps of the two grids and increasing diffusion parameters.

Another problem shown in Table 4.1 occurred early in the experiment and involved the incorrect handling of multiple boundary condition update files. Previous RAMS studies have used only two variable model files at a given time (the present and 12 hours in the future); however, the real-time version needed the 0, 12, 18 and 24-hour files in order to run 24 hours continuously. Otherwise manual intervention would have been required to restart the model at each of these times (an unacceptable solution when running a model overnight). Code was written to allow the files to be read in successively at their respective times but this proved to be machine dependent and took a few days to debug. Problems such as this could have been avoided if the break-in period could have been utilized to its full extent.

The most devastating problem occurred on four successive days from December 2 to December 5 and also on November 25. An obscure routine in the microphysics module was receiving a negative Kelvin temperature at a single grid point in space and at a single timestep which varied from simulation to simulation. This wasn't discovered until February, 1992, well after the FIRE II program was over. After many hours using the CRAY symbolic debugger, it was discovered that a temperature at a single grid point went from a well-behaved 274 K to -6.7 K in a single timestep! This is indicative of a memory overwrite, however the cause of it could not be isolated to a particular line of code; hence, a bypass was discovered whereby increasing the memory requested resolved the problem. This only occurred on the CRAY Y-MP and was duplicated more recently by a fellow student (Papineau, personal communication) with the same modification to the memory allocation applied.

4.2.3 Case study: 26 November 1991

Synoptic overview

On 26 November 1991, investigators involved in the FIRE II field experiment centered in Coffeyville, KS were delighted to see a broad area of cirrus clouds approaching from the west. The synoptic conditions at 1500 UTC for this day were as follows: a weak

surface low extended through the Dakotas with a weak cold front trailing back to the southern portions of Wyoming; a well-defined warm front extended south-east from the low center into northeast Kansas and south-central Missouri; a weak pressure trough existed between the two fronts oriented north-south through west-central Kansas and into the Texas panhandle. This trough was reflected throughout the entire depth of the troposphere as the 200 *mb* chart showed a weak trough in between two weak ridges. Also indicated by the 200 and 300 *mb* charts was a northwest-southeast oriented jet streak entering western Kansas. Some of these features are reflected in the satellite picture valid at 1443 UTC shown in Figure 4.20. The trough discussed above existed along the western edge of the north-south band of clouds on the right side of the figure.

Real-time RAMS forecast

The real-time RAMS forecast for this event was excellent in terms of placement of the upper level clouds. RAMS-predicted non-zero pristine ice and snow mixing ratios (the two active microphysical species) corresponded extremely well with areas of clouds as seen in Figure 4.20. This agreement can be seen by comparing the satellite photo to the RAMS 16-hr forecast of pristine ice crystal concentration shown in Figure 4.21. Model-predicted ice crystal concentration numbered up to 90 per liter at 7.35 *km* with lesser amounts above and below this level. Crystal concentrations from aircraft or other retrieval methods during FIRE II were unavailable, however, the maximum of 90 per liter is in an acceptable range based on measurements and other modeling studies. Unfortunately, investigation of the magnitude of pristine ice mixing ratios (water equivalent) revealed errors of at least an order of magnitude. A possible explanation to this is that the model is initialized with a moisture content that is too low at these upper levels. This may be caused by inaccurate or non-existent moisture measurements by rawinsondes at these altitudes. Further compounding this problem is that cirrus dynamics involve weak vertical velocities necessitating long time periods to increase model moisture/condensate to realistic values.

The model-predicted timing of the onset of cirrus clouds at a particular location was also handled well for the 26 November simulation. Figure 4.22 presents a time-height cross-section of RAMS-predicted ice crystal concentration valid at a grid point near Coffeyville,

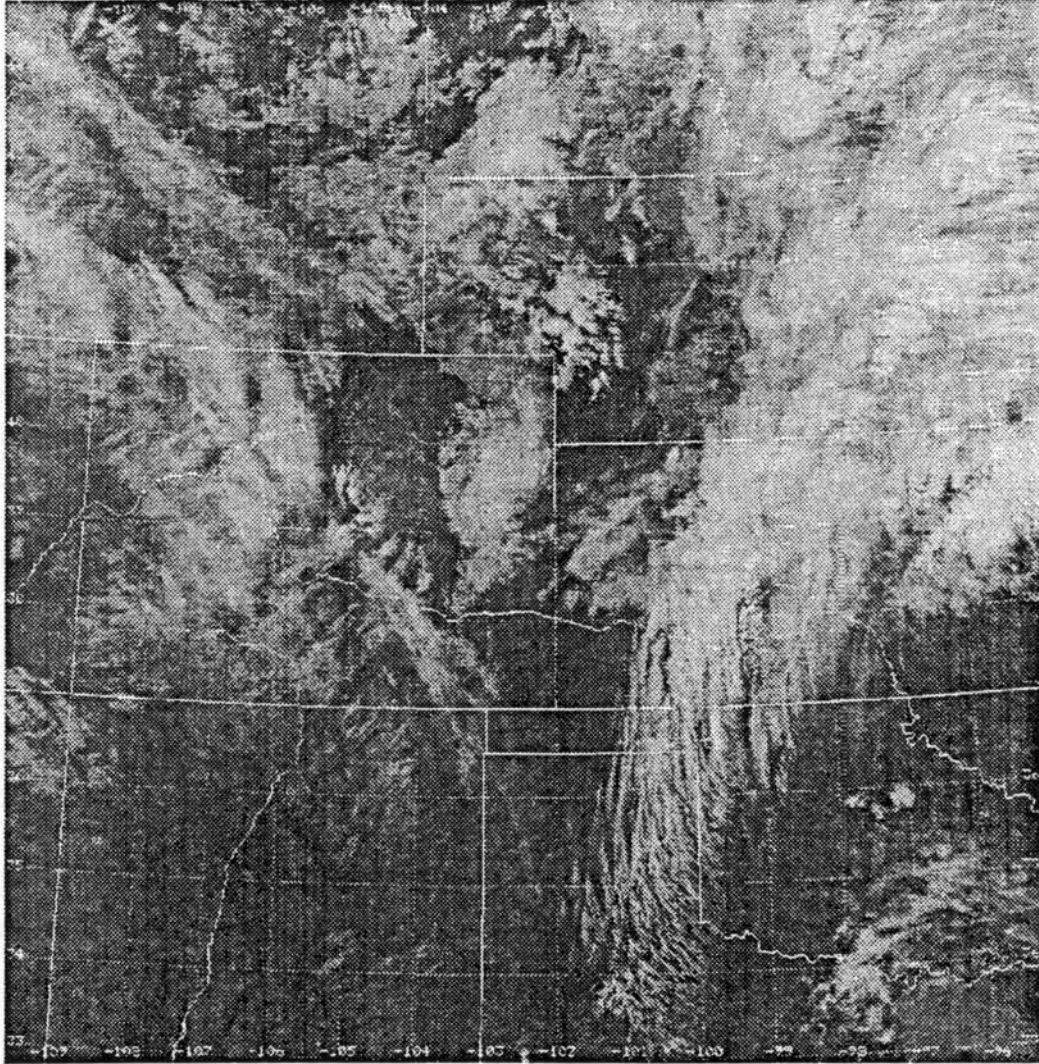
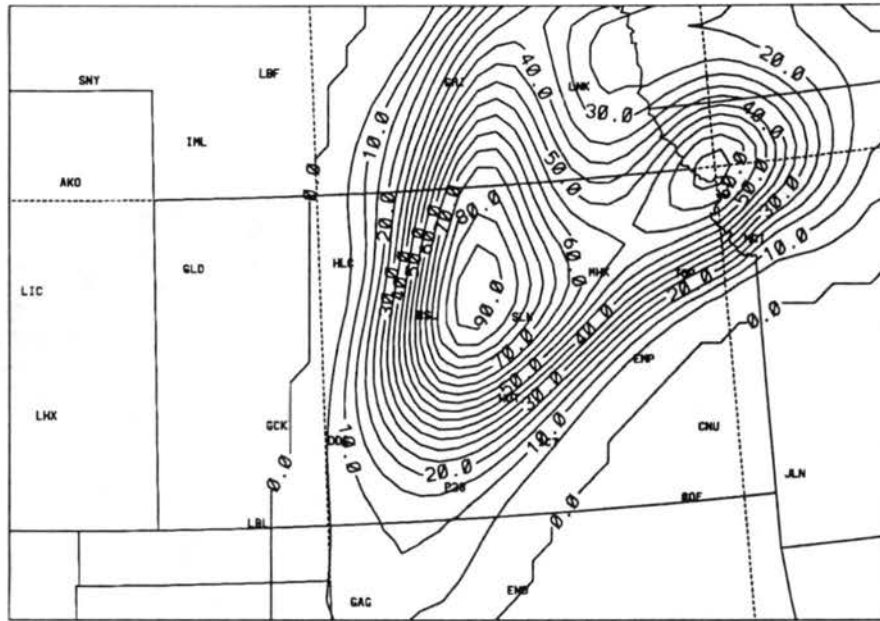


Figure 4.20: Infra-red satellite picture taken by NOAA-12 at 1443 UTC 26 November, 1991. Notice the high level clouds oriented north-south through the center of Kansas.



ICE CONCENTRATION (#/L)

Figure 4.21: RAMS 16-hr forecast ice concentration (/L) valid 1600 UTC 26 November, 1991. Notice the similarities between this plot and the clouds shown in Figure 4.20.

Kansas. Here we see the first evidence of a cloud at 16 hours (1600 UTC 26 Nov) at 8-10 km then increasing cloud depth through the remainder of the period with a 5-10 km cloud deck at 24 hours or 0000 UTC 27 November. Inspection of lidar images from the Coffeyville site showed the first evidence of a cloud at approximately 1615 UTC 26 November. The 200 m thick cloud located at 10 km was reportedly extensive and tenuous as blue sky was visible through the cloud (Intrieri et al., 1992). The cloud gradually thickened with time and existed from 8.25 - 10 km by 1730 UTC and was not detected by the Penn State 94 Ghz cloud radar until nearly 1830 UTC when cloud base lowered to 7 km (Mace and Ackerman, 1992). Cloud base continued to lower with a significant drop from 6 to 3 km between 2130 and 2200 UTC. Reproductions of the lidar images are presented in Figure 4.23 for comparison. The cloud deck abruptly dissipated at 2330 UTC. The PSU/NCAR MM4 model shared similar success by predicting the timing and height of clouds for the 26 November case well (Jensen et al., 1992).

Because of the apparent success of the RAMS 24 hour simulation, we decided to repeat the simulation initializing the model 24 hours earlier and forecasting out to 48 hours. The

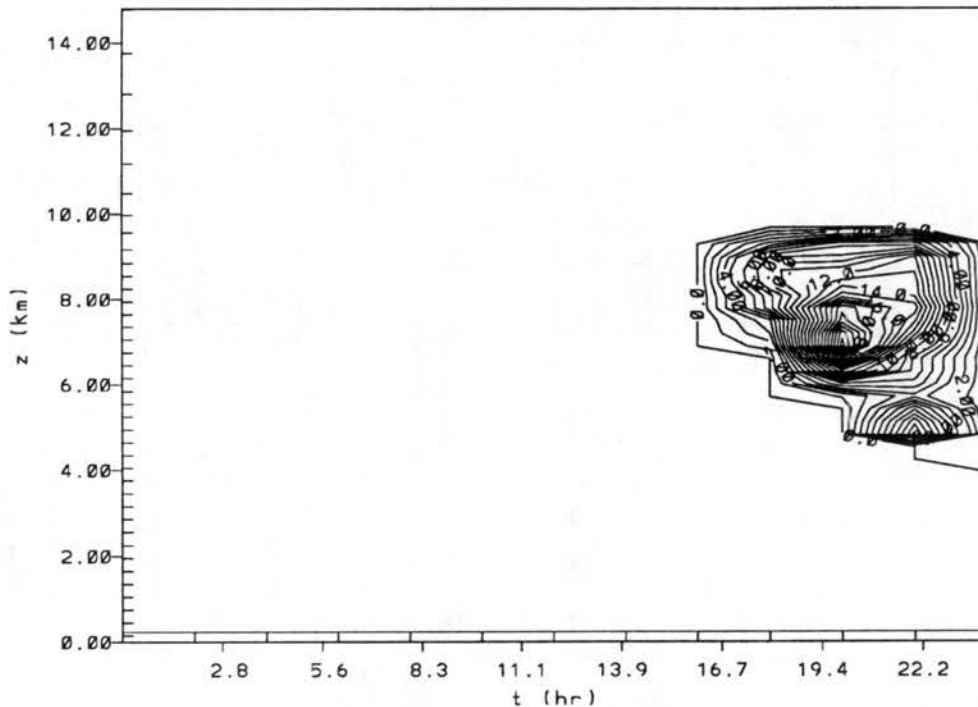


Figure 4.22: RAMS 24-hr time-height ice concentration (/L) plot valid at a model grid point near Coffeyville, Kansas from 0000 UTC 26 November to 0000 UTC 27 November, 1991.

result of this forecast was also accurate in the placement of the upper level clouds. Figure 4.24 was taken from the 48-hr simulation initialized at 0000 UTC 25 November. It shows the 40-hr RAMS forecast of the same field valid at the same time as Figure 4.21. Again, we see a strong resemblance to the clouds shown in Figure 4.20. Once again the mixing ratios are probably an order of magnitude too low, but ice crystal concentration numbered up to 6.4 per liter. It is difficult to say what caused the significant drop in predicted concentrations and which concentration is more accurate since measurements are currently unavailable.

4.2.4 Future & preliminary sensitivity studies

Much is yet to be learned from this program as the analysis of the huge volume of observational data has only begun. Work is continuing on modeling the above event as well as others during the FIRE II program. This modeling work will continue to use the forecast version of the model as well as the standard research configuration. Recently, Harrington (personal communication) has shown a sensitivity to the radiation scheme employed. He has repeated modeling efforts on the 26 November case and 5-6 December case and found

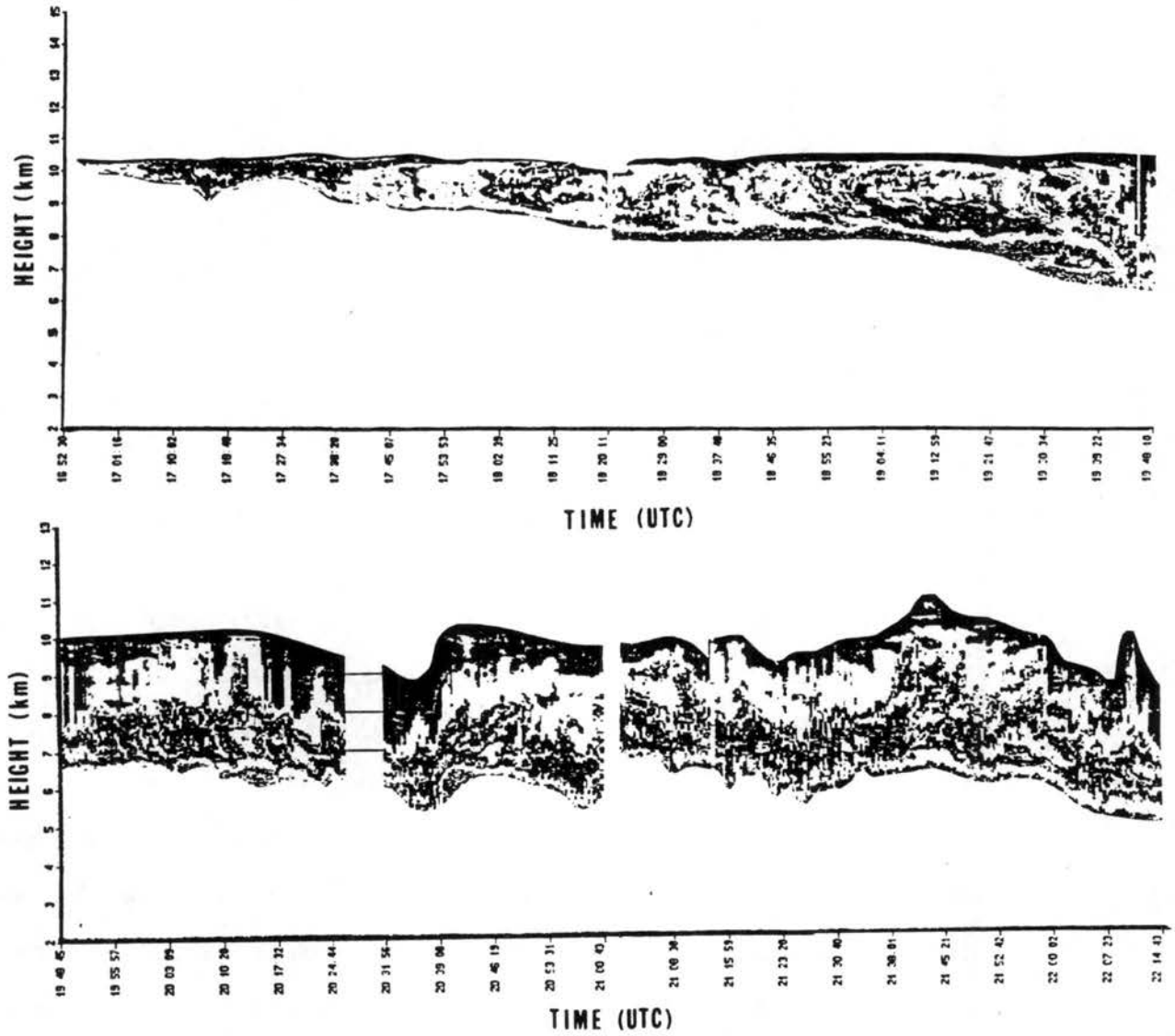
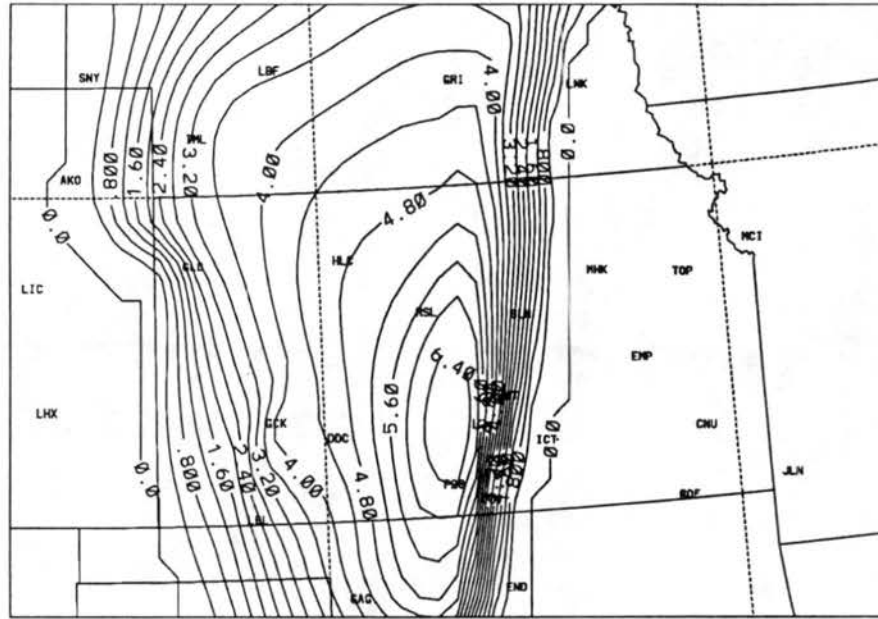


Figure 4.23: Lidar instrument time-height observations taken at Coffeyville, Kansas from 1652 UTC to 2214 UTC 26 November, 1991 indicating the locations of clouds.



ICE CONCENTRATION (#/L)

Figure 4.24: RAMS 40-hr forecast ice concentration (/L) valid 1600 UTC 26 November, 1991.

that by using the more complete RAMS radiation option, the mixing ratios are much higher. Work has also begun on including a homogeneous nucleation scheme (DeMott et al., 1993) in the microphysics. This may account for the majority of the cirrus crystals produced in the real atmosphere as much of the cirrus clouds on 26 November were in air with temperatures below -40°C . Furthermore, all the real-time forecasting included microphysics which were initiated only upon reaching water supersaturation. The current scheme does, however, allow ice microphysics upon ice supersaturation once a particular grid volume contains any microphysical species whether in frozen or liquid state. It will also allow ice microphysics when a species is advected in from another grid volume; it does not require that each grid volume reach water supersaturation. In the real atmosphere, condensate species are often initiated upon reaching supersaturation with respect to ice. These three factors all contribute to the discrepancy that mixing ratios were too low. Lastly, simulations are also underway where RAMS' other microphysical species - aggregates and graupel - are activated.

4.3 Computer Resources

Each decade a plethora of advances in computer technology is realized. In 1990, due to unprecedented advances in computer hardware, Reduced Instruction Set Computers (RISC)-based workstations have met and exceeded the capabilities of a single CRAY-1 processor (Pielke et al., 1992). RAMS, like all large scientific codes, had historically been targeted for the large mainframe supercomputer. Now, with the advent of fast RISC workstations, RAMS has been modified to run on a variety of platforms. In addition to the traditional supercomputers like CRAYs, the CYBER 205 and NEC machines, RAMS has been executed on machines such as DEC VAXs, IBM 3090, IBM RS/6000, Stardent, Silicon Graphics and Convex (Pielke et al., 1992). Following is a discussion of which computers were utilized for this study; including particular run-time statistics for each of the configurations discussed in previous sections and brief speculation of the future of RAMS computing.

All simulations pertaining to the Colorado investigation were performed on a Stardent 3000 with RISC architecture. Although this machine was used by many other users it had four processors to distribute the jobs. Unfortunately, RAMS was unable to use more than one processor at a time, however the code is being modified to allow parallel processing. A forty-eight hour simulation on the Stardent took from 10 to 12 hours of wall-clock time depending on machine load. This same job would take half as long on an IBM RS/6000 with a 320 processor and one-fourth that long on an IBM RS/6000 with a 560 processor. It is projected that with parallelization of the code on a cluster of six IBM processors, the same job could be accomplished in just over an hour and include the microphysics option as well (Tremback, personal communication).

Simulations pertaining to the FIRE II investigation were performed on a CRAY Y-MP supercomputer at the National Center for Atmospheric Research. A twenty-four hour simulation took nearly 8 hours of wall-clock time but only 3 to 4 hours of CPU time. The difference here being the Y-MP with its 8 processors, also has a huge number of jobs and a time-sharing queue. There are different categories involved in determining job priority in this queue: economy, regular, premium and real-time. The simulations performed for FIRE

II were in the highest priority, real-time queue and yet nearly as many hours were spent waiting in limbo as were spent on a processor.

From the discussions of two real-time forecasting investigations in this chapter, it was shown how RAMS was configured to best serve a particular purpose. For the Colorado investigation, RAMS was able to predict mesoscale features of importance to local forecasters. RAMS was configured in such a way as to improve local snow prediction. For the FIRE II investigation RAMS again was configured with the users' needs in mind. This time, high vertical resolution was required to improve upper-level cloud forecasts. In either case, real-time mesoscale forecasting was achieved over a selected region with the purpose of producing forecasts which were tailored to particular needs. More importantly, the time has arrived where this type of forecasting can be accomplished by anyone with the money for a RISC workstation and access to the analysis/forecast model data stream. A forecaster in an eastern seaboard metropolis (Boston, New York, Philadelphia, Baltimore or Washington for example) could improve forecasts of rain/snow/ice storms which frequent the region in winter months; a forecaster in Florida could improve predictions of sea breeze fronts; a forecaster in the Central Plains could improve predictions of low temperatures and possibly frost. These are all possible with current computers and code, however, the future could easily allow for much finer resolution and explicit microphysics extending the forecast applications to limitless proportions.

Chapter 5

STATISTICAL VERIFICATION

An area of increasing concern for research mesoscale numerical models is model verification. How accurately do mesoscale models predict mesoscale and synoptic scale weather? Is their accuracy better than established operational numerical models? This chapter will tackle these issues as a comprehensive statistical analysis has been performed on the cases discussed in the previous chapter and also on the entire 1991-92 winter season. Also included is a discussion of previously used statistical procedures and their inappropriateness to mesoscale model verification.

5.1 Introduction

Statistical verification of mesoscale model data is a difficult task, primarily because of the lack of observational data on this scale. As an example, refer back to the precipitation forecasted and observed for the 8-9 March case study. Figure 4.12 shows the forecast precipitation field valid at 1200 UTC 9 March and Figure 4.8 shows the observed amounts at this time. Notice the complete lack of data over the mountains of Colorado. This example only illustrates the difficulty of making objective comparisons between model output and observational data. Imagine the difficulty involved with a statistical analysis of these fields. A great deal of uncertainty is introduced upon interpolating observational values to a gridded field for statistical comparisons. Likewise, a gridded observational data field of different resolution than that from a model introduce similar uncertainties. This point is discussed further in Section 5.3 below.

From the above example, it is obvious that mountainous regions represent the worst scenario for verification; whereas special observing networks such as the Front Range mesonet-work in Colorado represent a better opportunity for an appropriate validation. While

mesonet network observing systems provide detailed data for surface parameters, the wind profiler system of the Central Plains provides detailed wind information through the depth of the troposphere, supplementing the radiosondes launched twice daily. These data sets represent the best sources of mesoscale data currently available. Incorporation of these data sets into the widely-available large-scale data will undoubtedly aid in statistical analysis of mesoscale models.

Statistical techniques for model verification should adhere to three criteria. First, the assumed distribution for the test statistic must correspond to the error distribution of the model data. If an artificial distribution is incorrectly assumed, then the conclusions drawn from the analysis may be totally wrong. Many previously-used statistical methods assume a normal distribution which is not always satisfied for model data. A more intuitive choice is that model errors follow a random distribution. The assumption that there exists a random allocation of objects to experimental treatments (termed the randomization assumption) provides a meaningful distribution called the permutation distribution (Mielke, 1991). The resulting statistical procedures which depend on the randomization assumption are called permutation methods. The second criterion is that the analysis space correspond with the space in which the data exist (Mielke, 1984, 1986). This criterion is widely neglected in statistical studies involving atmospheric models. Mielke (1984) shows that Student's *t*-test and analysis of variance methods are based on squared Euclidean distance. Analyses of numerical models and atmospheric measurements should be based on a distance function of the same space, namely, ordinary Euclidean distance. The squared Euclidean distance of widely-used methods such as the Student's *t*, correlation coefficient, threat scores and bias scores is a result of the normal distribution assumption, thus revealing the relationship between the first two criteria. Finally, the testing procedure should assess the probability that a predicted pattern could occur by chance alone while providing a quantitative measure of forecast skill (Tucker et al., 1989). The statistical technique used for this study satisfies all three above criteria by using multivariate randomized block permutation procedures (MRBP).

5.2 Description of MRBP

The initial presentations and theoretical development of MRBP are given in Brockwell and Mielke (1984), Mielke (1984, 1986), Mielke and Berry (1982), and Mielke and Iyer (1982), but a brief description and discussion of terminology is in order in this section. MRBP has been used for statistically analyzing numerical model output by McCoy (1988), Tucker et al. (1989), and Lee (1992). As with the research presented here, the aforementioned studies tested model output data that consisted of meteorological parameter values (e.g. pressure, temperature or geopotential heights) on grid points from a variety of cases against corresponding observed fields on the same grid points. More than one numerical model can be used (as in Tucker et al.) and data are partitioned into blocks, each block representing the data from a particular model. The observations also occupy a block. If there are $b - 1$ prediction models, then there are b blocks since each model's gridded data occupy a block and the observed data values occupy a block. Within each block, there are g treatments, each representing a specific case application (e.g. a 12- or 24-hour forecast) of all models and the observations (Tucker et al., 1989). Lastly, within each treatment, there are r responses or measurements. The r measurements represent temperature values, for instance, at individual grid points.

The MRBP statistic is given by:

$$\delta = \left[g \binom{b}{2} \right] \sum_{i=1}^g \sum_{j < k} \Delta(x_{ij}, x_{ik}) \quad (5.1)$$

where $\sum_{j < k}$ is the sum over all j and k such that $1 \leq j < k \leq b$ and $\Delta(x_{ij}, y_{ik})$ is the symmetric distance function value of the two points in Euclidean space. The symmetric distance function is defined by:

$$\Delta(x, y) = \left[\sum_{i=1}^r (x_i - y_i)^2 \right]^{\frac{\nu}{2}}. \quad (5.2)$$

As emphasized earlier, ordinary Euclidean distance is desired as the distance function since the meteorological data exist in ordinary Euclidean space, so we choose $\nu = 1$. If $\nu = 2$, squared Euclidean distance is used and the test becomes analogous to a more familiar statistical procedure, the correlation coefficient (Mielke, 1984).

From the form of δ in expression (5.1), Mielke (1991) computes the exact mean, variance, and skewness of δ under the null hypothesis, H_0 . The null hypothesis states that the distribution of δ assigns an equal probability to each of the:

$$M = (g!)^b \quad (5.3)$$

possible allocations of the g r -dimensional response measurements to the g treatment position within each of the b blocks (Mielke, 1991). For the present application, this means that data in each block have no resemblance to corresponding data in other blocks. From the mean, variance and skewness of δ , Mielke computes the probability that forecast patterns can be produced by chance alone, a criterion mentioned in the previous section. The test statistic is given by:

$$T = (\delta - \mu_\delta) / \sigma_\delta \quad (5.4)$$

where μ_δ is the exact mean and σ_δ^2 is the exact variance of the distribution of δ . The terminology used for this test statistic is P-value. Additionally, Mielke defines an agreement measure, ρ , as:

$$\rho = 1 - (\delta / \sigma_\delta). \quad (5.5)$$

This is the chance-corrected agreement which estimates the composite measurement agreement between blocks for all treatments. To achieve perfect agreement ($\rho = 1$), model-forecast values of a parameter (temperature, for instance) would have to be identical to observed values at every grid point in space, and for each treatment or event among a number of treatments. Again, for clarity, the model-predicted and observed values comprise b blocks; the grid points comprise r responses or measurements; and there can be g treatments or events. Values of ρ range from negative, indicating absolutely no correlation between data sets, to small positive indicating little agreement, to at most 1.0 when perfect agreement is achieved.

Mielke continues by noting the relationship between P-values and values of ρ . First, P-values are highly dependent on sample size (recall expression 5.4) whereas values of agreement measure, ρ , are not. He also states that large data sets can yield small positive values of ρ with very small P-values while small data sets can yield relatively large positive values

of ρ with fairly large P-values. Basically, more agreement is achieved when P-values are extremely small and ρ is large and positive. This is illustrated further by example in Tucker et al. (1989). Values of ρ provide a measure of agreement between model forecasts and observations and can be interpreted much like correlation coefficients, although direct magnitude comparisons with correlation coefficients cannot be made since they involve different analysis space. This concept is vividly illustrated by example in Tucker et al. as they run a test using $\nu = 2$ (squared Euclidean space) in MRBP for a simple 10-point data set. They note "the probability of correspondence between two data sets is more representative of the entire data set when $\nu = 1$; whereas, for $\nu = 2$, a deviation in only a pair of points can overwhelm the analysis." This was the driving force behind the initiation of MRBP procedures, since one of its first meteorological applications involved the statistical analysis of cloud-seeding experiments (Mielke, 1985). In this study, Mielke emphasizes the problems related to using traditional statistical methods when a single datum value is in question.

5.3 Procedure of Analysis

To use MRBP correctly, model forecast fields and observational data sets must exist at the same points in space. Observational data obviously exist in an irregularly-spaced manner while model output exists on its grid domain. RAMS grid points are shown in Figure 4.1 of Chapter 4. Recall that RAMS must be initialized at these points in order to execute, and that the MAPS data set was used for this purpose (the plot of MAPS grid points is shown in Figure 3.1). Thus, the MAPS analyses are used as the observational data sets against which RAMS forecasts are statistically verified. First, though, the MAPS analyses are horizontally and vertically interpolated via RAMS initialization in order to complete the task of grid point matching. This means that RAMS 12-, 24-, 36-, and 48-hour forecasts are verified against RAMS 0-hour forecasts valid at the same time.

Unfortunately, the model initialization procedure (as described in Chapter 3) using the MAPS (60 km spacing) analyses, initializes only the coarse grid (100 km spacing) directly from the MAPS data. The model's fine grid (25 km spacing) is then interpolated from the coarse grid data and not directly from the MAPS data. This is unfortunate since shorter wavelength features can easily be eliminated when interpolating from 60 km to

100 *km* and finally to 25 *km* grids. If, however, the fine grid was interpolated directly from the MAPS data, then the shorter wavelength features may be retained. A test was performed to resolve the magnitude of any errors involved in this procedure. The fine grid was initialized directly from the MAPS analysis for 9 March and close inspection of model initialization fields showed no noticeable differences in placement and magnitude of features. This only provided a qualitative comparison with the previous initialization method, however, MRBP was used on each procedure to provide a more objective analysis. The MRBP analysis was performed in the following manner. The 8 March 24-hour RAMS grid 2 forecast was compared against an analysis of grid 2 based on the standard method described above and then also against an analysis based on a direct interpolation from the MAPS analysis (without the intermediate grid 1 step). The statistical analysis showed insignificant differences with respect to method used. With the lack of differences in the statistical agreement for the two methods, it can be concluded that the RAMS forecast agreed equally to either analysis, hence no significant differences exist in the two analyses.

The reason that grid 2 was not interpolated directly from the MAPS analysis and instead was interpolated from grid 1, results from the more customary choices of data sources for variable initialization. Previous RAMS modeling was designed to access the standard archives of data at NCAR. These data sets generally contain horizontal spacing of 2.5°Lat by 2.5°Lon. Then, upon ingestion through ISAN, the horizontal spacing could effectively be reduced to 0.7-1.0°Lat/Lon or approximately 100 *km*. This spacing usually matched the coarse grid spacing of a RAMS configuration, and so, interpolation to the fine grid was justified. Now, however, the 60 *km* MAPS analysis is available and a new initialization method is being implemented. This new scheme will investigate the spacing of all model grids in relation to the spacing of the initialization source to determine when to interpolate solely from a coarser grid.

A problem more serious than the interpolation procedure when verifying mesoscale model data is the spacing of the observational data set. Mesoscale models such as RAMS predict on grids with much smaller spacing than any available data set. The smallest grid spacing in this study was 25 *km* for the Colorado investigation and 20 *km* for the FIRE II investigation, however, other RAMS modeling efforts have used grid spacings of

less than a kilometer. To truly analyze a mesoscale model statistically, it is only fair to use observed data similarly gridded. Low resolution observational data sets can sometimes reduce the amplitude of shorter wavelength mesoscale features and occasionally eliminate them altogether. Then, upon statistical analysis of model data, it may appear that the model performed poorly when in fact the model predicted a mesoscale feature well. As an example, suppose a model with 25 *km* spacing predicted a weak disturbance which was evident at 500 *mb*. Spacing of 25 *km* translates to a model resolution of nearly 100 *km* since it usually requires four grid points to truly resolve a disturbance within a given 2-D area. Now suppose the data set used for verification has horizontal spacing of 60 *km*. This spacing then translates to a resolution of 240 *km*, to assure that a feature is resolved in the analysis. One can quickly see that, with this new resolution, a disturbance can be smoothed by a reduction in magnitude, or an increase in wavelength. Statistical analysis of model results, therefore, can be contaminated because features which really did exist in the atmosphere were not analyzed by the verification data set. Hence, caution must be taken when interpreting results of statistical analyses performed for grid spacing which does not match both the model data and the observations.

Variables which can be verified immediately using MRBP include ones that are readily available from model output files, for instance: *u*- and *v*-wind components, temperature, and mixing ratio. Many other variables can then be diagnosed from these including: absolute vorticity, relative humidity, geopotential heights and reduced mean sea-level pressure. Variables which were not be analyzed include ones which do not exist at the 0-hour model time. Examples are: *w*-wind component, microphysical species (masses or concentrations) and cloud water. If, however, an observational data set of one of these variables did exist (e.g. using normal mode initialization to get a *w* component), then analyzing the model statistically for these fields is possible. A scenario where this could occur exists as intensive field observational data from the FIRE II or other field programs become available. The *w*-wind component, for instance, was measured by the wind-profiler network. Examples of other intensive observations for use in statistical evaluation of models include satellite, radar, sodar and lidar data. These data sources can provide an unprecedented observational database for model verification.

Variables which were analyzed in this study are: u- and v-wind components, speed, absolute vorticity, temperature, relative humidity, perturbation Exner function (Exner function based on a reference state and should be considered similar to geopotential heights), mean sea-level pressure, and geopotential heights at 850, 700, 500, and 250 *mb*. MRBP statistical analyses were performed on a sigma-by-sigma level basis for all except the last five variables listed since these only have meaning at one vertical level. Through analysis in this fashion, one can quickly infer model strong/weak points vertically (ie. surface parameters should generally indicate lesser correlation than their mid-level counterparts). To avoid contamination by the "nudging" on lateral boundary regions, the statistical analyses compare all grid points from grid 1 except the zone of five points along boundaries directly affected by the nudging. As for grid 2, computational limits required verifying every other grid point.

The computer time needed for statistically analyzing model forecasts varies greatly depending on the application. Increasing the number of treatments increases the computer time dramatically since forecast data sets are evaluated for chance correlation. Also, increasing the number of grid points or responses causes an increase in computational expense. For the analysis shown here, approximately 30 seconds of computer time was needed on a RISC workstation when analyzing one coarse grid forecast of one variable on one level. Analyzing one forecast of all twelve variables (listed above) through all sigma levels for both grids required nearly an hour of computer time. Increasing the number of treatments by analyzing an entire month's worth of 12-hour forecasts can take a day or longer, however, this represents the extreme case as most common applications require very little computational expense.

5.4 Results

Presented in this section are the results of the MRBP analyses for a variety of RAMS forecast categories. The first category is a whole season analysis of the real-time experiment performed during the winter of 1991-92. Here, MRBP was used to analyze the statistical agreement between all of the 12-, 24-, 36-, and 48-hour forecasts and their corresponding observations. In other words, the 12-hour forecast from 0000 UTC 8 November was analyzed

against observations taken at 1200 UTC 8 November; the 24-hour forecast from the same time was analyzed against observations at 0000 UTC 9 November and so on for the 36- and 48-hour forecasts. Then the cycle was repeated for the forecasts initialized 24 hours later (recall that RAMS was run once a day beginning at 0000 UTC). This was done for all of the forecasts made during the 1991-92 winter season. In all, eighty-two 12-hour forecasts, sixty-five 24-hour forecasts, forty-five 36-hour forecasts and thirty-four 48-hour forecasts were analyzed. These analyses help determine specific strengths and weaknesses that RAMS had throughout the entire season as well as illustrate the reduction in accuracy as the forecast times increase.

The second category encompasses the case studies discussed in the previous chapter. The 8-9 March 1992 blizzard case study is analyzed first including each variation discussed in Chapter 4. By analyzing the results of these variations, a sensitivity analysis is performed and the true potential of MRBP is realized. This application will show how MRBP can be used to improve forecast skill. The next case study is from the 23 November 1992 RAMS simulation. This was chosen as an additional analysis on a snowstorm in the Front Range of Colorado. The last case study analyzed here is a 26 November 1991 FIRE II RAMS forecast. Here the 18-hour forecast is analyzed since this time was crucial as cirrus was being observed over the field site. Generally, 18-hour forecasts are not used for statistical analysis since observational times correspond with 12 hour intervals; however, an 1800 UTC data set was available from the MAPS analysis.

The results of the MRBP analyses are presented as a series of graphs. The graphs consist of agreement measure, ρ , versus sigma level. Each figure will have results of grid 1 shown in the top-half and grid 2 results are presented in the bottom portion of a figure. On the left of each half are the results for forecast u- and v-wind components, speed, and absolute vorticity (named totvort in plots). The five non-sigma-dependent variables are mean sea-level pressure (mslp), and geopotential heights at 850, 700, 500, and 250 mb (named geo850, geo700, geo500, and geo250 respectively). These are denoted with a X and plotted nearest the sigma level where such variables can be found. For instance, typical 850 mb geopotential heights are 1500 m, so the 850 mb height agreements are denoted by a X and plotted at sigma=5 since this RAMS vertical level is approximately 1500 m from the

surface. Likewise, typical 500 *mb* heights are 5600 *m* so a *X* denotes its agreement and is plotted at $\sigma=12$, since this roughly corresponds to 5600 *m* above the model's surface. Lastly, mslp agreement is plotted at $\sigma=2$ since this is the first level above the model surface. Also on the same plots are relative humidity (*relhum*), temperature (*tempc*), and perturbation Exner function (*pistar* or π^*). All of these variables can be found in the graphs on the right side of the figures.

5.4.1 Whole season

The MRBP results from the eighty-two 12-hour forecasts analysis are shown in Figure 5.1. As expected, temperature and geopotential heights (as well as the related perturbation Exner function) show the highest agreement whereas relative humidity reflects the lowest agreement. The related variables of *u*- and *v*-wind components, speed and absolute vorticity lie in-between, with agreement measures between 20 and 60 percent. The momentum variables show minor changes in agreement measure with respect to height, with the highest agreement close to the tropopause near $\sigma=18$. Temperature, on the other hand, reflects poorer agreement near the tropopause than in lower levels. This is most likely due to the dramatic gradient in temperature at the tropopause and any small error in prediction of the tropopause height causes poor agreement in the temperature agreement near tropopause levels. Temperature also has poor agreement at the surface as does relative humidity, not unlike most numerical models. The statement that perturbation Exner function (π^*) resembles geopotential heights is supported by the graphical representation of Figure 5.1 as agreement increases with height. Notice *geo850*, *geo700*, *geo500* and *geo250* points fall nearly on the *pistar* curve. Grid 2 reflects all of these trends and characteristics but generally has lower agreement measures. These lower agreements may not indicate poorer performance but, instead, may be a result of the poorer resolution of the observational data as discussed in the previous section.

The results of the sixty-five 24-hour forecasts MRBP analysis are displayed in Figure 5.2. As expected, the agreement measure of all variables decreases from the 12-hour analysis to the 24-hour analysis, although decreases ranged from only 5 to 10 percent. This trend continues into the forty-five 36-hour forecasts analysis shown in Figure 5.3 and the

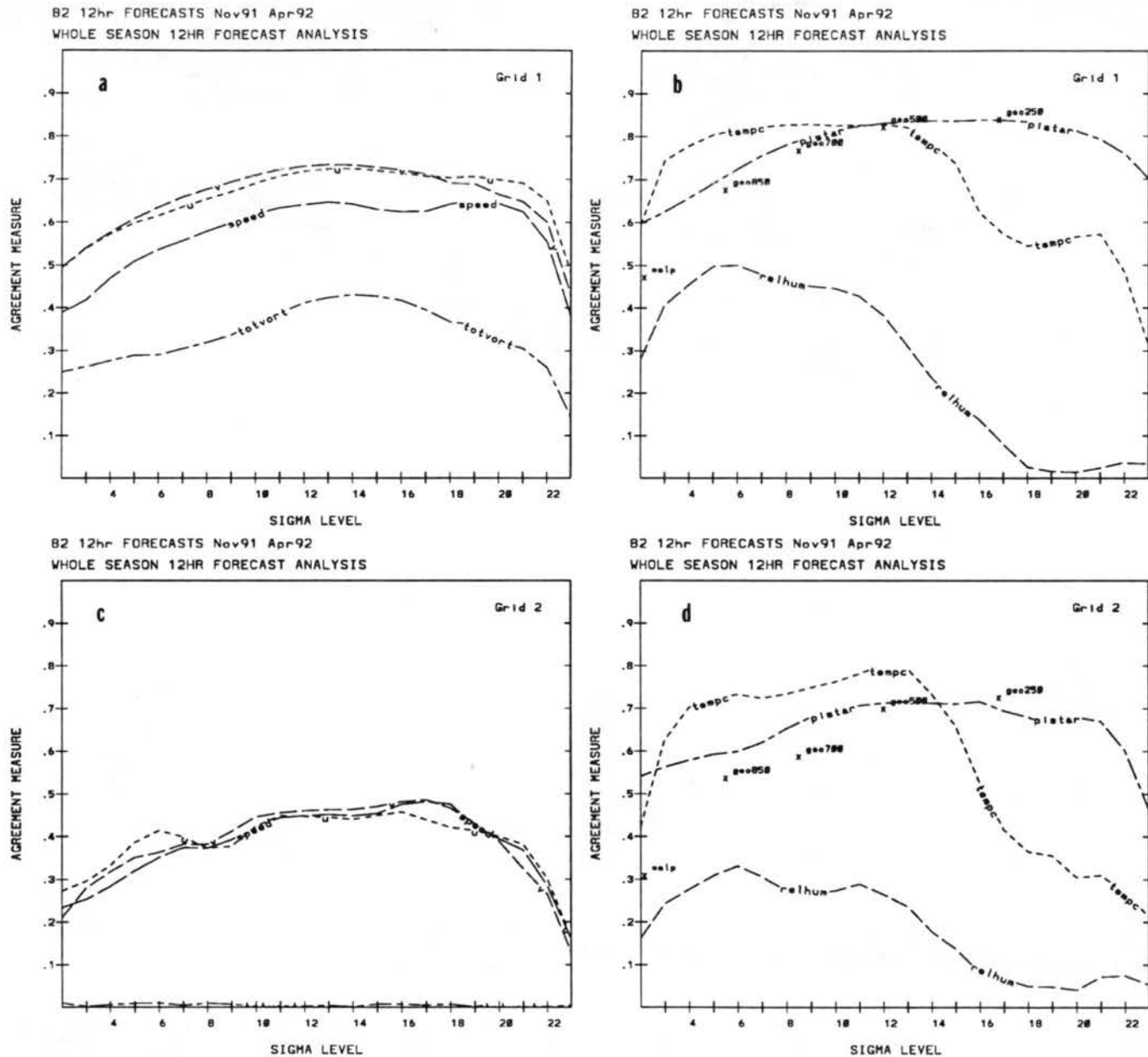


Figure 5.1: MRBP results for whole season of RAMS 12 hour forecasts. Statistical agreement measure is plotted versus model sigma level (see text for details). Panel a shows wind-related variables for grid 1, while thermodynamic variables for grid 1 are shown in panel b. Panels c and d have same information but for grid 2.

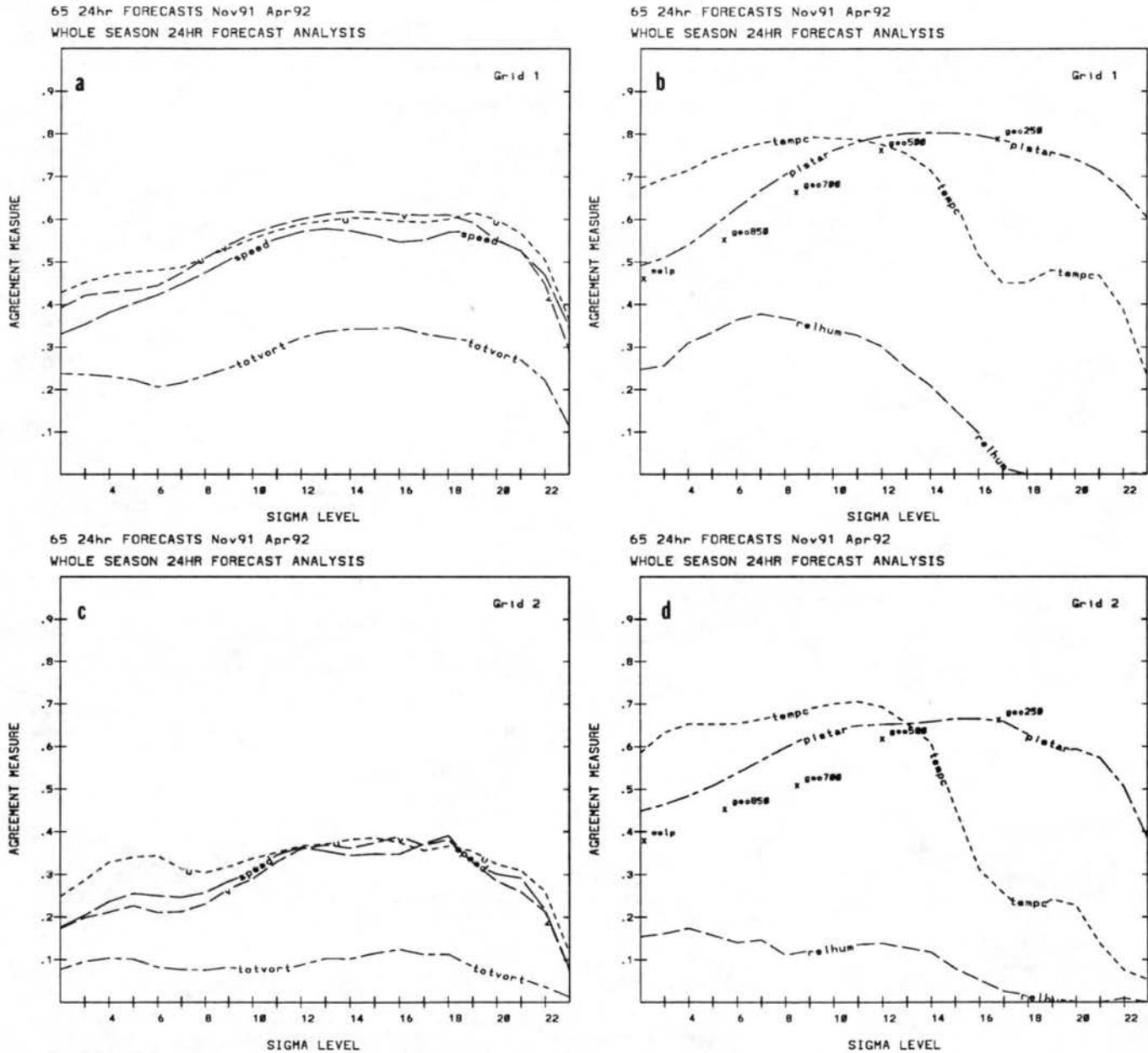


Figure 5.2: MRBP results for whole season of RAMS 24 hour forecasts, otherwise same as Figure 5.1.

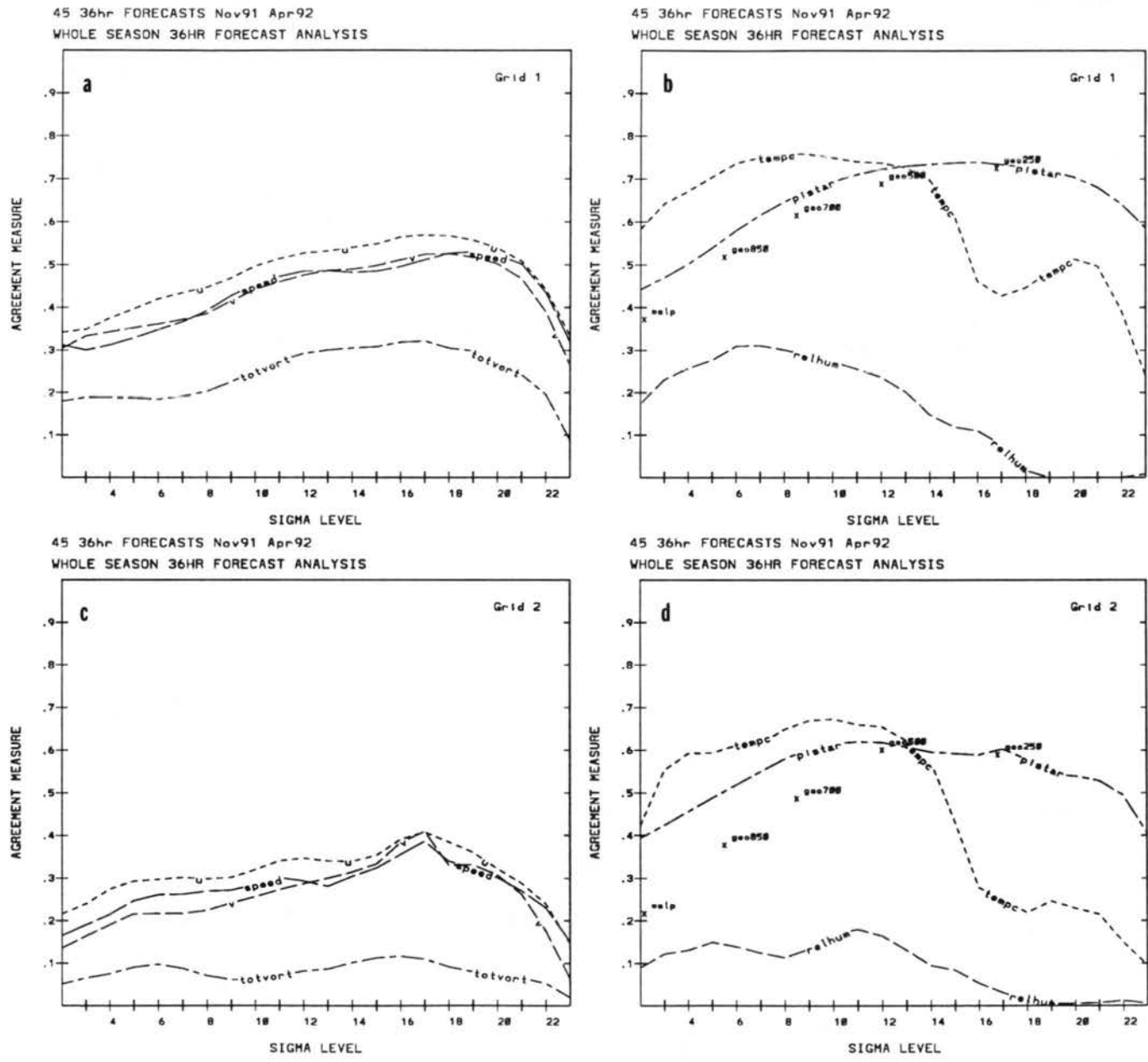


Figure 5.3: MRBP results for whole season of RAMS 36 hour forecasts, otherwise same as Figure 5.1.

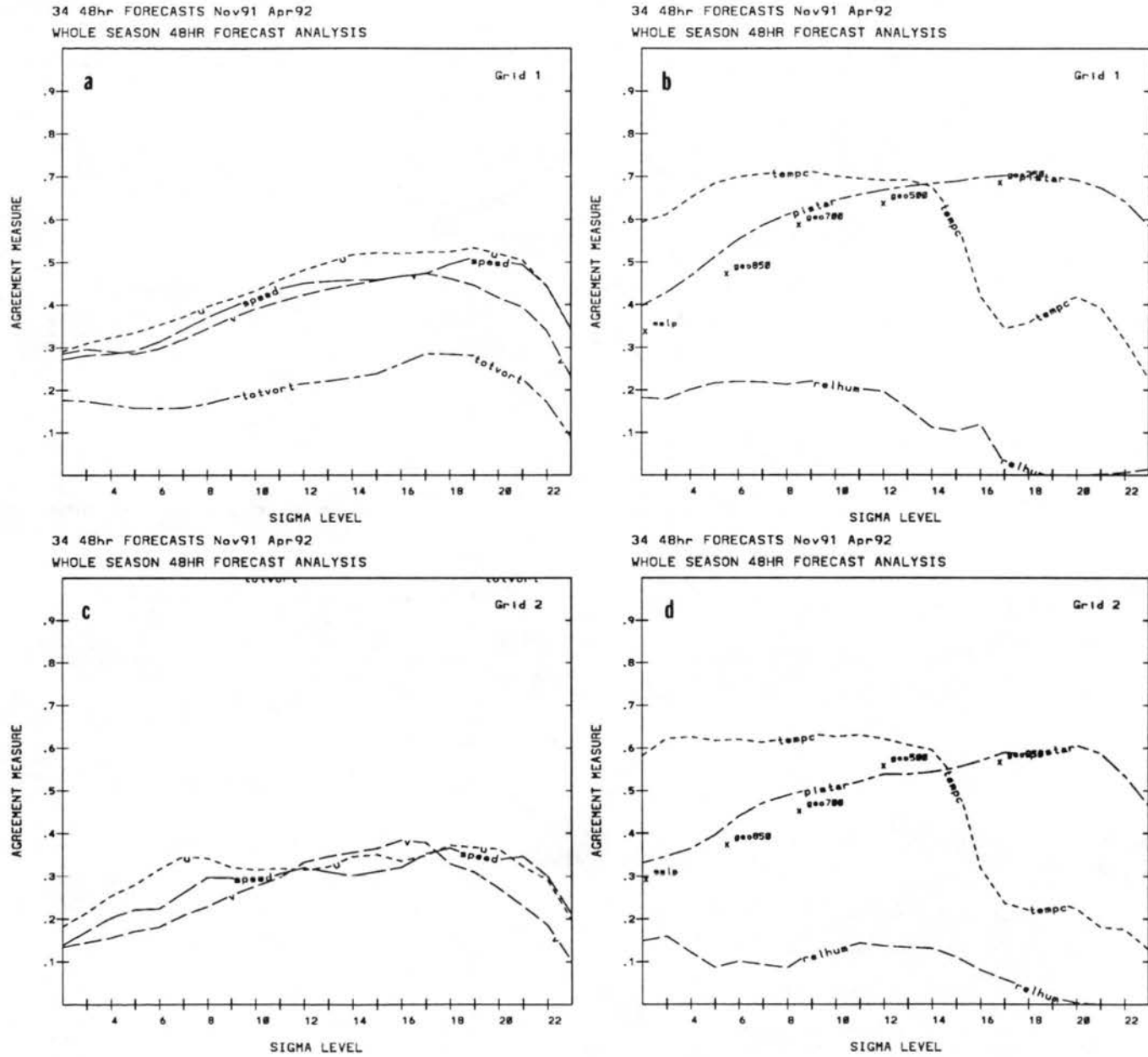


Figure 5.4: MRBP results for whole season of RAMS 48 hour forecasts, otherwise same as Figure 5.1.

thirty-four 48-hour forecasts MRBP analysis shown in Figure 5.4. Temperature shows the least variations through these times whereas relative humidity and mean sea-level pressure reflect the largest changes in agreement measure. Another possible application which would be similar to this one is to categorize different portions of a synoptic scale pattern and provide an analysis based on these classifications. This type of analysis would be similar to the study done by McCoy (1988) except an entire season's analysis could be performed to evaluate, for instance, the agreement for arctic air outbreaks or warm sectors of extra-tropical cyclones.

5.4.2 8-9 March case study

The results of the MRBP analysis for the 8 March 1992 simulation including the many configurations discussed in Chapter 4 show how MRBP can be used for model improvements. First, the MRBP analysis of the original 24-hour forecast initialized at 0000 UTC 8 March is discussed. This will be referred to as the V2c simulation since it was made using RAMS Version 2c. Then the analysis of the 24- and 36-hour forecasts with the modifications discussed in Section 4.1.6 is discussed. This simulation will be referred to as NEW2c since an updated Version 2c model code was utilized. Next, the forecast which included the above modifications and the microphysics option (referred to as MICRO) is analyzed statistically. Finally, the simulation which used the ETA forecasts for boundary nudging is discussed. This run is named LBC-ETA in subsequent paragraphs. After each of these sensitivity study analyses are discussed, comparisons are made with the NMC numerical models to evaluate the potential that RAMS forecasts had greater accuracy than the NGM or ETA models for this particular event.

Results of MRBP analysis of simulation V2c

Analysis of the original 24-hour RAMS forecast (V2c) from 0000 UTC 8 March is shown in Figure 5.5. Notice that the agreement measure for this single forecast is generally higher than the agreement for the whole season of 24-hour forecasts. The relhum curve, though, shows an exception as it exhibits low agreements near the surface.

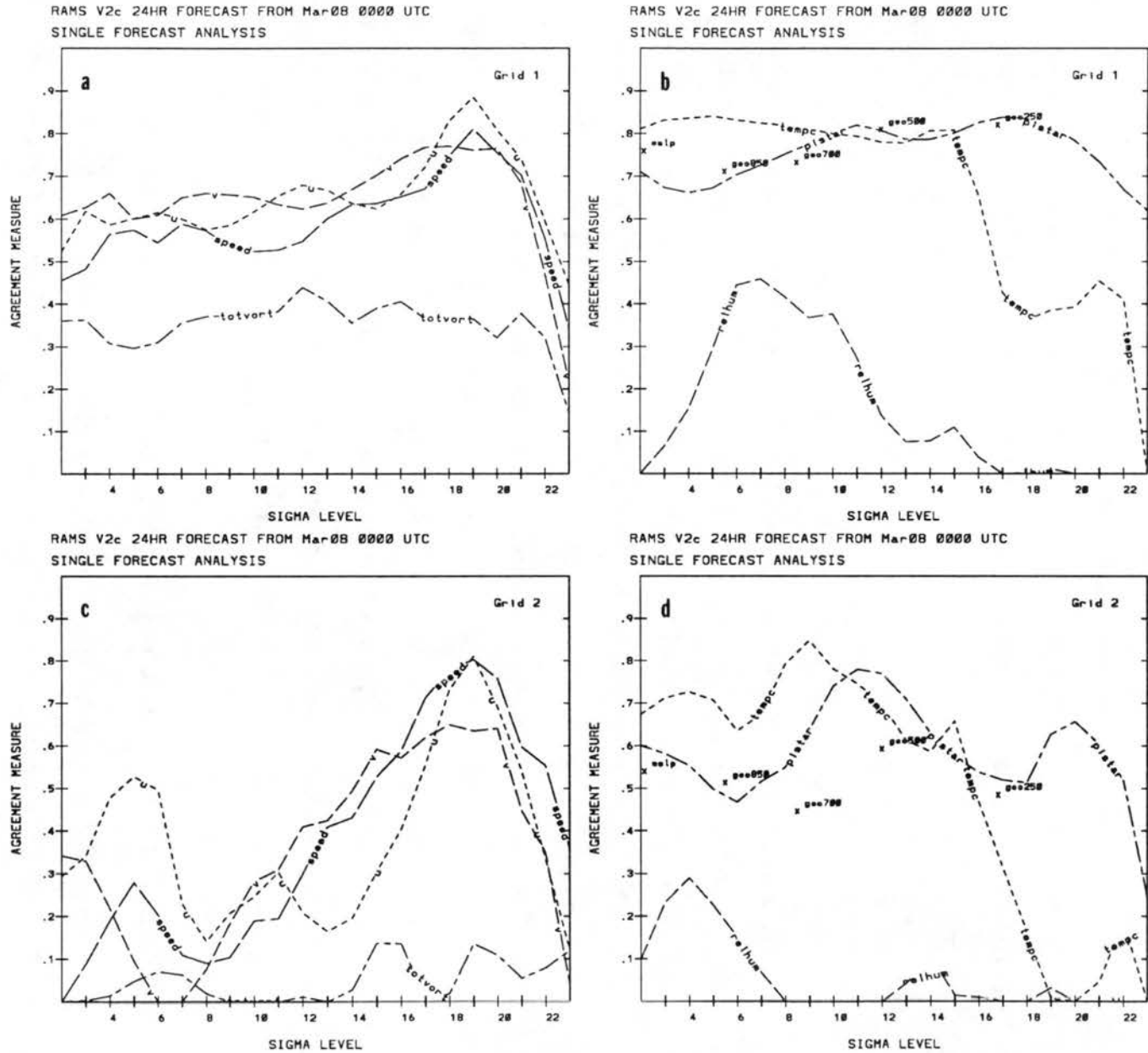


Figure 5.5: MRBP results for a single RAMS 24-hour forecast from sensitivity run V2c beginning 0000 UTC 8 March, 1992, otherwise same as Figure 5.1

Results of MRBP analysis of simulation NEW2c

Next, compare this figure with Figure 5.6 which shows an analysis of the NEW2c RAMS forecast. Both analyses are made using a RAMS 24-hour forecast begun at the same time yet the NEW2c analysis shows dramatic improvements in agreement measure. In particular, notice the increase in grid 1 near-surface relhum agreement from 0% to 50%. Improvement is even greater for grid 2 as relhum agreement increases throughout the entire lower half of the troposphere. Also improving dramatically is the wind-related variables on grid 2. These variables have the largest impact on Colorado snowstorms so their accurate prediction is of utmost importance for predicting the amount and locations of snowfall. Unfortunately, the strong performance of the relhum variable did not continue for grid 2 at 36 hours. Figure 5.7d shows the decrease in agreement as values drop to below 10% that were previously near 60%. This may be attributable to the crude precipitation scheme since the majority of the precipitation occurred between 24 and 36 hours.

To help demonstrate the relationship between the statistical agreement measure and an actual application, a RAMS 24-hour forecast of grid 2 mean sea-level pressure and wind vectors is shown in Figure 5.8a and the 0-hour forecast used as the verification is shown in Figure 5.8b. MRBP results shown in Figure 5.6 indicated that grid 2 mslp had an agreement measure of 62% and grid 2 u- and v-wind components at $\sigma=2$ have agreements of 56% and 58%, respectively. These values were obtained by applying MRBP analysis to the data represented in Figure 5.8 and give an illustration of this measure as it is discussed throughout this chapter.

Results of MRBP analysis of simulation MICRO

To see the impact that the addition of microphysics has on statistical agreement, compare Figures 5.9 and 5.6. Figure 5.9 shows the MICRO statistical analysis and exhibits only small variations in agreement for variables on grid 1. However, grid 2 agreement has dropped for all variables except wind-related ones where slight improvements are noticeable. Relhum also shows an improvement near the surface but somehow exhibits less accuracy at mid-levels. Relhum agreement does, however, improve again near $\sigma=18$ and this improvement was discussed in Chapter 4 (recall discussion of Figure 4.16). The decreases in

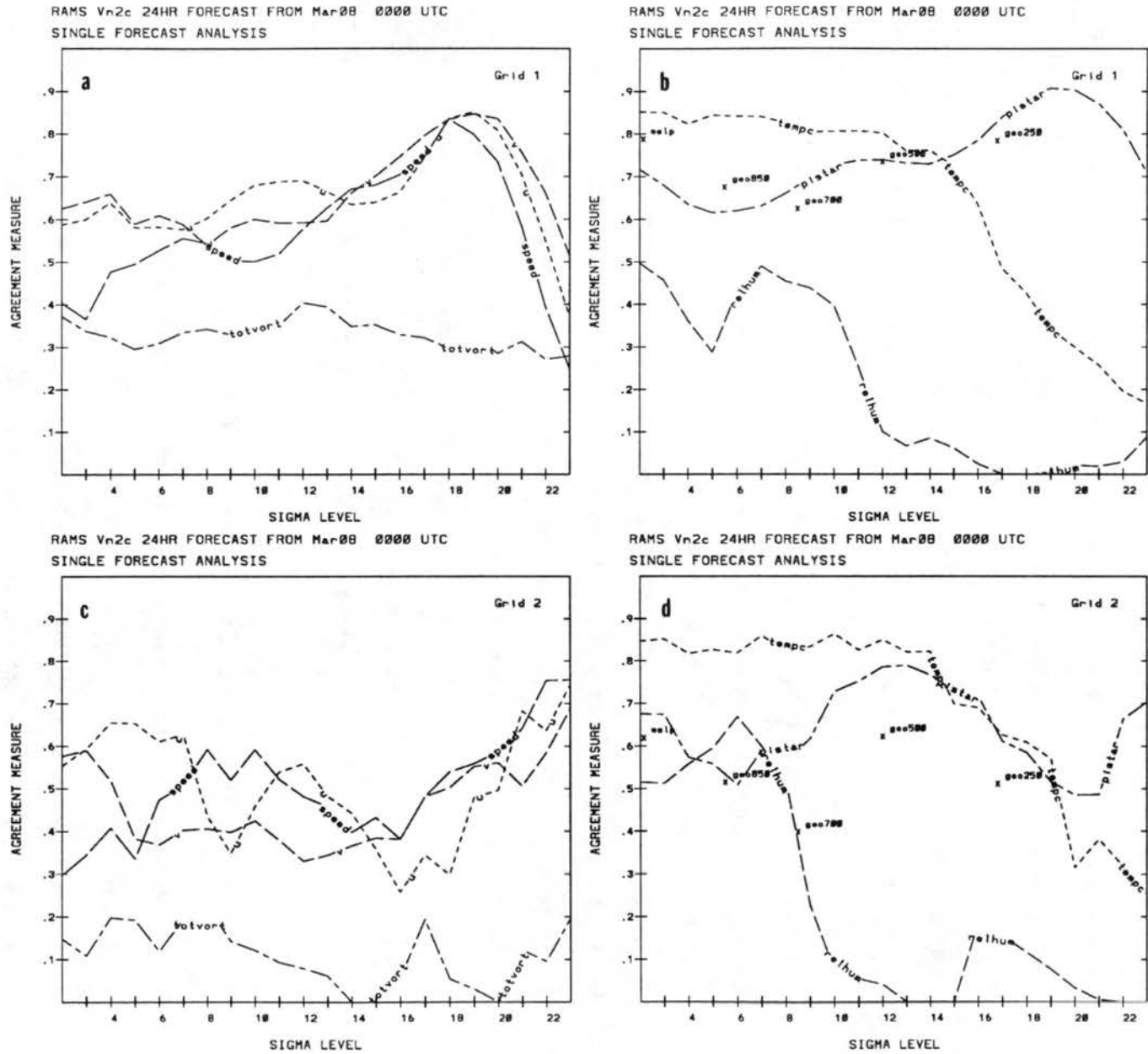


Figure 5.6: MRBP results for a single RAMS 24-hour forecast from sensitivity run NEW2c, otherwise same as Figure 5.5.

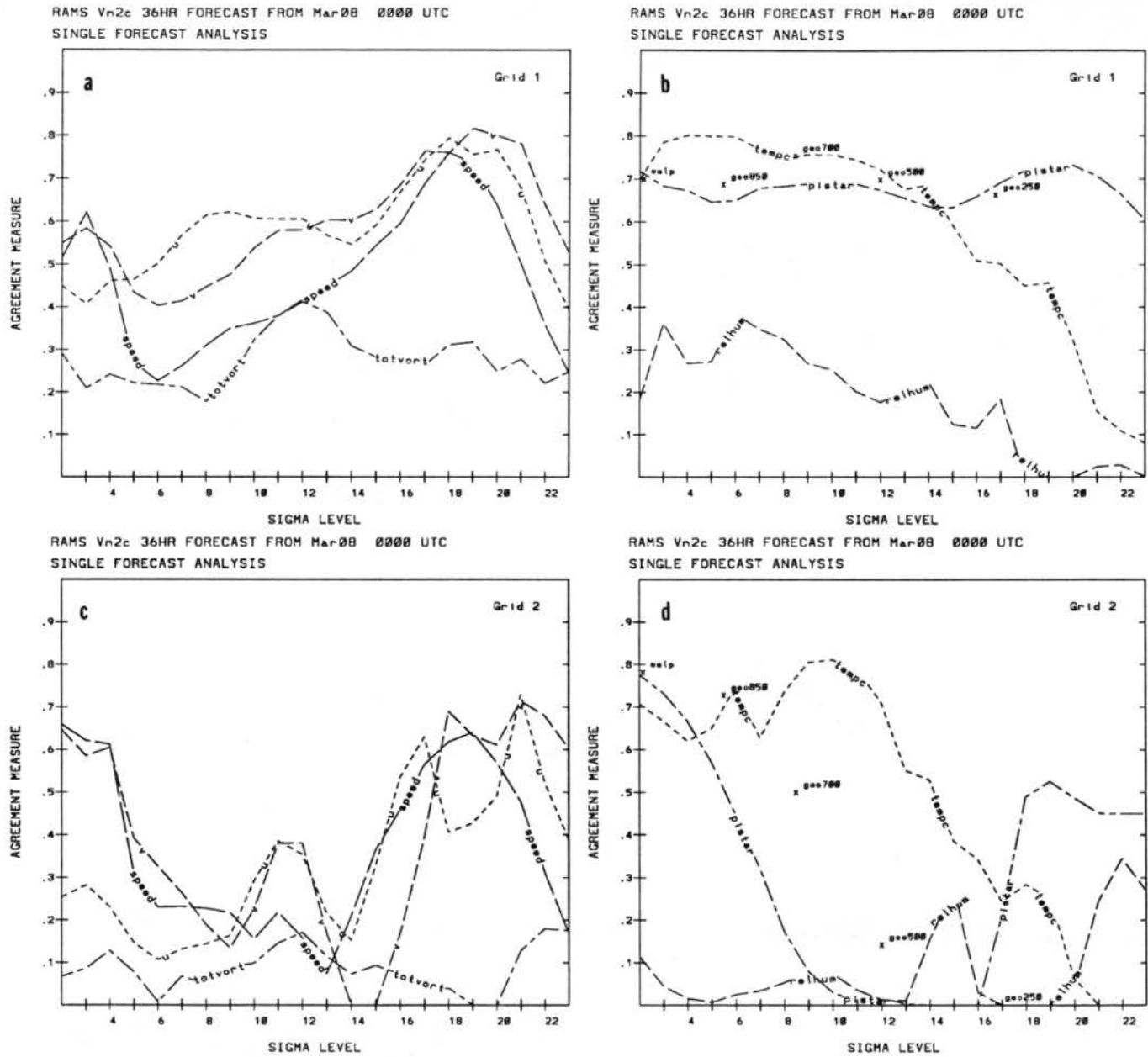
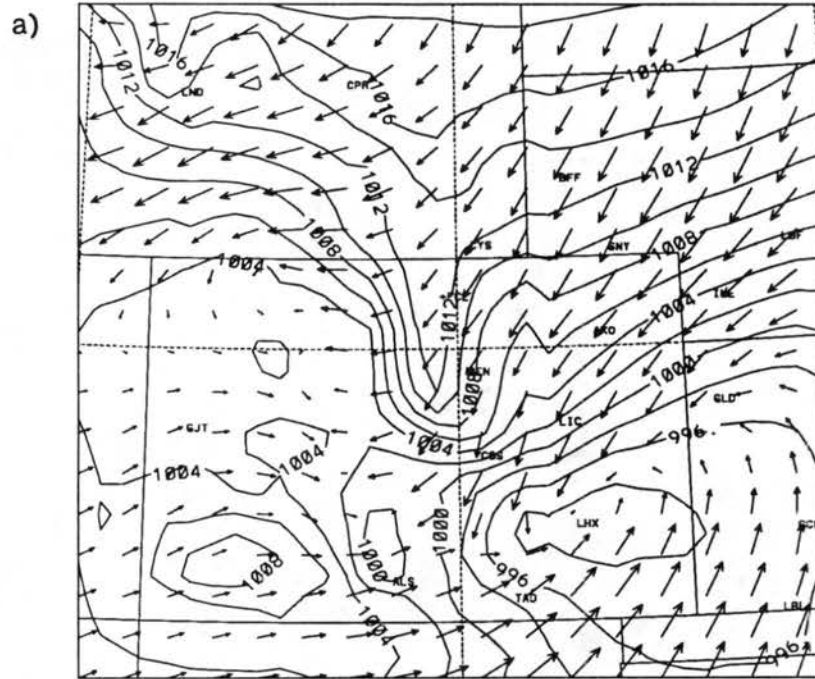
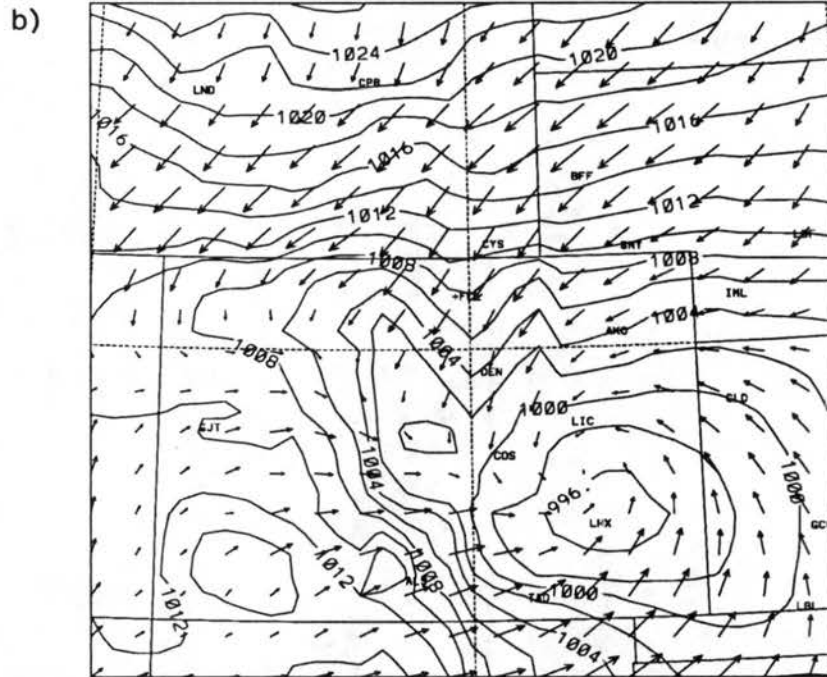


Figure 5.7: MRBP results for a single RAMS 36-hour forecast from sensitivity run NEW2c, otherwise same as Figure 5.6.



REDUCED MSLP (mb)
24HR FCST VALID 0000 UTC 03/09/92



REDUCED MSLP (mb)
00HR FCST VALID 0000 UTC 03/09/92

Figure 5.8: RAMS grid 2 mean sea-level pressure (mb) with wind vectors valid 0000 UTC 9 March, 1992 a) 24-hour forecast and b) 0-hour forecast.

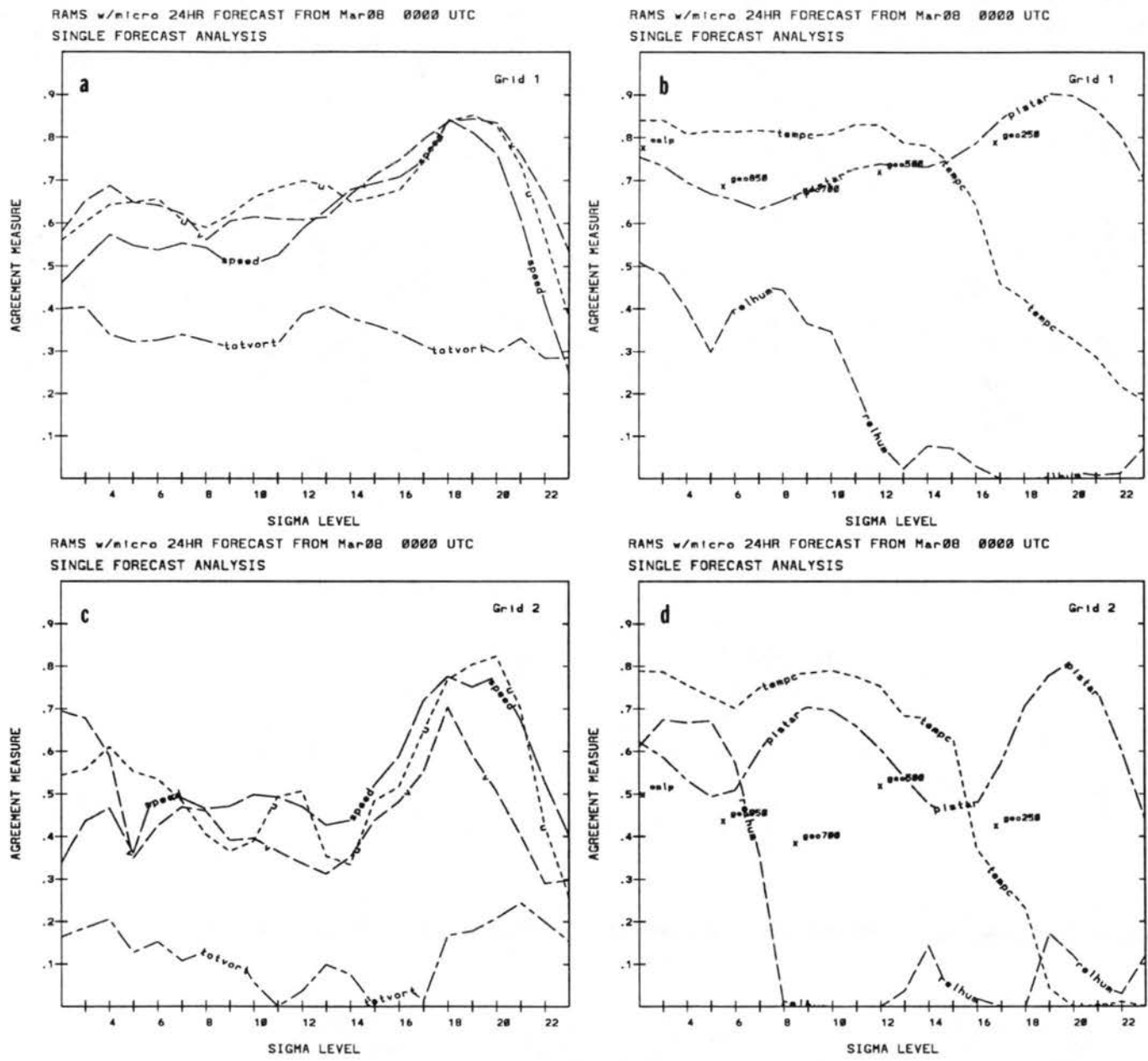


Figure 5.9: MRBP results for a single RAMS 24-hour forecast from sensitivity run MICRO, otherwise same as Figure 5.7.

agreement are not too large and, had a statistical analysis of precipitation been performed, the addition of microphysics would show large increases in model accuracy for the precipitation field. Comparisons of the 36-hour MICRO forecast with the NEW2c 36-hour forecast showed only minor statistical differences; however, the relhum variable in the MICRO simulation did have higher agreement possibly indicating that the crude precipitation scheme causes poor relative humidity forecasts.

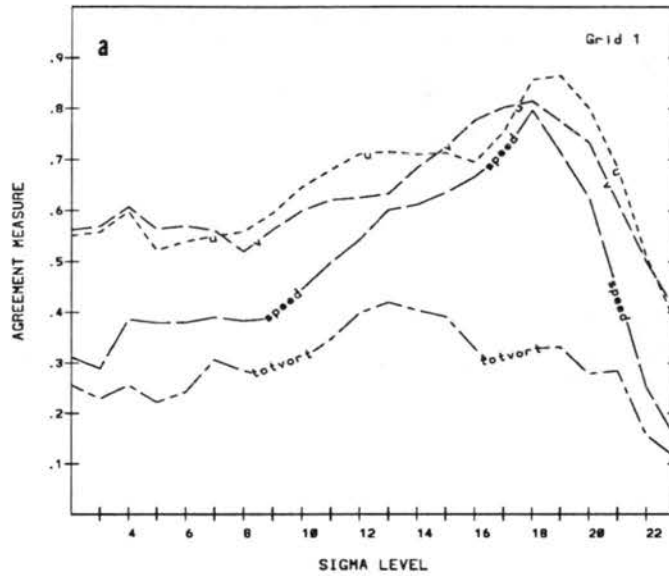
Results of MRBP analysis of simulation LBC-ETA

Analysis of the LBC-ETA sensitivity study showed general decreases in agreement when compared with the NEW2c simulation. Recall that the LBC-ETA study refers to the RAMS forecast that used the ETA model forecasts to nudge the lateral boundaries. Figure 5.10 presents the 24-hour LBC-ETA MRBP analysis and Figure 5.11 presents the 36-hour LBC-ETA analysis. Both forecast analyses show similarities with the NEW2c forecast analyses, but agreements are generally lower. One exception to this is the 36-hour grid 2 relhum comparison. The LBC-ETA analysis shows higher agreement for grid 2 relative humidity than the NEW2c analysis (compare Figures 5.11d and 5.7d). It was stated in Chapter 4 that a better relative humidity vertical resolution data set was needed for the lateral boundary nudging. The ETA data sets did provide this increased resolution and apparently agreement has increased, although isolation to this factor alone is not feasible. Nonetheless, more forecasts using this configuration are necessary before determining that the ETA model provides an unacceptable decrease in model accuracy. It is thought that perhaps this example reflects poorly on the ETA model; however, this certainly cannot be ascertained from just this one example.

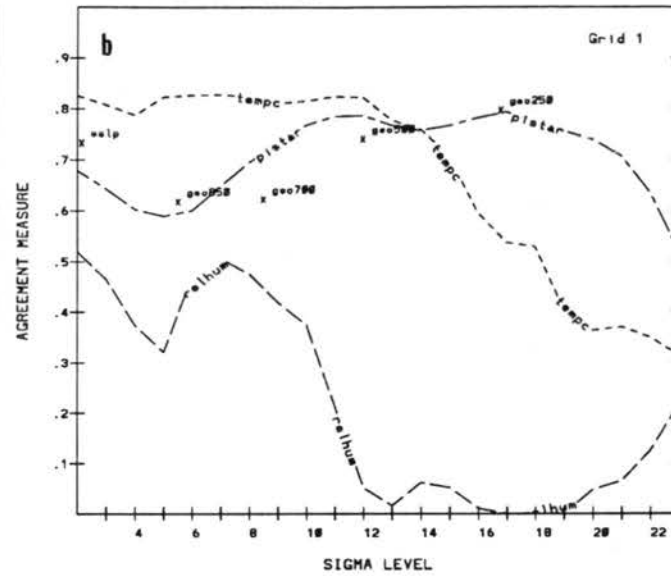
Discussion

From the results of these MRBP analyses on the 8-9 March sensitivity studies, it appears as though the NEW2c model configuration provided the highest overall accuracy. Certain improvements, however, were achieved by both the addition of microphysics and the use of ETA model forecasts for lateral boundary conditions. In particular, better relative humidity forecasts resulted from each of these variations. Perhaps a model run

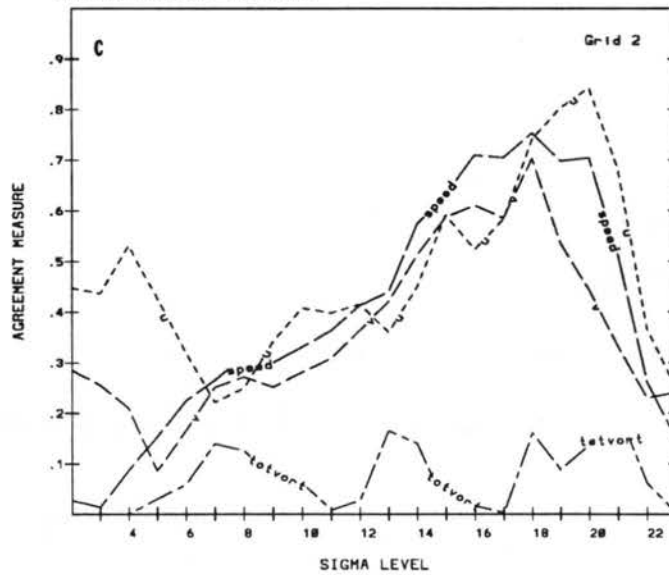
RAMS w/eta 24HR FORECAST FROM Mar-08 0000 UTC
SINGLE FORECAST ANALYSIS



RAMS w/eta 24HR FORECAST FROM Mar-08 0000 UTC
SINGLE FORECAST ANALYSIS



RAMS w/eta 24HR FORECAST FROM Mar-08 0000 UTC
SINGLE FORECAST ANALYSIS



RAMS w/eta 24HR FORECAST FROM Mar-08 0000 UTC
SINGLE FORECAST ANALYSIS

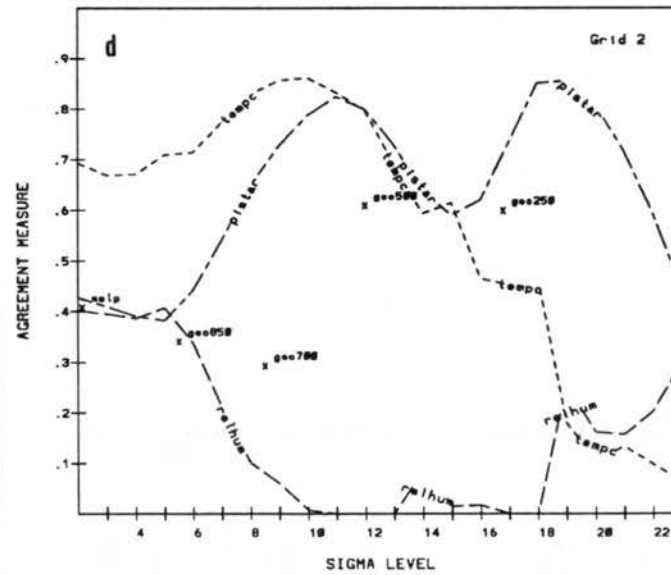


Figure 5.10: MRBP results for a single RAMS 24-hour forecast from sensitivity run LBC-ETA, otherwise same as Figure 5.9.

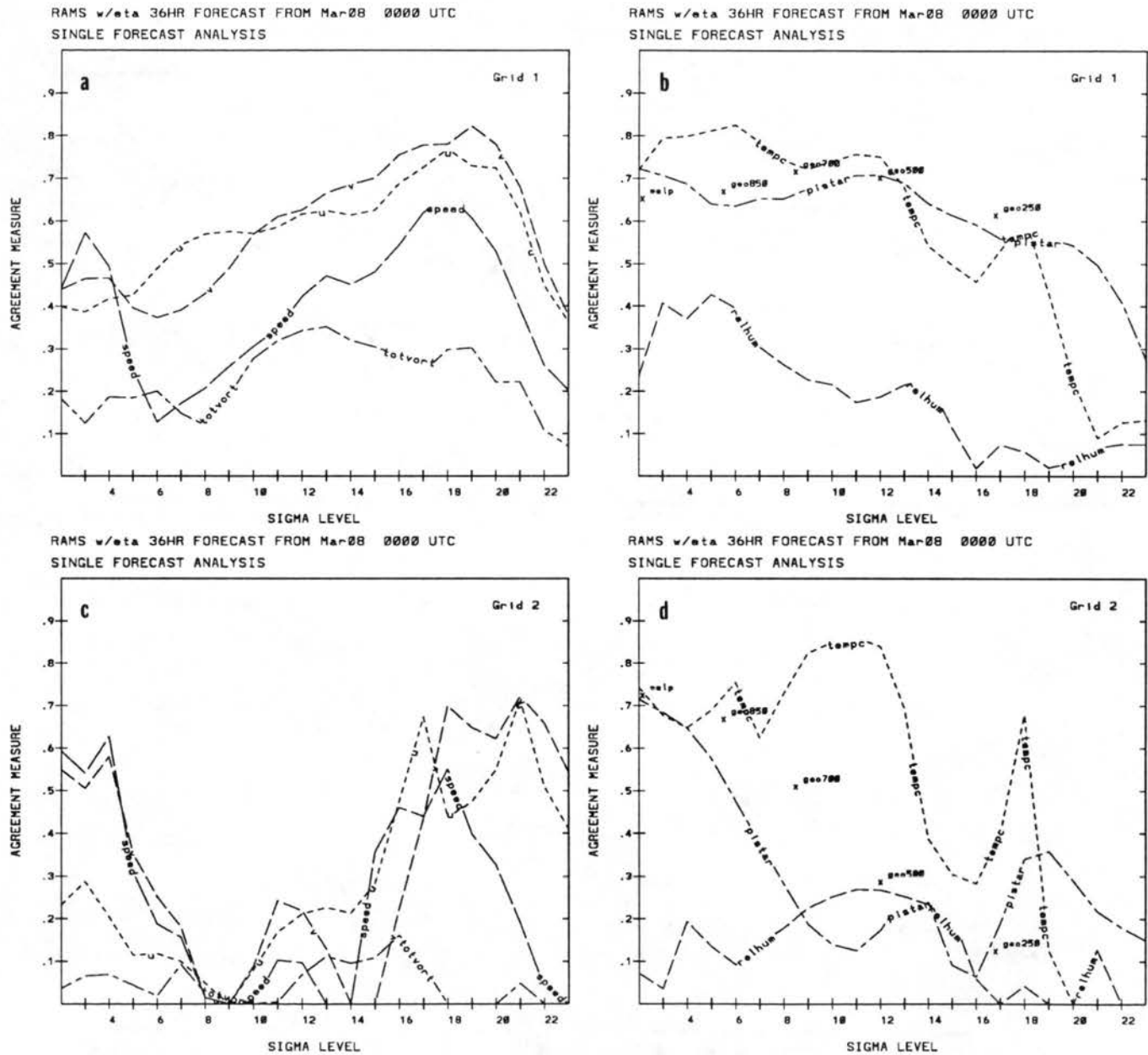


Figure 5.11: MRBP results for a single RAMS 36-hour forecast from sensitivity run LBC-ETA, otherwise same as Figure 5.7.

using aspects of all three variations, version new 2c code, microphysics option, and ETA boundary nudging, could produce the highest accuracy in the relative humidity field.

Comparison of RAMS, NGM and ETA model performance

Statistical analyses were also performed on the NGM and ETA numerical models to determine if RAMS had higher accuracy in predicting features of the 8-9 March event. This was accomplished by interpolating the NGM and ETA forecasts to RAMS grid points. The NGM and ETA forecasts then were verified statistically against the same data sets which RAMS forecasts were verified against - the MAPS analyses interpolated to RAMS grid points. The interpolation step had already been performed in order to provide RAMS with lateral boundary information so this verification procedure was easily attainable. This procedure is important when interpreting results of a NGM statistical analysis; since 150 *km*-spaced NGM forecast products (recall Figure 3.3) are interpolated to 100 and 25 *km* grids. Also keep in mind the vertical resolution of the NGM data sets, since the verification occurs on twice as many vertical levels as the original data. For these reasons, comparisons of statistical agreement between RAMS forecasts and NGM forecasts must be viewed with a degree of skepticism. The ETA model, on the other hand, provided a good statistical data set; since output was provided at 80 *km* grid increments and 19 vertical levels from 1000 to 100 *mb*. Therefore, comparisons of statistical agreement between RAMS forecasts and ETA forecasts are more trustworthy.

Results of the 24- and 36-hour NGM forecast analyses are shown in Figures 5.12 and 5.13. Again, these forecasts were taken from the 0000 UTC 8 March simulation and are valid at 0000 UTC and 1200 UTC 9 March respectively. Comparing these figures to previous ones showing RAMS statistical agreements, we see some common characteristics. For instance, panel a of Figures 5.12 and 5.6 exhibit increasing agreement with height for variables *u*, *v* and speed until the tropopause. Common trends are also evident in the other panels. Generally speaking, RAMS statistical agreement is higher than the NGM although certain variables on certain levels do reflect higher agreement for the NGM forecasts. The grid 1 *pistar* and grid 2 *relhum* curves show higher accuracy in the RAMS model whereas the grid 2 *v* curve indicates higher accuracy at mid-levels for the NGM model. The 36-hour

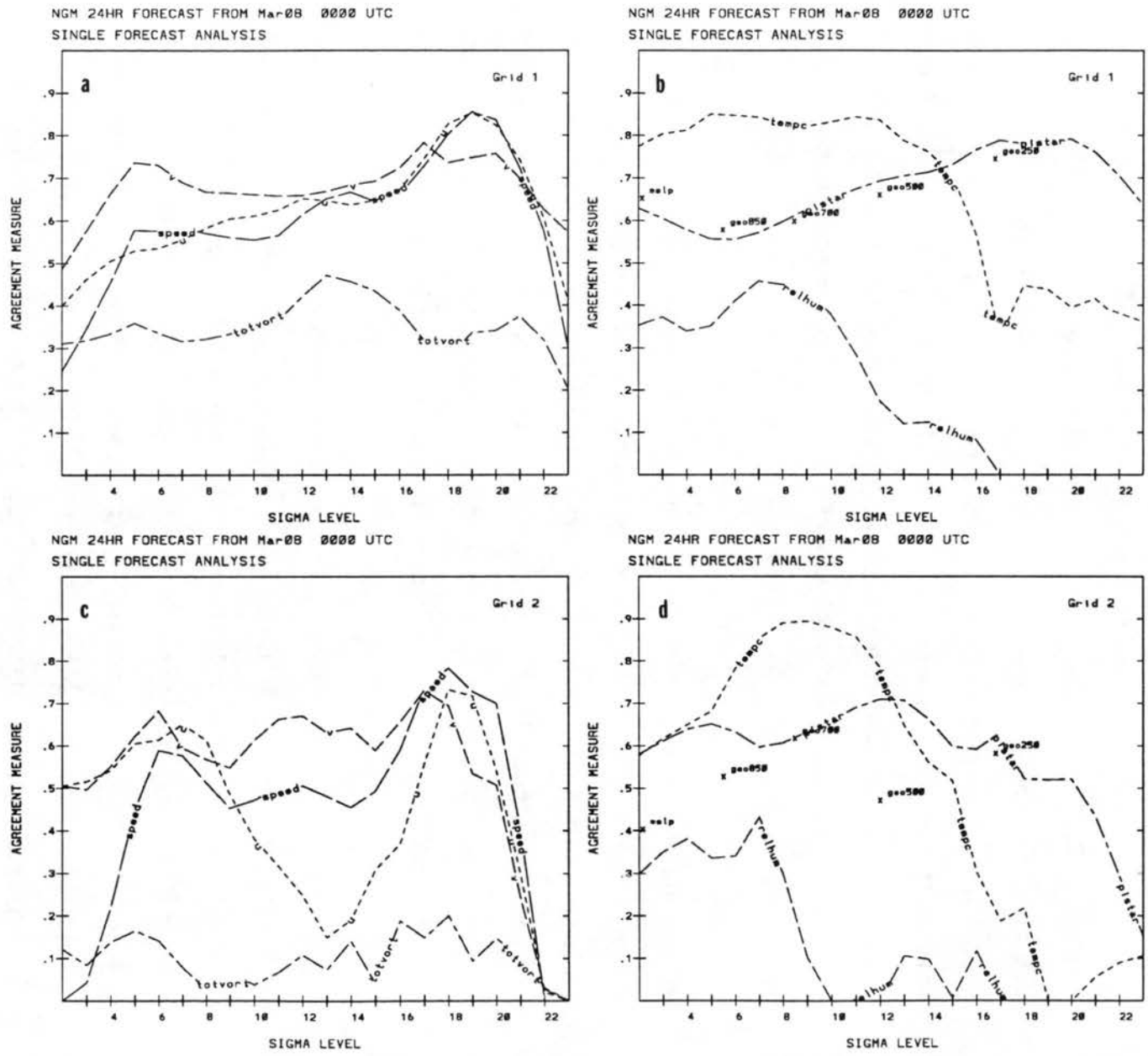


Figure 5.12: MRBP results for a single NGM 24-hour forecast beginning 0000 UTC 8 March, 1992, otherwise same as Figure 5.6.

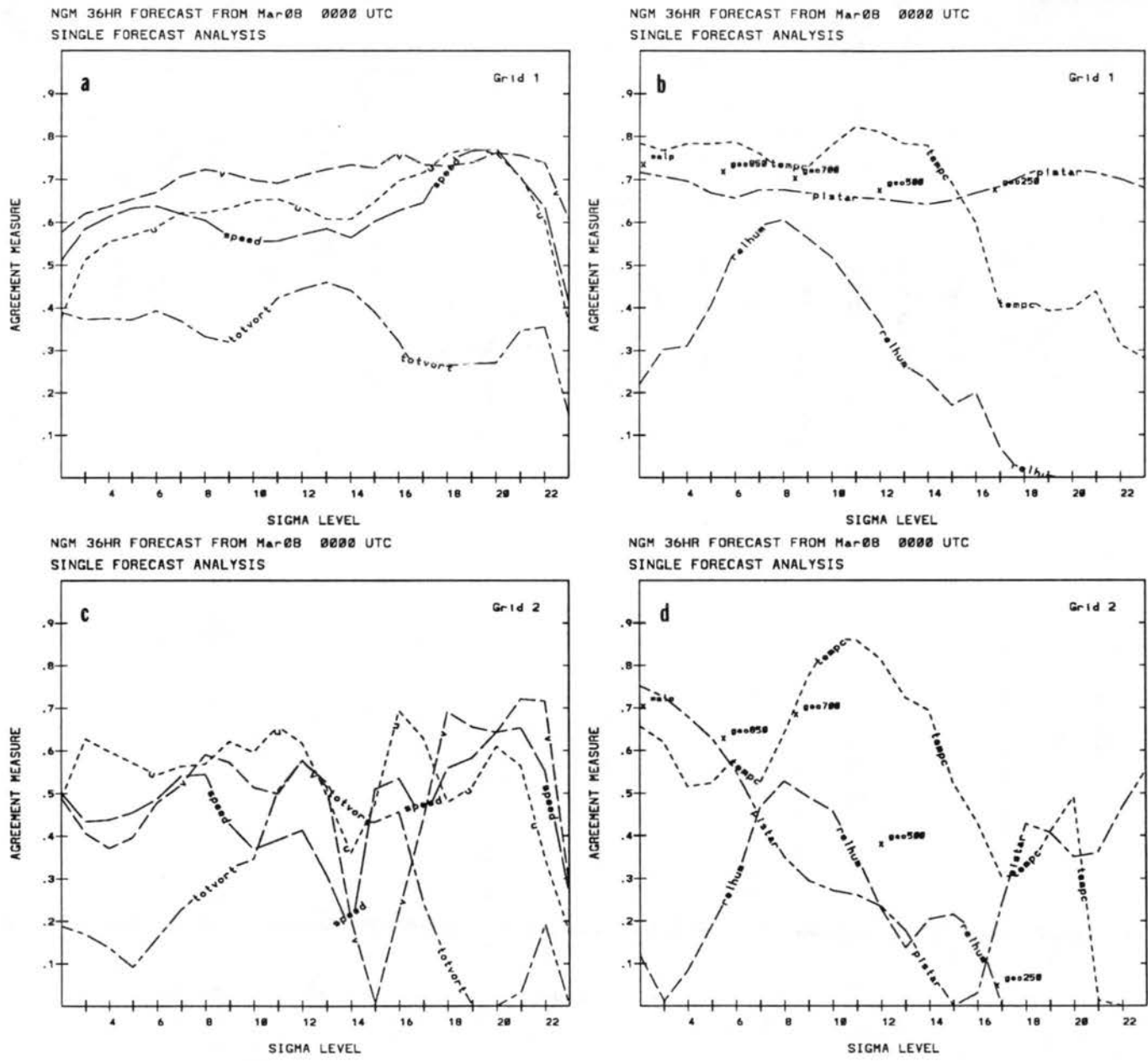


Figure 5.13: MRBP results for a single NGM 36-hour forecast beginning 0000 UTC 8 March, 1992, otherwise same as Figure 5.7.

forecast analysis, on the other hand, indicates many parameters that were forecast better by the NGM model. This is evident when comparing Figures 5.13 and 5.7. Notice the relhum curves for both grids show higher agreement in Figure 5.13 than Figure 5.7. Other variables show similar improvements in agreement measure.

Comparisons can also be made between the RAMS statistics and ETA statistics. The results of the 24- and 36-hour ETA forecast analyses are presented in Figures 5.14 and 5.15. The ETA model statistics reflect the identical trends and characteristics as the NGM model statistics did in the two previous figures; indicating that perhaps the resolution and interpolation procedures involved with the NGM do not produce unrealistic results. Since the NGM and ETA analyses contain common trends, comparing the ETA statistics with RAMS statistics presents the same discussion of each model's strengths and weaknesses. One interesting feature when comparing the ETA and NGM analyses is that the ETA analysis shows higher correlation for the 24-hour forecast, yet the NGM analysis generally indicates higher correlation for the 36-hour forecast. The biggest conclusion drawn from all these statistical analyses of the 8-9 March case is not a surprising one: each model exhibits particular strength and weaknesses.

5.4.3 MRBP analysis of a 23 November 1992 forecast

As an additional comparison between RAMS and NGM model performance, a 36-hour forecast from 23 November 1992 was analyzed. This forecast was chosen because a snowstorm again affected the Colorado Front Range, this time producing near-blizzard conditions. Many Denver weather forecasters placed heavy emphasis on the NGM model output and, therefore, predicted blizzard conditions of strong winds and heavy snowfall. RAMS model output, though, indicated that the storm would take a slightly different track thereby reducing the severity of the storm in the Front Range region.

The statistical analysis of the RAMS forecast is shown in Figure 5.16 and the NGM statistics are shown in Figure 5.17. Through comparison of these two figures, it is obvious that RAMS has higher agreement measure for all variables except grid 2 relhum, geo700 and geo500. In fact mslp on grid 2 is shown to have 30% higher agreement in the RAMS statistical analysis. The grid 2 relhum curve shows lower agreement in RAMS than the

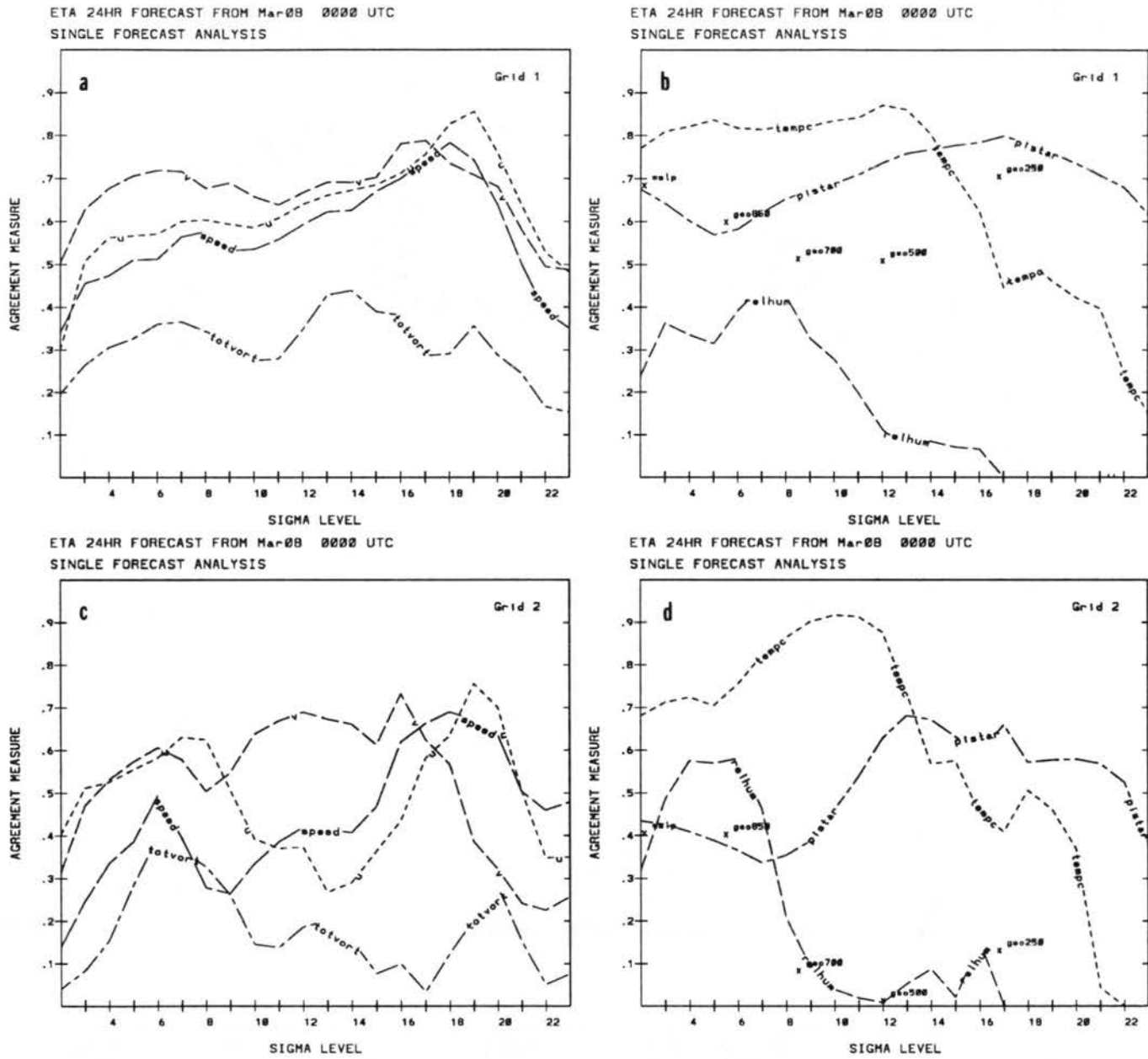


Figure 5.14: MRBP results for a single ETA 24-hour forecast beginning 0000 UTC 8 March, 1992, otherwise same as Figure 5.12.

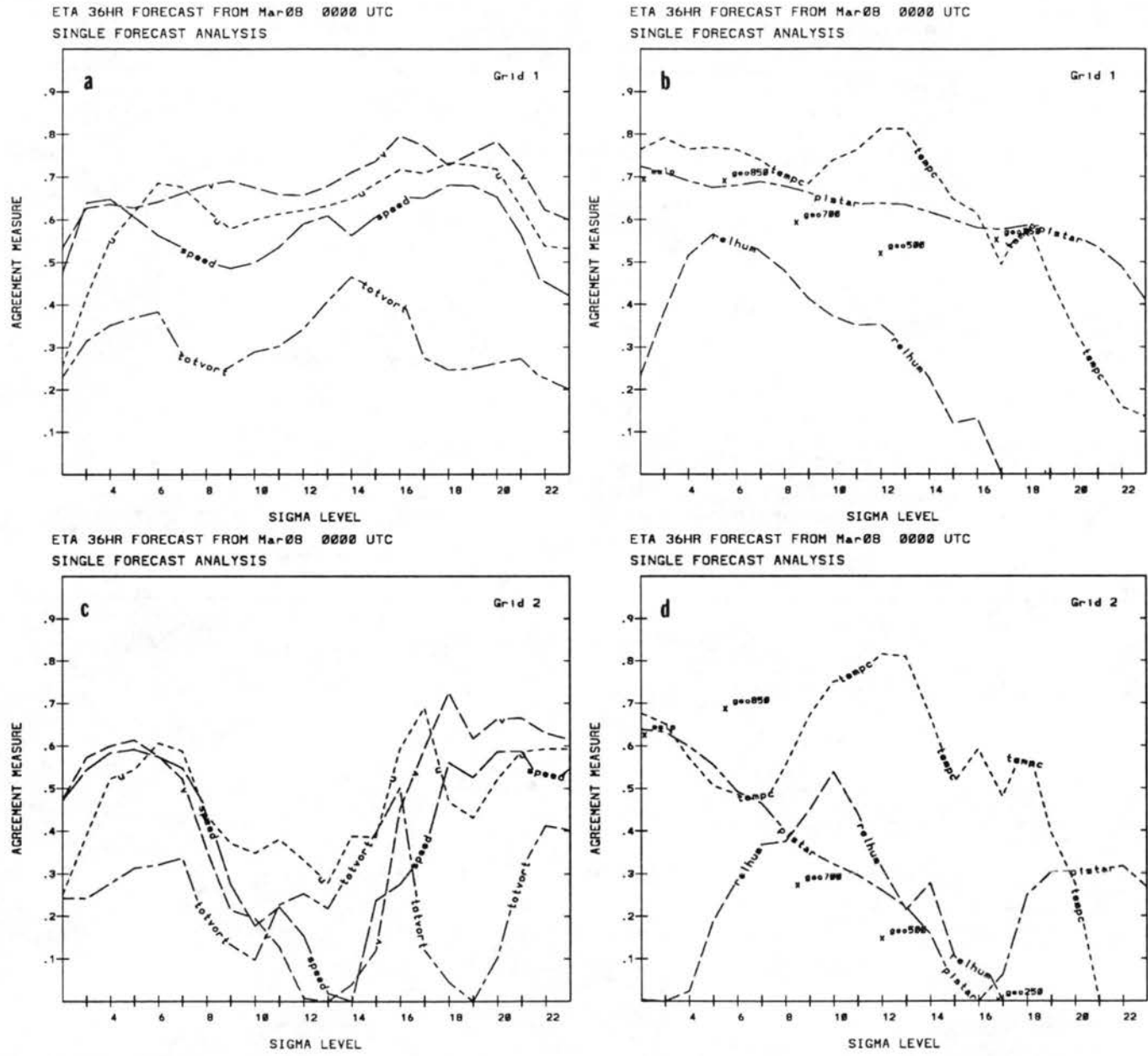


Figure 5.15: MRBP results for a single ETA 36-hour forecast beginning 0000 UTC 8 March, 1992, otherwise same as Figure 5.13.

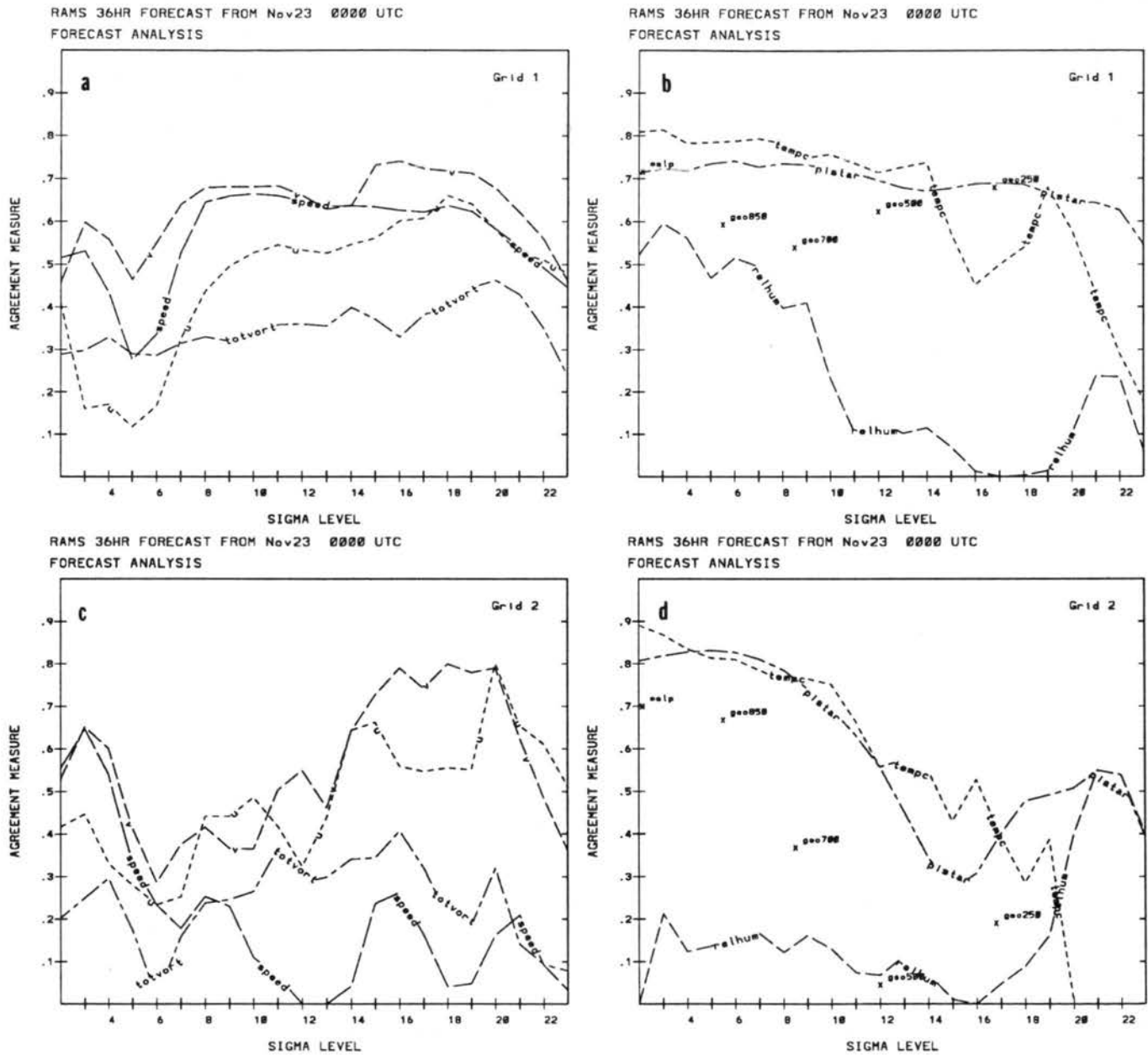


Figure 5.16: MRBP results for a single RAMS 36-hour forecast beginning 0000 UTC 23 November 1992, otherwise same as Figure 5.7.

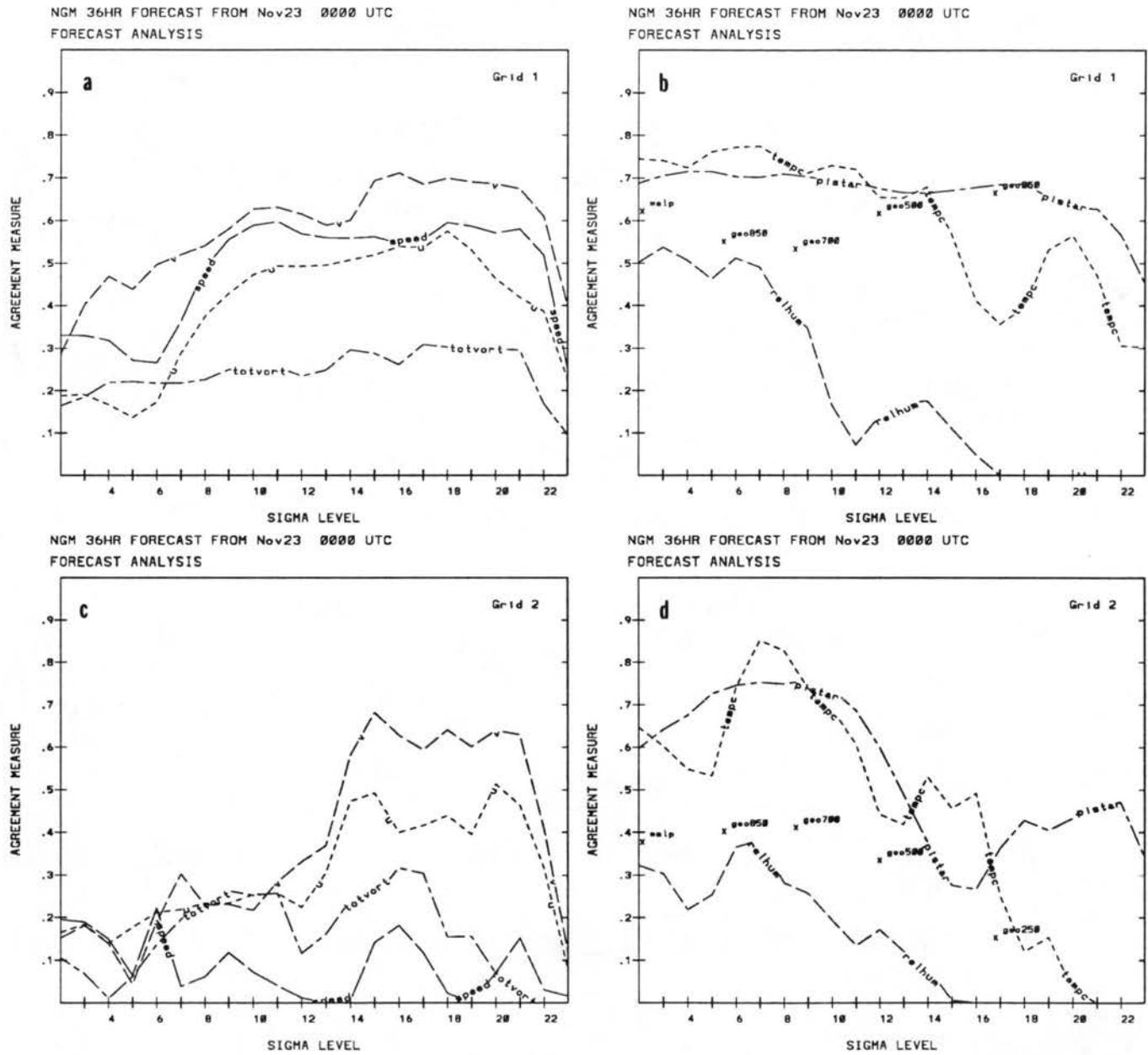


Figure 5.17: MRBP results for a single NGM 36-hour forecast beginning 0000 UTC 23 November 1992, otherwise same as Figure 5.16.

NGM and may be a result of the crude precipitation scheme. All other curves clearly show that RAMS has higher agreement with observations.

5.4.4 26 November FIRE II case study

The last analysis shown here is the MRBP statistics of the 26 November FIRE II case study discussed in the previous chapter. Figure 5.18 shows the results of the statistics for the 18-hour RAMS forecast from 0000 UTC 26 November 1991. These plots reflect only the upper-troposphere agreement as the first plotted sigma level is 15, which corresponds to roughly 4.3 *km* above ground level. Again, the same trends are indicated as tempc and pistar show the highest agreement, and relhum and totvort reflect lower agreements. Comparing this to the NGM 18-hour forecast analysis shown in Figure 5.19, we see that the two analyses differ very little on grid 1 (panels a and b) and have small variations in the wind-related variables on grid 2, hence, neither model showed any strengths over the other. Also shown in these figures is that the relative humidity agreement drops off quickly near the tropopause which is not surprising since the NGM data sets had no relative humidity information above 300 *mb* and RAMS was nudged using these data sets, so it too reflected poor agreement near these levels. Unfortunately, observational data of cloud mixing ratio or microphysical species concentration was unavailable so statistical agreement of these variables could not be included. Otherwise, the agreement in the model results shown in Chapter 4 could be demonstrated.

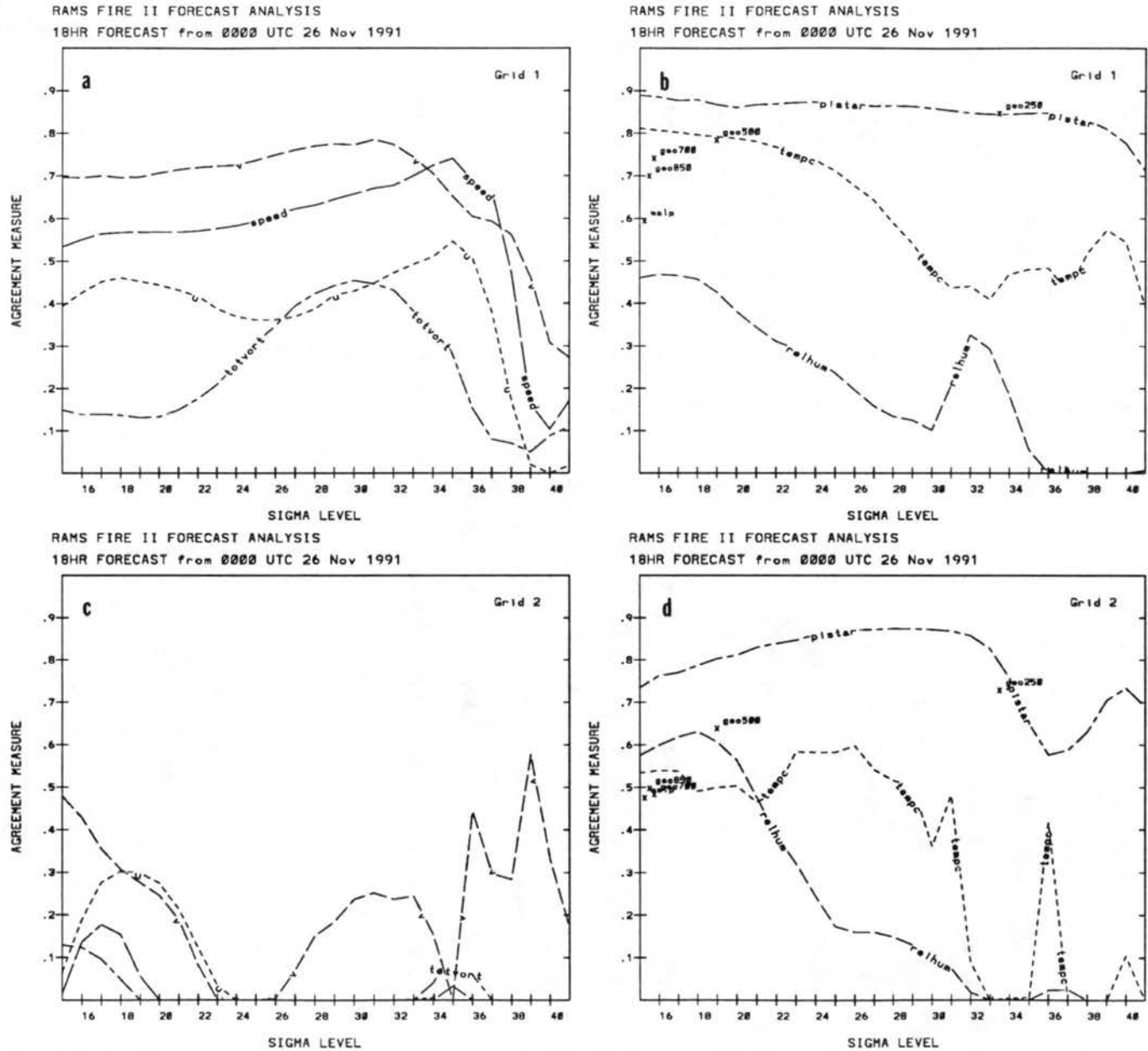


Figure 5.18: MRBP results for a single RAMS 18-hour forecast beginning 0000 UTC 26 November 1991, otherwise same as Figure 5.16.

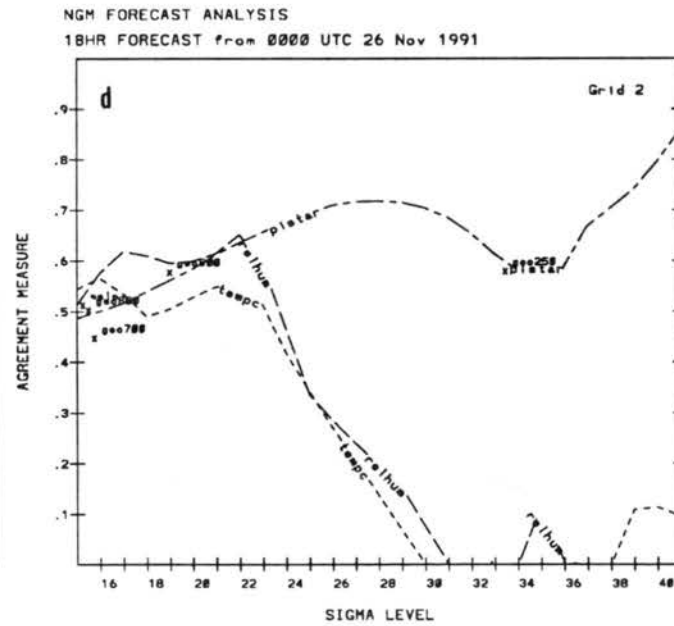
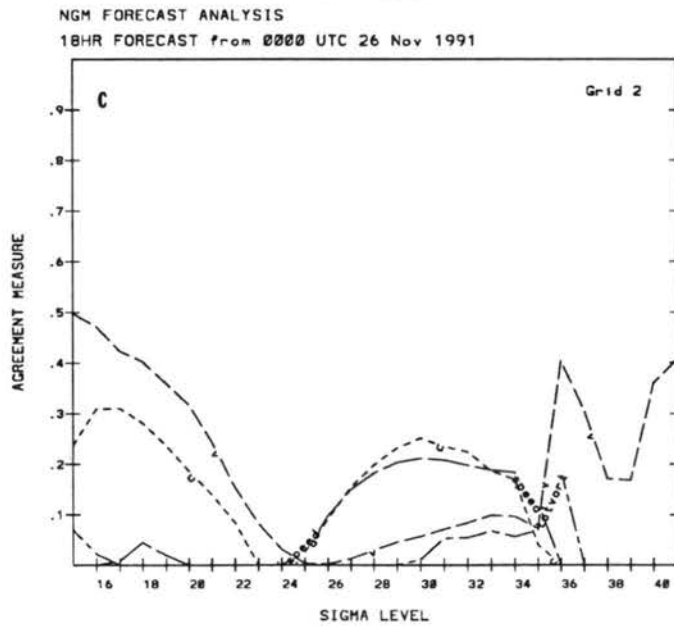
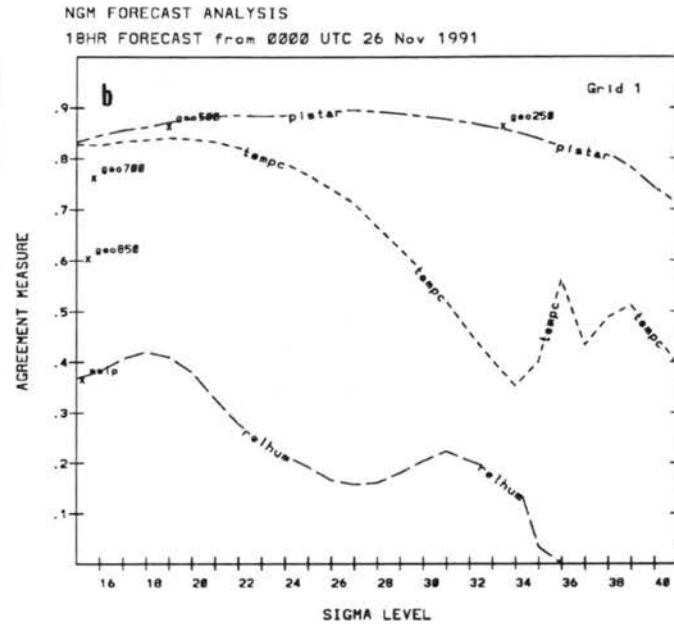
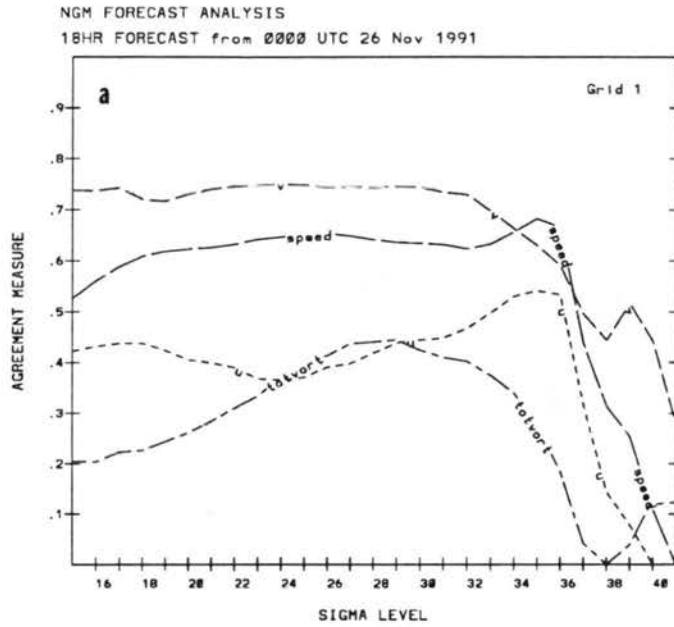


Figure 5.19: MRBP results for a single NGM 18-hour forecast beginning 0000 UTC 26 November 1991, otherwise same as Figure 5.17.

Chapter 6

SUMMARY AND CONCLUSIONS

6.1 Summary

This study first showed how the Regional Atmospheric Modeling System (RAMS) was modified to create a real-time forecast system. A new data source was used to initialize the RAMS model. The MAPS data set provided a superior initialization because of the 60 *km* grid spacing and the incorporation of aircraft reports and wind profiler data. The model's lateral boundary conditions were provided by the NGM forecasts instead of observations, creating a true forecast model. Previous RAMS modeling has shown the advantage of using a research mesoscale model to investigate case study applications, however, this study demonstrated how RAMS was adapted to perform daily real-time forecasting.

Once a real-time forecast system was achieved, RAMS was configured to satisfy two projects: predict wintertime orographic precipitation in Colorado and predict upper-level clouds in support of the FIRE Phase II field program. The Colorado investigation used a 100 *km* course grid increment over the western two-thirds of the U.S. and a 25 *km* fine grid covering Colorado and portions of bordering states. Real-time forecasting was performed once a day (initialized at 0000 UTC) on workstations at CSU with emphasis on predicting orographically-forced precipitation. The FIRE II investigation had a similar course grid domain with 80 *km* spacing and a fine grid with 20 *km* grid increments covering Kansas. Real-time RAMS prediction corresponded with the duration of the program, 13 November to 6 December, and was carried out on a CRAY Y-MP at NCAR. Not only did the increased speed and power of the CRAY allow for finer grid spacing but also the inclusion of RAMS' most complex precipitation physics. The Colorado experiment, on the other hand, relied on a crude precipitation scheme whereby all supersaturation was removed from the atmosphere and translated to the ground as precipitation. All other microphysical processes

were neglected because of time constraints. RAMS FIRE II forecasts were produced daily with emphasis on the prediction of upper-level clouds to support the forecasting products available to scientists at the Coffeyville, Kansas research site.

Within the discussions of these two experiments, a case study from each was analyzed to assess the effectiveness of incorporating real-time RAMS forecasts into already established operational numerical model output. In particular, RAMS demonstrated its ability to accurately predict mesoscale features by comparing forecasts of the 8-9 March 1992 Colorado Front Range blizzard with observations; and also by comparing forecasts of upper-level cloud features for the 26 November 1991 FIRE II case study day against observations. Also shown in this section was how RAMS forecasts were tailored to serve the needs of FIRE II field investigators, particularly mixing ratios and concentration of microphysical species such as pristine ice crystals. No other operational model available provided these specific forecast products.

The comparisons with observations mentioned above were not only performed in the usual manner of presenting forecast maps and observational data maps but also statistically. The statistical analysis performed in this study utilized multivariate randomized block permutation methods (MRBP). MRBP statistical procedures were chosen over more well-known methods because MRBP satisfies three critical criteria:

- the analysis space should correspond with the space in which the data exist
- the assumed distribution for the test statistic should correspond to the error distribution of the model data
- the testing procedure should assess the probability that a predicted pattern could occur by chance alone while providing a quantitative measure of forecast skill.

Commonly-used methods such as the Student's t-test, correlation coefficients, threat scores and bias scores do not adhere to all three criteria and therefore are inappropriate for use in model verification.

The MRBP analyses confirmed suspicions of particular strengths and weaknesses of the model. Some of the model strengths were:

- forecasts of temperature and perturbation Exner function
- forecasts of geopotential heights
- forecasts of wind-related variables such as u- and v-wind components and speed.

While weaknesses included the following:

- forecasts of surface temperatures
- forecasts of mean sea-level pressure
- forecasts of relative humidity especially those with the crude precipitation scheme
- forecasts of precipitation amounts without using the microphysics option.

These model strengths and weaknesses are not unlike many other numerical models. Improved boundary layer parameterizations and surface interactions will undoubtedly improve forecasts of surface temperatures and moisture.

6.2 Conclusions

With today's faster, more powerful computers, rather complicated, high resolution model configurations can be run in real-time. More importantly, a real-time forecast system using two interactive nested grids and non-hydrostatic code can be attained on workstations for a very reasonable price. A super-computer such as a CRAY provides increased capabilities such as finer grid spacing and microphysics but current workstations provide an adequate platform for a real-time forecast system.

Two major problem areas were obvious throughout most of the 1991-92 winter season. The first problem related to the precipitation scheme utilized. The crude "dump bucket" method did not consider fundamental atmospheric processes such as latent heat release, evaporation of cloud water or precipitation or inclusion of an ice phase. This resulted in poor relative humidity forecasts as well as inaccurate forecast precipitation. The addition of microphysics improves these features yet cannot maintain the real-time operating constraints on the workstations available during this study. A new microphysics code, however,

is currently being implemented and is nearly ten times faster than the code used here. The addition of microphysics to the 8-9 March case study showed marked improvement in forecast precipitation, surface winds and position of the surface cold front. The latter two improvements may have resulted from the additional upward motion caused by latent heat release thereby producing stronger surface convergence.

The other major problem area was with surface temperature forecasts. Discrepancies were due to the radiation scheme used, which did not include cloud effects explicitly. This resulted in inaccurate parameterizations of net long- and short-wave radiative fluxes reaching the surface. The more complete radiation option available in RAMS caused the model to run much slower. Therefore, a scheme which includes cloud effects yet remains computationally inexpensive is necessary to correct this problem. Fortunately, a new, faster, "two-stream" radiation scheme is currently being implemented and will soon be available to the real-time RAMS forecast system.

An associated problem to the surface temperature discrepancies is the low-level relative humidity agreement. Recall that every statistical analysis showed lower agreement of surface relative humidity than the level just above. This may be due to the initialization of the soil model. Soil model temperature and moisture profiles are initialized based on the temperature and moisture (relative humidity) of the atmospheric level in contact with the soil. Sensitivity simulations performed on the initialization method showed dramatic differences in lower atmosphere thermodynamic profiles. Ideally, accurate soil model initialization will contribute to increased statistical agreement; however, real-time measurements of these parameters are currently non-existent, making this task difficult.

Not only are improvements necessary in the soil model initialization, but also in the surface characteristics in general. Non-homogeneous soil type, vegetation cover, albedo and roughness length could improve forecasts of boundary layer thermodynamic information. Furthermore, the inclusion of a snow model would also aid in these forecasts. This is yet another area of the RAMS model which is currently under development at Colorado State University.

The FIRE II case study analysis showed how RAMS can be configured to satisfy the requirements of scientists involved with field programs. Not only did the horizontal and

vertical grid spacing need attention, but specific forecast products such as microphysical species concentration needed attention as well. This case study certainly shows how RAMS can be adapted to serve as an additional forecast tool for a field program and it is hoped that the opportunity will emerge again.

Conclusions from the MRBP statistical analysis are as follows: the analyses of the whole season confirmed suspicions that temperature and relative humidity forecasts have less accuracy near the surface than levels just above; mean sea-level pressure was predicted with less accuracy than 500 *mb* geopotential heights; and as expected, forecast agreement decreases with length of forecast.

Another conclusion drawn from the MRBP analyses is that MRBP can provide a powerful tool for improving the model. Modifications to the model code such as including the effects of "pseudo clouds" and a parameterized vegetated surface caused marked increases in agreement measure for nearly all meteorological variables analyzed. Further modifications such as the addition of microphysics and the use of ETA forecasts for lateral boundary nudging show that improvements can be attained after applying MRBP to the model results. Lastly, although MRBP showed that RAMS overall performed slightly better than the NGM model, it also highlighted some need for improvement as certain features were predicted with higher accuracy in the NGM.

6.3 Suggestions for Further Research

Areas for further research encompass two categories: the real-time forecast system and the additional applications of MRBP statistical procedures. Further research into the real-time forecast system should include the feasibility of including faster yet more complete microphysics and radiation schemes. Also, the addition of more representative surface characteristics and their impact on model performance should be investigated. Another area now being investigated is the inclusion of synoptic data into the initialization and four-dimensional data assimilation. Satellite and radar-derived products could be incorporated into the data assimilation process detailing precipitation regions, cloud information, rain rates and many others. Perhaps the inclusion of these products will result in enhanced moisture analysis.

There is a large number of potential real-time mesoscale forecast applications. RAMS could be extended to summer use where maximum/minimum temperatures, deposition of dew, evaporation/transpiration rates and quantitative precipitation forecasts could be investigated in real-time. Airports could use real-time RAMS forecasting to aid in prediction of ceilings, visibility, aircraft icing, turbulence and severe weather. These applications represent only the "tip of the iceberg". Future increases in computer power and code efficiency (parallel processing and multi-tasked code) will undoubtedly unleash this huge potential.

The other category for further research relates to statistical verification of mesoscale model data and has equal potential. MRBP is an excellent tool for showing statistical ramifications due to changes in model code. The need for finer resolution data sets against which model data can be compared is critical. Future MRBP analyses should investigate model performance through comparisons with comparable data scales. An area left untouched by this study was verification of precipitation and vertical motion. The intensive observations taken during the FIRE II program should provide an excellent database to compare vertical motions and microphysical species.

Lastly, MRBP could be used simultaneously on many meteorological variables (hence the name Multivariate) instead of one at a time as in this study. (Hence, a more appropriate name for the statistical procedures used in this study is Univariate Randomized Block Permutations, URBP.) For example, multiple meteorological variables such as u- and v-wind components, speed, and absolute vorticity could have been analyzed simultaneously to provide a common statistical agreement for the wind related variables. Likewise, thermodynamic information could be grouped together for obtaining a single statistical agreement for all model thermodynamic variables.

References

- Arakawa, A. and V.R. Lamb, 1981: A potential enstrophy and energy conserving scheme for the shallow water equations. *Mon. Wea. Rev.*, **109**, 18-36.
- Barnes, L.L., 1973: Mesoscale objective map analysis using weighted time series observations. NOAA Tech. Memo. ERL NSSL-62, 60 pp. [NTIS COM-73-10781].
- Benjamin, S.G., K.A. Brewster, R. Brummer, B.F. Jewett, T.W. Schlatter, T.L. Smith, and P.A. Stamus, 1991: An isentropic three-hourly data assimilation system using ACARS aircraft observations. *Mon. Wea. Rev.*, **119**, 888-906.
- Benjamin, S.G., T.L. Smith, P.A. Miller, D. Kim, T.W. Schlatter, and R. Bleck, 1991: Recent improvements in the MAPS isentropic-sigma data assimilation system. Preprint Volume of the Ninth Conference on Numerical Weather Prediction, October 1991, AMS, Denver, CO, 118-121.
- Benjamin, S.G., 1989: An isentropic mesoalpha-scale analysis system and its sensitivity to aircraft and surface observations. *Mon. Wea. Rev.*, **117**, 1586-1603.
- Black, T.L., 1987: A comparison of key forecast variables derived from isentropic and sigma coordinate regional models. *Mon. Wea. Rev.*, **115**, 3097-3114.
- Bossert, J.E., 1990: Regional-scale flows in complex terrain: An observational and numerical investigation. PhD dissertation, Atmos. Sci. Paper No. 472, Colorado State University, Dept. of Atmos Sci., Fort Collins, CO, 254pp.
- Branson, M.D., 1991: An historical evaluation of a winter orographic precipitation model. Masters thesis, Atmos. Sci. Paper No. 505, Colorado State University, Dept. of Atmos. Sci., Fort Collins, CO, 116 pp.

- Brockwell, P.J. and P.W. Mielke, 1984: Asymptotic distributions of matched-pairs permutation statistics based on distance measures. *Aust. J. Stat.*, **24**, 33-41.
- Chappell, C.F. 1970: Modification of cold orographic clouds. PhD dissertation, Atmos. Sci. Paper No. 173, Colorado State University, Dept. of Atmos. Sci., Fort Collins, CO, 196pp.
- Chen, C. and W.R. Cotton, 1983: Numerical experiments with a one-dimensional higher order turbulence model: Simulation of the wargara day 33 case. *Boundary-Layer Meteorol.*, **25**, 375-404.
- Cotton, W.R., M.A. Stephens, T. Nehr Korn, and G.J. Tripoli, 1982: The Colorado State University three-dimensional cloud/mesoscale model - 1982, Part II: an ice parameterization. *J. Rech. Atmos.*, **16**, 295-320.
- Cram, J.M., 1990: Numerical simulation and analysis of the propagation of a prefrontal squall line. PhD dissertation, Atmos. Sci. Paper No. 471, Colorado State University, Dept. of Atmos. Sci., Fort Collins, CO, 332 pp.
- Davies, H.C., 1983: Limitations of some common lateral boundary schemes used in regional NWP models. *Mon. Wea. Rev.*, **111**, 1002-1012.
- DeMott, P.J., M.P. Meyers, and W.R. Cotton, 1993: Parameterization and impact of ice initiation processes relevant to numerical model simulations of cirrus clouds. Submitted to *J. Atmos. Sci.*
- Dirks, R.A. 1973: The precipitation efficiency of orographic clouds. *J. Rech. Atmos.*, **7**, 177-184.
- Doesken, N.J. 1987: The contribution of snotel precipitation measurements to climate analysis, monitoring and research in Colorado. Presented at the Western Snow Conference, 14-16 April 1987, Vancouver, BC, Canada.
- Flatau, P.J., G.J. Tripoli, J. Verlinde, and W.R. Cotton, 1989: The CSU-RAMS cloud microphysics module: General theory and code documentation. Technical Report 451, Colorado State University, Fort Collins, Colorado 80523.

- Gal-Chen, T. and R.C.J. Somerville, 1975: On the use of a coordinate transformation for the solution of the Navier-stokes equations. *J. Comput. Phys.*, **17**, 209-228.
- Grasso, L.D., 1992: A numerical simulation of tornadogenesis. Masters thesis, Atmos. Sci. Paper No. 495, Colorado State University, Dept. of Atmos Sci., Fort Collins, CO, 102pp.
- Heckman, S.T., 1991: Numerical simulation of cirrus clouds - FIRE case study and sensitivity analysis. Masters thesis, Atmos. Sci. Paper No. 483, Colorado State University, Dept. of Atmos. Sci., Fort Collins, CO, 132pp.
- Heckman, S.T., and W.R. Cotton, 1993: Mesoscale numerical simulation of cirrus clouds-FIRE case study and sensitivity analysis. Accepted *Mon. Wea. Rev.*.
- Henry, S.L., 1991: Impact of inferred latent heating rates on predictions of convective storms. Masters thesis, Atmos. Sci. Paper No. 487, Colorado State University, Dept. of Atmos. Sci., Fort Collins, CO, 127 pp.
- Hoke, J.E., N.A. Phillips, G.J. DiMego, J.T. Tuccillo, and J.G. Sela, 1989: The Regional Analysis and Forecast System of the National Meteorological Center. *Mon. Wea. Forecasting*, **4**, 323-334.
- Intrieri, J.M., W.L. Eberhard, J.B. Snider, and T. Uttal, 1992: Multi-wavelength observations of a cirrus cloud event from FIRE II: Preliminary lidar, radar and radiometer measurements. Preprint Volume of the Eleventh International Conference on Clouds and Precipitation, August, 1992, AMS, Montreal, Canada, 537-540.
- Jensen, E.J., D.L. Westphal, O.B. Toon, and S. Kinne, 1992: Three dimensional microphysical modeling of cirrus clouds during the 1991 FIRE IFO. Preprint Volume of the Eleventh International Conference on Clouds and Precipitation, August, 1992, AMS, Montreal, Canada, 477-479.
- Klemp, J.B. and R.B. Wilhelmson, 1978: Simulations of right- and left-moving storms produced through storm-splitting. *J. Atmos. Sci.*, **35**, 1097-1110.

- Lee, T.J., 1992: The impact of vegetation on the atmospheric boundary layer and convective storms. PhD dissertation, Atmos. Sci. Paper No. 509, Colorado State University, Dept. of Atmos. Sci., Fort Collins, CO, 137pp.
- Mace, G.G. and T.P. Ackerman, 1992: Large scale forcing of middle and upper level clouds: Preliminary results from a FIRE cirrus case study. Preliminary lidar, radar and radiometer measurements. Preprint Volume of the Eleventh International Conference on Clouds and Precipitation, August, 1992, AMS, Montreal, Canada, 537-540.
- Mahrer, Y. and R.A. Pielke, 1977: A numerical study of the airflow over irregular terrain. *Beitr. Phys. Atmos.*, **50**, 98-113.
- McCoy, M.C. 1988: Application of the CIMMS mesoscale model to operational short-range forecasting. Masters thesis. Colorado State University, Dept. of Atmos Sci., Fort Collins, CO, 97pp.
- Mesinger, F., T.L. Black, D.W. Plummer, and J.H. Ward, 1990: Eta model precipitation forecasts for a period including tropical storm Allison. *Wea. and Forecasting*, **5**, 483-493.
- Mesinger, F., Z.I. Janjic, S. Nickovic, and D. Gavrilov, 1988: The step mountain coordinate: Model description and performance for cases of Alpine lee cyclogenesis and for a case of an Appalachian redevelopment. *Mon. Wea. Rev.*, **116**, 1493-1518.
- Meyers, M.P., 1990: An evaluation of the factors affecting wintertime quantitative precipitation forecasts in an explicit cloud model over mountainous terrain. Masters thesis, Atmos. Sci. Paper No. 450, Colorado State University, Dept. of Atmos Sci., Fort Collins, CO, 127pp.
- Mielke, P.W., 1991: The application of multivariate permutation methods based on distance functions in the earth sciences. *Earth-Science Rev.*, **31**, 55-71.
- Mielke, P.W. 1986: Non-metric statistical analyses: Some metric alternatives. *J. Stat. Plann. Inference*, **13**, 377-387.

- Mielke, P.W. 1885: Geometric concerns pertaining to application of statistical tests in the atmospheric sciences. *J. Atmos. Sci.*, **42**, 1209-1212.
- Mielke, P.W. 1984: Meteorological applications of permutation techniques based on distance functions. In: P.R. Krishnaiah and P.K. Sen (Editors), *Handbook of Statistics*, Vol. 4. North-Holland, Amsterdam, pp. 813-830.
- Mielke, P.W. and K.J. Berry, 1982: An extended class of permutation techniques for matched pairs. *Commun. Stat. Theory Methods*, **11**, 1192-1207.
- Mielke, P.W. and H.K. Iyer, 1982: Permutation techniques for analyzing multiresponse data from randomizing block experiments. *Commun. Stat. Theory Methods*, **11**, 1427-1437.
- Neiburger, M. 1949: Reflection, absorption, and transmission of insolation by stratus cloud. *J. Appl. Meteor.*, **6**, 98-104.
- Perkey, D.J. and C.W. Kreitzberg, 1976: A time-dependent lateral boundary scheme for limited-area primitive equation models. *Mon. Wea. Rev.*, **104**, 744-755.
- Pielke, R.A., W.R. Cotton, R.L. Walko, C.J. Tremback, W.A. Lyons, L.D. Grasso, M.E. Nicholls, M.D. Moran, D.A. Wesley, T.J. Lee and J.H. Copeland, 1992: A comprehensive meteorological modeling system - RAMS. *Meteorol. Atmos. Phys.*, **49**, 69-91.
- Rhea, J.O., 1978: Orographic precipitation model for hydrometeorological use. PhD dissertation, Atmos. Sci. Paper No. 287, Colorado State University, Dept. of Atmos. Sci., Fort Collins, CO, 199 pp.
- Rhea, J.O. and L.O. Grant, 1974: Topographic influences on snowfall patterns in mountainous terrain, *Advanced Concepts and Techniques in the Study of Snow and Ice Resources*, Nat'l Academy of Sci., Washington, DC, 182-192.
- Tripoli, G.J., 1986: A numerical investigation of an orogenic mesoscale convective system. PhD dissertation, Atmos. Sci. Paper No. 401, Colorado State University, Dept. of Atmos. Sci., Fort Collins, CO, 290 pp.

- Tripoli, G.J. and W.R. Cotton, 1982: The Colorado State University three-dimensional cloud/mesoscale model - 1982. Part I: General theoretical framework and sensitivity experiments. *J. Rech. Atmos.*, **16**, 185-220.
- Tucker, D.F., P.W. Mielke and E.R. Reiter, 1989: The verification of numerical models with multivariate randomized block permutation procedures. *Meteo. Atmos. Phys.*, **40**, 181-188.
- Tremback, C.J., 1990: Numerical simulation of a mesoscale convective complex: model development and numerical results. PhD dissertation, Atmos. Sci. Paper No. 465, Colorado State University, Dept. of Atmos. Sci., Fort Collins, CO, 274 pp.
- Tremback, C.J., and R. Kessler, 1985: A Surface temperature and moisture parameterization for use in mesoscale numerical models. Preprint Volume of the Seventh Conference on Numerical Weather Prediction, June 1985, AMS, Montreal, Canada, 355-358.
- Tremback, C.J., G.J. Tripoli, and W.R. Cotton, 1985: A regional scale atmospheric numerical model including explicit moist physics and a hydrostatic time-split scheme. Preprint Volume of the Seventh Conference on Numerical Weather Prediction, June 1985, AMS, Montreal, Canada, 355-358.
- Warner, T.T. and N.L. Seaman, 1990: A real-time mesoscale numerical weather-prediction system for research, teaching, and public service at Pennsylvania State University. *Bull. Amer. Meteor. Soc.*, **71**, 792-805.
- Wesley, D.A., 1991: An investigation of the effects of topography on Colorado Front Range winter storms. PhD dissertation, Atmos. Sci. Paper No. 489, Colorado State University, Dept. of Atmos. Sci., Fort Collins, CO, 197pp.
- Wesley, D.A. and R.A. Pielke, 1990: Observations of blocking-induced convergence zones and effects on precipitation in complex terrain. *Atmos. Res.*, **25**, 235-276.

496133 R